USGS
science for a changing world

Mineral Resources Program

# Tungsten Resources of the Northern Rocky Mountains, Montana and Idaho—A Synthesis and Quantitative Assessment of Skarn-Hosted Resources


Scientific Investigations Report 2023-5012

U.S. Department of the Interior
U.S. Geological Survey

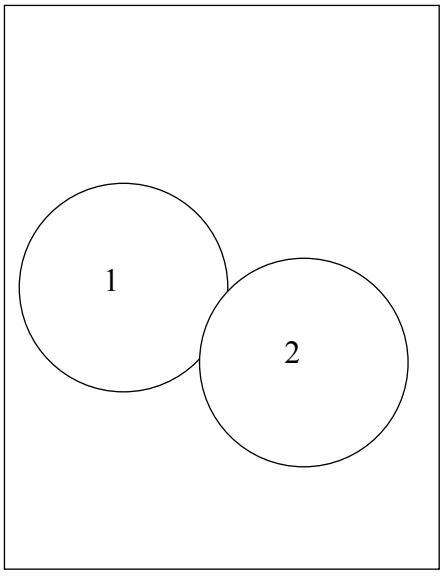


**Cover:** Massive scheelite sample from the Browns Lake tungsten skarn deposit, Beaverhead County, Montana. Images are captured under standard fluorescent light (1) and short wave, 254 nanometer, ultraviolet light (2). The scheelite mineral fluoresces or glows a light blue under ultraviolet light, which can be a useful indication of its concentration in a sample. Historically, tungsten has been mined from scheelite-bearing skarn rock. Photographs by Heather Parks, U.S. Geological Survey.

# Tungsten Resources of the Northern Rocky Mountains, Montana and Idaho—A Synthesis and Quantitative Assessment of Skarn-Hosted Resources

By Allen K. Andersen, Margaret A. Goldman, Mitchell M. Bennett, Connie L. Dicken, Philip J. Brown, and Heather L. Parks

Mineral Resources Program

Scientific Investigations Report 2023-5012

**U.S. Department of the Interior**
**U.S. Geological Survey**

U.S. Geological Survey, Reston, Virginia: 2023



Suggested citation:
Andersen, A.K., Goldman, M.A., Bennett, M.M., Dicken, C.L., Brown, P.J., and Parks, H.L., 2023, Tungsten resources of the northern Rocky Mountains, Montana and Idaho—A synthesis and quantitative assessment of skarn-hosted resources: U.S. Geological Survey Scientific Investigations Report 2023-5012, 87 p., https://doi.org/10.3133/sir20235012.

Associated data for this publication:
Goldman, M.A., Dicken, C.L., Brown, P.J., Andersen, A.K., Bennett, M.M., and Parks, H.L., 2022, Spatial data associated with tungsten skarn resource assessment of the northern Rocky Mountains, Montana and Idaho: U.S. Geological Survey data release, https://doi.org/10.5066/P9094RVV.

ISSN 2328-0328 (online)

# Contents

## Figures

## Tables



# Conversion Factors

International System of Units to U.S. customary units

| Multiply | By | To obtain |
|---|---|---|
| | Length | |
| centimeter (cm) | 0.3937 | inch (in.) |
| meter (m) | 3.281 | foot (ft) |
| kilometer (km) | 0.6214 | mile (mi) |
| | Area | |
| square kilometer ($km^2$) | 247.1 | acre |
| square meter ($m^2$) | 10.76 | square foot ($ft^2$) |
| square kilometer ($km^2$) | 0.3861 | square mile ($mi^2$) |
| | Mass | |
| gram (g) | 0.03527 | ounce, avoirdupois (oz) |
| kilogram (kg) | 2.205 | pound avoirdupois (lb) |
| metric ton (t) | 1.102 | ton, short [2,000 lb] |
| metric ton (t) | 0.9842 | ton, long [2,240 lb] |
| | Pressure | |
| kilopascal (kPa) | 0.01 | bar |
| kilopascal (kPa) | 0.00001 | kilobar |

Temperature in degrees Celsius (°C) may be converted to degrees Fahrenheit (°F) as follows:

$$°F = (1.8 \times °C) + 32.$$

Temperature in degrees Fahrenheit (°F) may be converted to degrees Celsius (°C) as follows:

$$°C = (°F - 32) / 1.8.$$

## Datum

Vertical coordinate information is referenced to the North American Vertical Datum of 1988 (NAVD 88).

Horizontal coordinate information is referenced to the North American Datum of 1983 (NAD 83).

Altitude, as used in this report, refers to distance above the vertical datum.

## Abbreviations

| | |
|---|---|
| AGRS | airborne gamma ray spectrometry |
| AI | alkalinity index |
| ASI | aluminum saturation index |
| CV | commodity value |
| DMA | Defense Minerals Administration |
| DMEA | Defense Minerals Exploration Administration |
| EMAG | Earth Magnetic Anomaly Grid |
| GFTZ | Great Falls tectonic zone |
| GIS | geographic information system |
| GUI | graphical user interface |
| IGS | Idaho Geological Survey |
| MALI | modified alkali-lime index |
| MBMG | Montana Bureau of Mines and Geology |
| MRDS | Mineral Resources Data System |
| MRR | metallurgical recovery rate |
| MSC | Marshall-Swift cost updating index |
| MT | magnetotelluric |
| NOAA | National Oceanic and Atmospheric Administration |
| NPV | net present value |
| NURE | National Uranium Resource Evaluation |
| P-T-X | pressure-temperature-composition |
| USGS | U.S. Geological Survey |
| USMIN | USMIN Mineral Deposit Database |
| RAEF | Resource Assessment Economic Filter |
| SGMC | State Geologic Map Compilation |

# Chemical Notation

| | |
|---|---|
| Ag | silver |
| Al | aluminum |
| As | arsenic |
| Au | gold |
| Bi | bismuth |
| Ca | calcium |
| CaO | calcium oxide |
| $CO_2$ | carbon dioxide |
| Cu | copper |
| F | fluorine |
| Fe | iron |
| FeO | ferrous iron oxide |
| $Fe_2O_3$ | ferric oxide |
| Hf | hafnium |
| K | potassium |
| $K_2O$ | potassium oxide |
| Li | lithium |
| MgO | magnesium oxide |
| Mn | manganese |
| Mo | molybdenum |
| $MoS_2$ | molybdenum disulfide |
| Na | sodium |
| NaCl | sodium chloride |
| $Na_2O$ | sodium oxide |
| Nd | neodymium |
| Pb | lead |
| Sb | antimony |
| $SiO_2$ | silicon dioxide (silica) |
| Sr | strontium |
| Sn | tin |
| Th | thorium |
| U | uranium |
| W | tungsten |
| $WO_3$ | tungsten trioxide |
| Zn | zinc |

# Tungsten Resources of the Northern Rocky Mountains, Montana and Idaho—A Synthesis and Quantitative Assessment of Skarn-Hosted Resources

By Allen K. Andersen, Margaret A. Goldman, Mitchell M. Bennett, Connie L. Dicken, Philip J. Brown, and Heather L. Parks

## Abstract

Mineral resource assessments performed by the U.S. Geological Survey provide a synthesis of available information about the location of known and suspected mineral deposits. This study focuses on skarn-hosted tungsten resources in the northern Rocky Mountain region of east-central Idaho and western Montana which have seen moderate tungsten trioxide production in the past from a variety of mineralization styles including skarn, vein and replacement, and wolframite-quartz veins. The area's geology is dominated by large Cretaceous and Tertiary plutons that are emplaced into a belt of Mesoproterozoic to Permian sedimentary rock and affected by tectonism related to the Sevier and later Laramide orogenies. Known tungsten skarn mineral sites are associated with contacts between Cretaceous plutons and calcareous and argillaceous sedimentary or metasedimentary rocks, including two skarn deposits in Montana (Calvert and Browns Lake) that are consistent with an updated grade and tonnage model.

This study (1) delineates permissive tracts where undiscovered tungsten skarn deposits may occur within 1 kilometer of the surface; (2) presents a tungsten mineral site dataset from a variety of public sources; (3) evaluates currently available geochemical, geophysical, and radiometric age data in support of tract delineation; (4) provides probabilistic estimates of the amount of tungsten and tungsten-mineralized rock that could be contained in undiscovered deposits within one major tract; (5) estimates the value of total undiscovered deposits using economic filter analysis; and (6) provides a synthesis of metallogenic controls on regional tungsten skarn and granitoid-related mineral deposits.

Two permissive tracts were delineated: the Great Falls tectonic zone (GFTZ)-Cretaceous tract, for which a quantitative assessment was performed, and the Bitterroot tract, which was assessed in a qualitative manner. The quantitative three-part assessment, conducted in August 2019, indicates that undiscovered tungsten resources might exist in skarn-type deposits within the study area. Using a negative binomial function, a mean of 4 undiscovered deposits was calculated from panel estimates. Simulation results that combine an updated grade and tonnage model with estimates of undiscovered deposits include the amounts of ore and contained tungsten trioxide at different levels of uncertainty. A mean of 250,000 metric tons and median of 200,000 metric tons contained tungsten trioxide was calculated for the undiscovered deposits within the GFTZ-Cretaceous tract. The value of undiscovered deposits was estimated using a new economic filter that considers factors such as mine type, deposit depth, deposit geometry, metallurgical recovery rate, cutoff grade, and tract area.

A review of the regional Archean to Paleogene geology suggests that ore metal (copper, molybdenum, and tungsten) variations in intrusion-related deposits of Montana and Idaho may be controlled by a number of factors including the age and composition of underlying basement terranes, depth of emplacement, pluton chemistry and degree of fractionation, redox conditions, and aqueous fluid-melt partition coefficients.

## Introduction

The purpose of this study was to assess the potential for undiscovered tungsten deposits in the Northern Rocky Mountains of Idaho and Montana, with specific emphasis on skarn-hosted resources. Tungsten was identified as 1 of 35 commodities deemed vital to the United States' economy and national security as outlined in the Department of the Interior's Final List of Critical Minerals 2018 (U.S. Office of the Secretary, 2018), pursuant to Executive Order 13817 of December 20, 2017, "A Federal Strategy to Ensure Secure and Reliable Supply of Critical Minerals." This paper describes geologic and domestic resource information for one of the few critical commodities not covered in U.S. Geological Survey Professional Paper 1802: "Critical Mineral Resources of the United States—Economic and Environmental Geology and Prospects for Future Supply" (Schulz and others, 2017).

Tungsten is a very hard, dense metal with an extremely high melting temperature, high tensile strength, high thermal and electrical conductivities, and is resistant to corrosion (Brown and Pitfield, 2014). These properties have led to applications in aerospace (superalloys for jet engines), defense (munitions), energy (drilling equipment and petroleum catalysts), and telecommunications (filaments and cellular phones) (Fortier and others, 2018). The high

criticality of tungsten is due to three main factors: (1) there is currently no domestic production of tungsten from mining, (2) the United States is 100-percent reliant on net imports while consumption has remained consistent in recent years, and (3) production is limited to only a few countries where risk of disruption is high (McCullough and Nassar, 2017; U.S. Geological Survey, 2019).

This assessment is part of a broader effort by the U.S. Geological Survey (USGS) to identify areas with undiscovered tungsten resource potential in the United States. The USGS effort includes three tungsten-rich metallogenic provinces, two of which were delineated by Hobbs and Tooker (1979) but were not quantitatively assessed for undiscovered resource potential: the Northern Rocky Mountains of Montana, Idaho, and Washington; and the Great Basin of California and Nevada. Assessments complementary to this one focus on the Western Great Basin in California and Nevada (Lederer and others, 2021) and the Yukon-Tanana uplands in Alaska (Case and others, 2022; fig. 1). Collectively, this USGS effort represents the first study of domestic tungsten resources in over twenty years.

The northern Rocky Mountains study area includes twelve 1°×2° quadrangles, centered on Montana's Butte and Dillon quadrangles (fig. 2), which contain a high number of known tungsten mineral sites and were the focus of two previous assessments of Fe, Cu, Mo, W, Au, and Ag potential under the USGS Conterminous United States Mineral Assessment Program (Elliott and others, 1993; Pearson and


**Figure 1.** Map of North America showing three U.S. Geological Survey tungsten skarn assessment study areas located mostly within the North American Cordillera. The three study areas are the Yukon-Tanana uplands (Case and others, 2022), the Great Basin (Lederer and others, 2021), and the Northern Rocky Mountains of Montana and Idaho (this study).

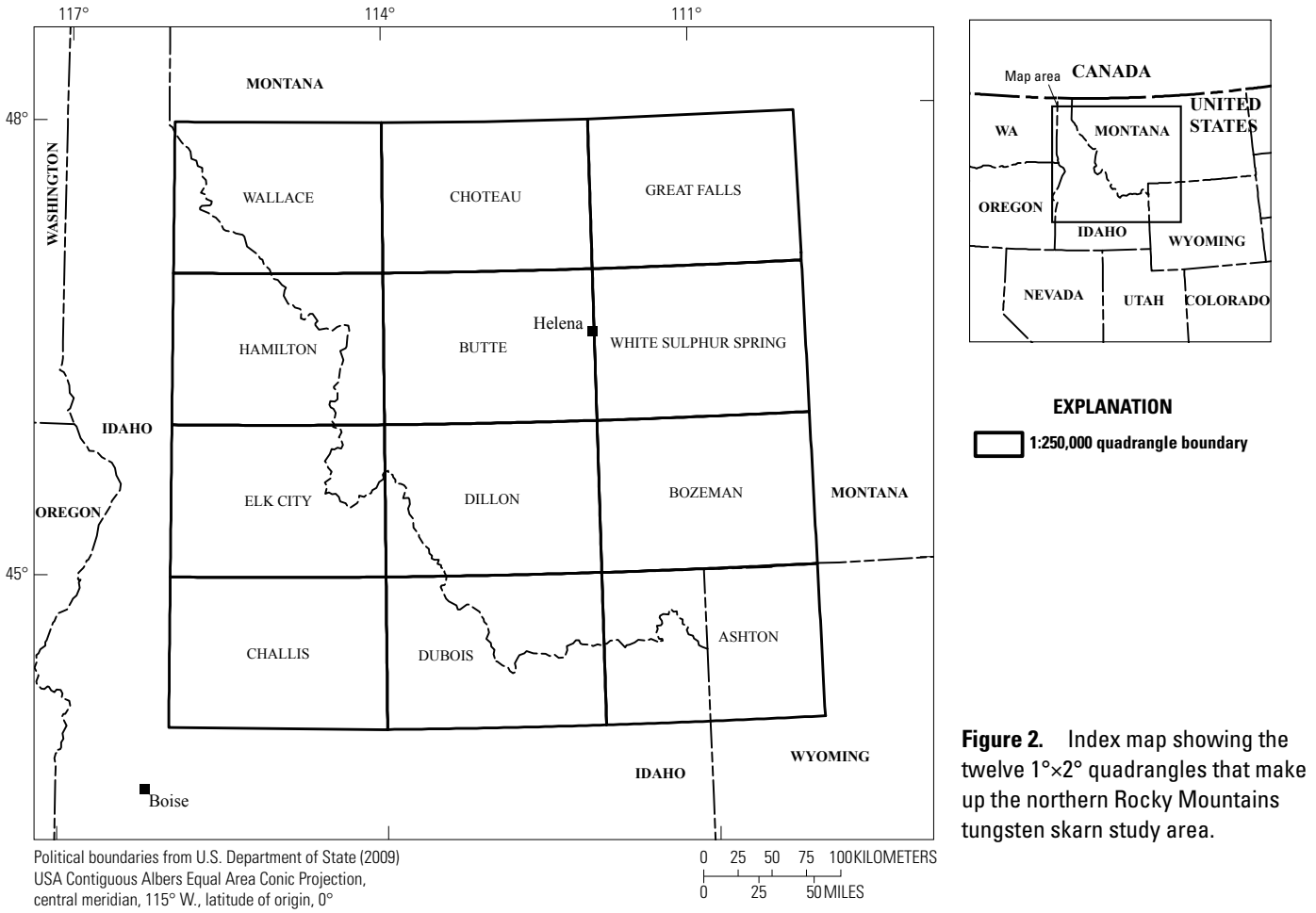


**Figure 2.** Index map showing the twelve 1°×2° quadrangles that make up the northern Rocky Mountains tungsten skarn study area.

others, 1992b). USGS Bulletin 1658 A-S (McIntyre, 1985) and USGS Professional Paper 1525 (Fisher and Johnson, 1995) previously described the geology and mineral resource potential, including tungsten, in the Challis 1°×2° quadrangle in Idaho. Tungsten was historically produced from scheelite-bearing skarn, hübnerite-quartz veins, breccia-fill or vein and replacement, and placer deposits, most of which was mined between 1932 and 1962. The eastern half of the Ashton 1°×2° quadrangle includes the northeastern corner of Wyoming that is Yellowstone National Park. The National Park was excluded from the study area and mineral resource potential in this area was not evaluated as part of this assessment.

This report contains the results of a three-part quantitative mineral resource assessment following the methods of Singer (1993) and Singer and Menzie (2010). Part 1 consists of grade and tonnage information for identified tungsten skarn resources in the northern Rocky Mountains study area in conjunction with an updated global grade and tonnage model (Green and others, 2020). Part 2, delineation of permissive tracts, relies on maps that identify areas with favorable geologic characteristics for the occurrence of tungsten skarn mineralization on the basis of criteria derived from the tungsten skarn descriptive deposit model. Permissive tracts were interpreted by integrating geoscience information from a variety of sources including maps of regional geology, seven publicly available mineral resource databases, rock and stream sediment geochemistry, and airborne magnetic and radiometric data. Part 3 involves a panel of experts who estimated the number of undiscovered deposits from information used to delineate permissive tracts, including tungsten mineral site locations and classifications.

In addition to the conventional three-part methodology, the estimates for undiscovered deposits and the global grade and tonnage model for tungsten skarn deposits are used as inputs to MapMark4 (Ellefsen, 2017b), an open-source, R-based, software tool designed to implement probability calculations. Using a Monte Carlo simulation with 20,000 iterations, MapMark4 estimates contained tungsten resources for undiscovered deposits from which probability distributions of contained ore and tungsten trioxide metal ($WO_3$) are calculated. The Resource Assessment Economic Filter of Shapiro and Robinson (2019) was applied to the simulation results to estimate the economic value of undiscovered tungsten skarn deposits in Idaho and Montana and to determine the proportion of resources that may be economic to extract.

Using the quantitative three-part method, estimates of in-ground tungsten resources were calculated for a single permissive tract: the Great Falls tectonic zone-Cretaceous tract

(herein referred to as GFTZ-Cretaceous tract). Qualitative results include a discussion of supporting data for an additional tract (the Bitterroot tract) and other styles of tungsten mineralization. For the Bitterroot tract, insufficient data preclude a quantitative estimate of tungsten mineral resources using only a skarn-type deposit model. Because 62 percent of the study area is administered as Federal lands (principally the U.S. Forest Service and Bureau of Land Management) or designated as wilderness areas (Frank Church–River of No Return Wilderness and Selway–Bitterroot Wilderness, among others; fig. 3), information on the undiscovered mineral resource potential represents an important consideration for land management decisions and Federal policy.

The terminology used in this report is intended to represent standard definitions that reflect general usage by the minerals industry and the resource-assessment community. Definitions are presented in the "Glossary" section of this report. Names for the many igneous intrusive bodies and intrusive complexes mentioned in this report come from Zientek and others (2005), unless otherwise noted.

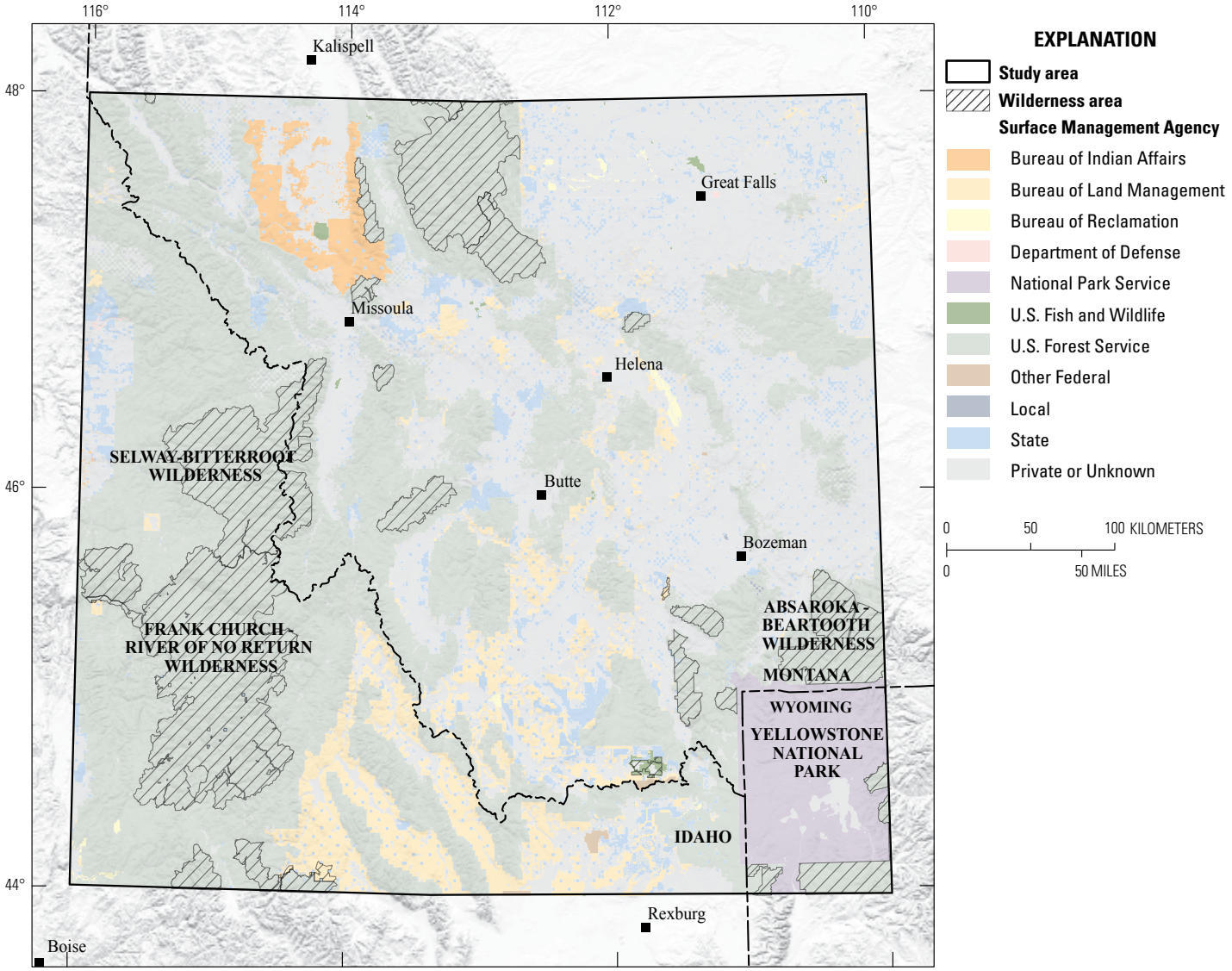


Political boundaries from U.S. Department of State (2009); Shaded relief from U.S. Geological Survey, National Geospatial Program; USA contiguous Albers Equal Area Conic Projection, central meridian 113° W. latitude of origin, 0°; North American Datum of 1983

**Figure 3.** Map showing ownership, including Federal land ownership and wilderness areas in the northern Rocky Mountains study area.

## Study Responsibilities

Introductory materials specific to the study area were initially compiled by J. Hammarstrom, M. Mihalasky, M. Zientek, and H. Parks. Coauthors of this report were involved in the several integrated aspects of the study, which include geographic information systems (GIS) analysis, data compilation, tract delineation, figure preparation, assessment meeting participation, and economic filter analysis. A. Andersen served as lead scientist, editor, and author for the study. Data compilation, radiometric data analysis, and mineral site ranking procedures were performed by M. Goldman. GIS analysis was performed principally by M. Goldman and C. Dicken. Descriptive models and orebody characteristics of tungsten in the study area were summarized by M. Bennett and A. Andersen. Review and analysis of geophysical data were performed by P. Brown. Figures were prepared by M. Goldman and C. Dicken with contributions from H. Parks, A. Andersen, and J. Wallis.

## Geologic Setting of the Study Area

Major geologic features of the 12-quadrangle study area include the Cretaceous to Tertiary Idaho batholith, Tertiary volcanic and intrusive rocks of the Challis magmatic belt, Mesoproterozoic metasedimentary rocks of the Belt Supergroup, Neoproterozoic metasedimentary (Windermere Group) and plutonic rocks, the Rocky Mountain Basin and Range (Sonder and Jones, 1999), the Sevier fold-and-thrust belt, and the foreland basin (figs. 4 and 5*A*, *B*). Underlying Precambrian basement terranes include the Archean Wyoming province; deformed continental margin assemblages of the Trans-Montana fold-and-thrust belt; and accreted terranes of the Trans-Montana orogen including an Archean micro-continent known as the Medicine Hat block and Paleoproterozoic magmatic arc known as the Wallace terrane (Sims and others, 2004; Sims and others, 2005). The basement domains of Lund and others (2015; fig. 6) were partially based on previously published basement, lithotectonic, and terrane maps, and are roughly consistent with the basement terranes described above. In this report, we refer to the basement domains of Lund and others (2015) in discussions of basement geology.

The Great Falls tectonic zone is a corridor of high-angle faults and lineaments trending from northeast to southwest across west-central Montana and continuing into Idaho as the Trans-Challis Fault System. The Great Falls tectonic zone is described as a ~200-kilometer (km)-wide zone of Phanerozoic faults resulting from reactivation of basement structures along the Proterozoic collisional suture between the Archean Wyoming province (3.5–2.6 billion years [Ga]) and the Archean Medicine Hat block (3.3–2.6 Ga; O'Neill and Lopez, 1985; Mueller and others, 2005; Gifford and others, 2014). In this report, the term "Great Falls tectonic zone" is retained informally to describe the highly disturbed tectonic zone between the respective plates of the Trans-Montana orogen, consistent with the definition of Sims and others (2004). It includes the major northeast-trending structures shown on figure 6, from north to south, the Great Falls shear zone, the Dillon suture (shear) zone, the Mirror Lake shear zone, and the Madison mylonite zone. Alternative models consider the Great Falls tectonic zone to be an intracontinental shear zone or a transcurrent fault reactivated during the Paleoproterozoic (Boerner and others, 1998; Lemieux and others, 2000). Regardless of its origin, there is a clear spatial association between the structure and Cretaceous to Tertiary plutonism with associated epigenetic mineral systems.

Studies of (1) Proterozoic rocks (1.86 Ga) in the Little Belt Mountains (figs. 6 and 7) that were uplifted within the Great Falls tectonic zone during Tertiary magmatism and (2) inherited zircons in Cretaceous and Tertiary granitic rocks within the corridor have led to the hypothesis that a single linear Paleoproterozoic arc (the Little Belt arc) existed within the region defined as the Great Falls tectonic zone (Mueller and others, 2002; Foster and others, 2006; Probst, 2007; Gifford and others, 2014). Foster and others (2006) suggest that the Idaho batholith, Bitterroot lobe is underlain by Proterozoic crust at 2.4–1.6 Ga but with a major component distinctly younger (1.75–1.73 Ga) than crust within the Great Falls tectonic zone. This region west of the Great Falls tectonic zone (the Selway terrane of Foster and others, 2006) is roughly equivalent to the Wallace terrane of Sims and others (2004; 2005; fig. 6). On the basis of Neoarchean (2.66 Ga) and Paleoproterozoic (1.86 Ga) uranium-lead zircon ages from orthogneisses of the Clearwater and Priest River complexes, Vervoort and others (2016) suggest that much of the area between the Little Belt Mountains in Montana and Priest River complex in northern Idaho may be underlain by similar Paleoproterozoic (1.86 Ga) crust.

Sedimentary rocks of the Belt Supergroup (the Purcell Supergroup in Canada) occur throughout the study area as an allochthon and series of thrust plates, having been transported northeastward over Phanerozoic strata. Sediment of the Belt and Purcell Supergroups was deposited during the Mesoproterozoic (1,500–1,370 Ma) (Evans and others, 2000; Lydon, 2000), and the basin subsequently experienced deformation during Neoproterozoic to early Paleozoic continental rifting, Cordilleran thrusting, and Tertiary extension (Sears, 2007). The total thickness of the Proterozoic sedimentary package exceeds 15 km within the study area. Although much of the Belt and Purcell Supergroups consist of clastic formations, specific carbonate and phosphate units represent potential host lithologies for tungsten skarn mineralization.

Neoproterozoic through Paleozoic marine strata were deposited along the ancient continental margin, shelf, and basin from east to west across the study area (Lund and others, 2016; fig. 8). Rocks within and east of the Sevier fold-and-thrust belt include marine Paleozoic strata with a total thickness of at least 2,400 meters (m). The Paleozoic sedimentary rocks are part of a shallow-water carbonate-dominant shelf sequence which ranges from the basal Middle Cambrian

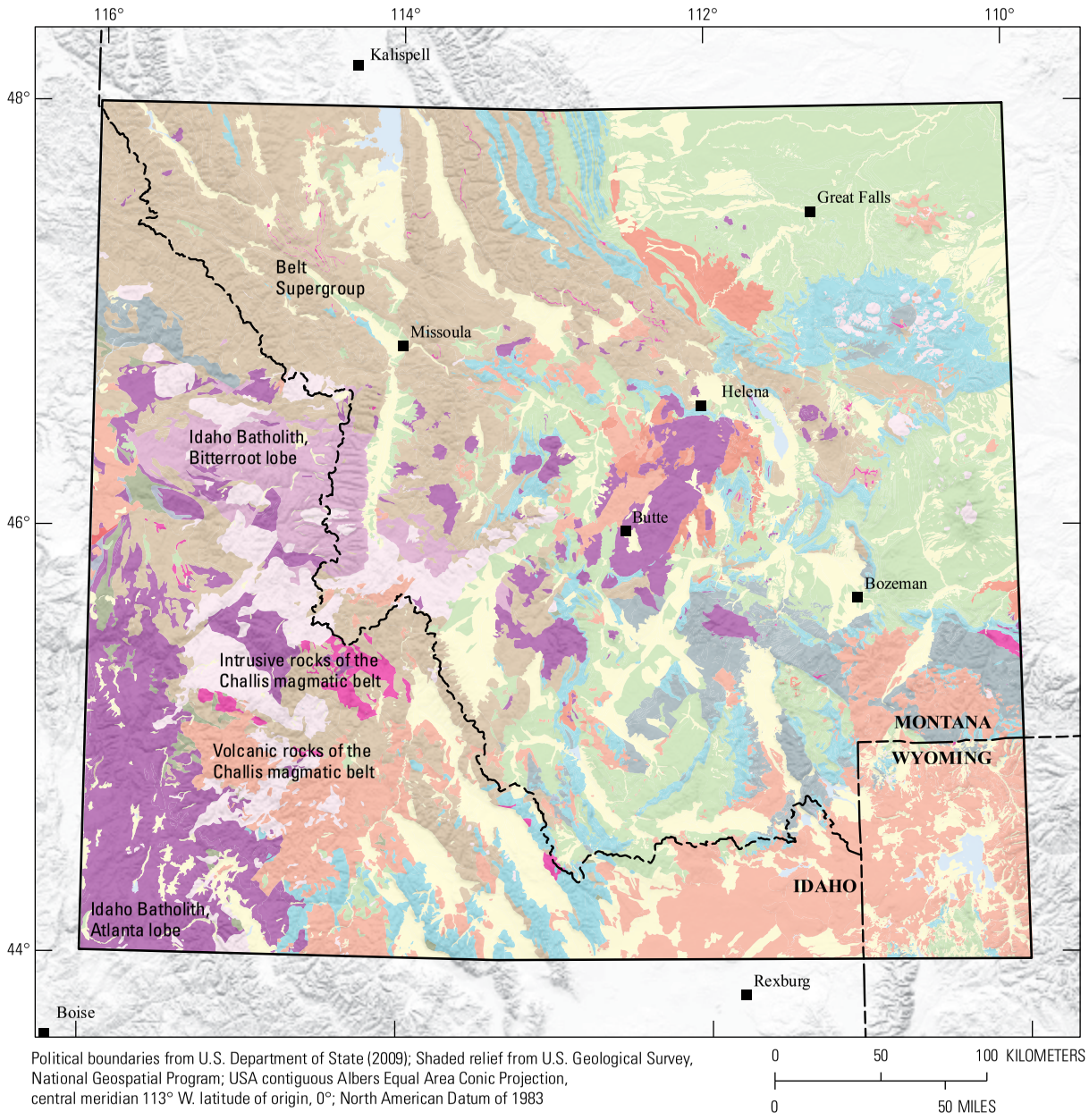


**Figure 4.** Generalized geologic map of the northern Rocky Mountains tungsten skarn study area based on work by Zientek and others (2005) and Horton (2017).

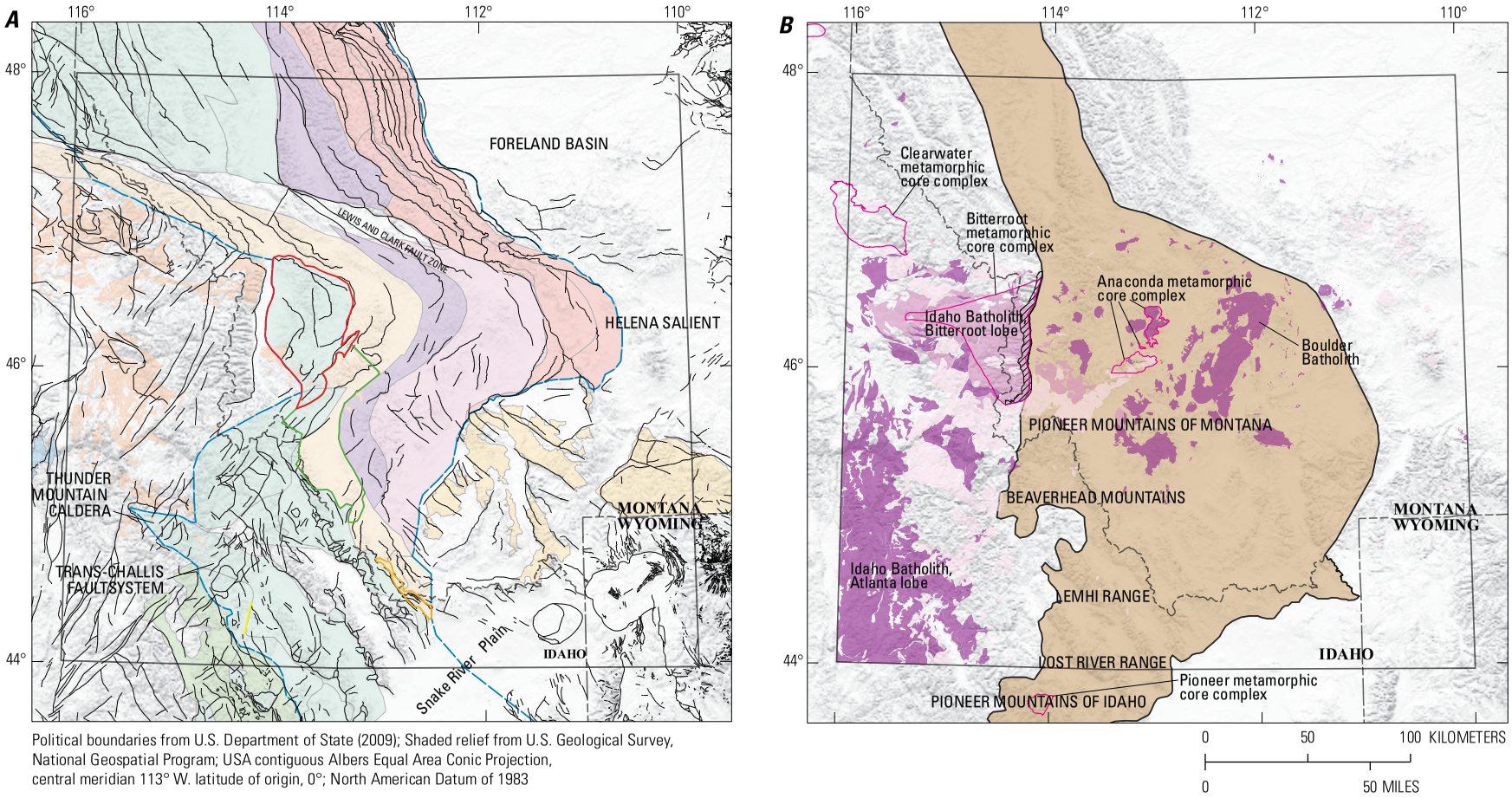


Political boundaries from U.S. Department of State (2009); Shaded relief from U.S. Geological Survey, National Geospatial Program; USA contiguous Albers Equal Area Conic Projection, central meridian 113° W. latitude of origin, 0°; North American Datum of 1983

## EXPLANATION

**Basement-Cored Uplifts and Thrust Plate Complexes**

- Laramide basement-cored uplift
- Laramide fold-thrust complex above shallow decollement
- Sevier to Laramide thrust complex above eastward-shallowing decollement ramp
- Sevier to Laramide thrust complex above moderately deep decollement
- Sevier thrust complex above moderately deep decollement
- Sevier thrust complex above ramp in decollement
- Metamorphic remnants of Sevier thrust-complex above deep decollement
- Sevier (?) thrust complex in area of Antler allocthon
- Sonoman (?) to Nevadan (?) thrust complex
- Sonoman (?) thrust complex in area of possible Antler allocthon

**Pluton age**

- Tertiary
- Tertiary to Cretaceous
- Cretaceous

- **Study area**
- **Sevier-Laramide fold-and-thrust belt**
- **Grasshopper thrust plate**
- **Medicine Lodge thrust plate**
- **Sapphire-Georgetown thrust plate**
- **Core complexes**
- **Bitterroot mylonite zone**
- **Rocky Mountain Basin and Range**
- **Salmon River Lineament**
- **Major faults**

**Figure 5.** Maps showing tectonic features of the northern Rocky Mountains study area. *A*, Map showing the major faults and thrust-plate complexes. *B*, Map of areas of Neogene Basin and Range normal faulting (labeled as Rocky Mountain Basin and Range), Eocene metamorphic core complexes, and Cretaceous to Tertiary plutons. Structural features from Zientek and others (2005), Vuke and others (2007), and Horton (2017). Rocky Mountain Basin and Range modified from Reynolds (1979), Kuntz and others (1992), Sonder and Jones (1999), and Camp and others (2015).

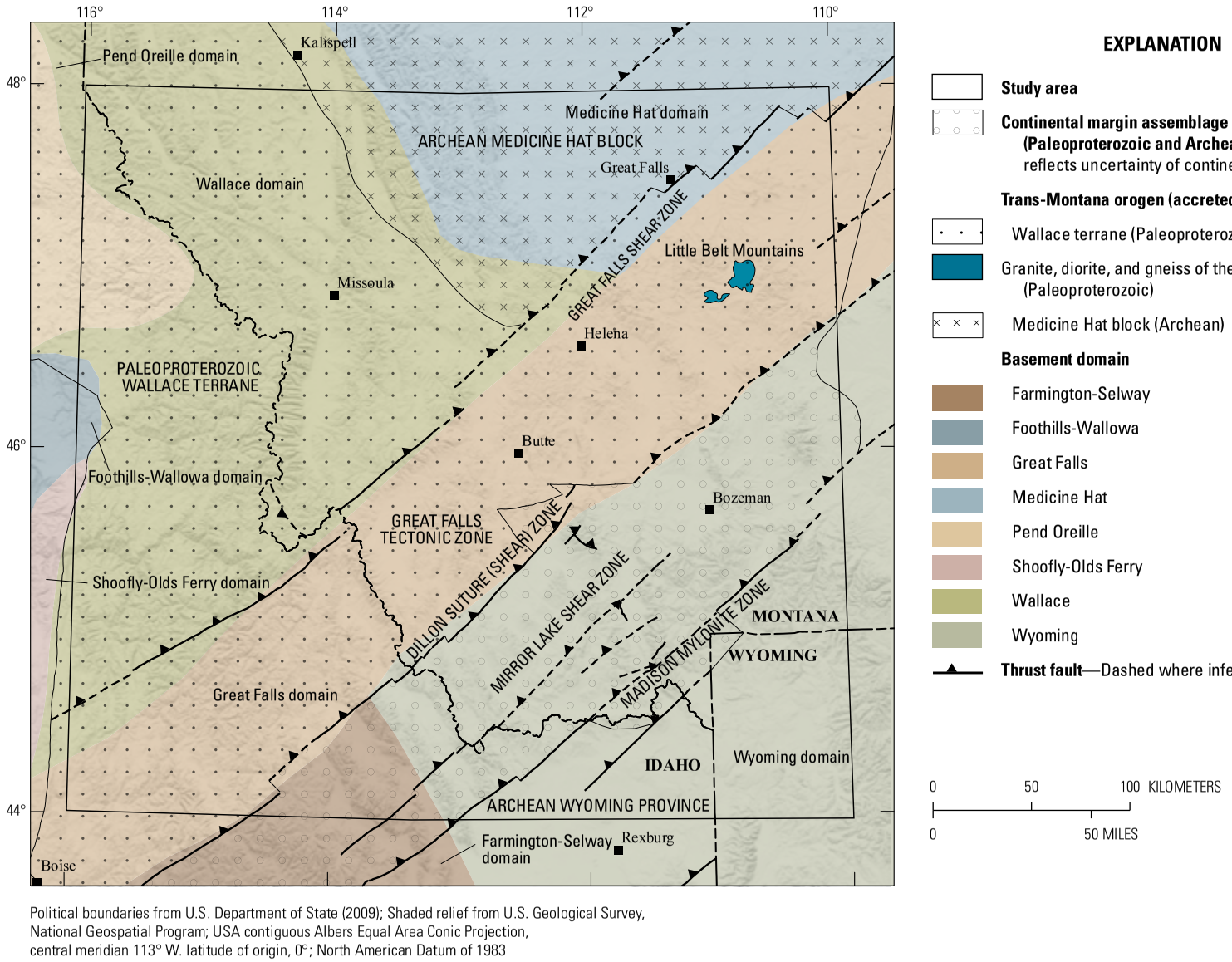


Political boundaries from U.S. Department of State (2009); Shaded relief from U.S. Geological Survey, National Geospatial Program; USA contiguous Albers Equal Area Conic Projection, central meridian 113° W. latitude of origin, 0°; North American Datum of 1983

**Figure 6.** Map showing basement domains of the northern Rocky Mountains study area from Lund and others (2015). The Continental margin assemblage (Fold-and-thrust belt), Trans-Montana orogen (accreted terranes) and thrust faults (certain and inferred) were modified from Sims and others (2004, 2005).

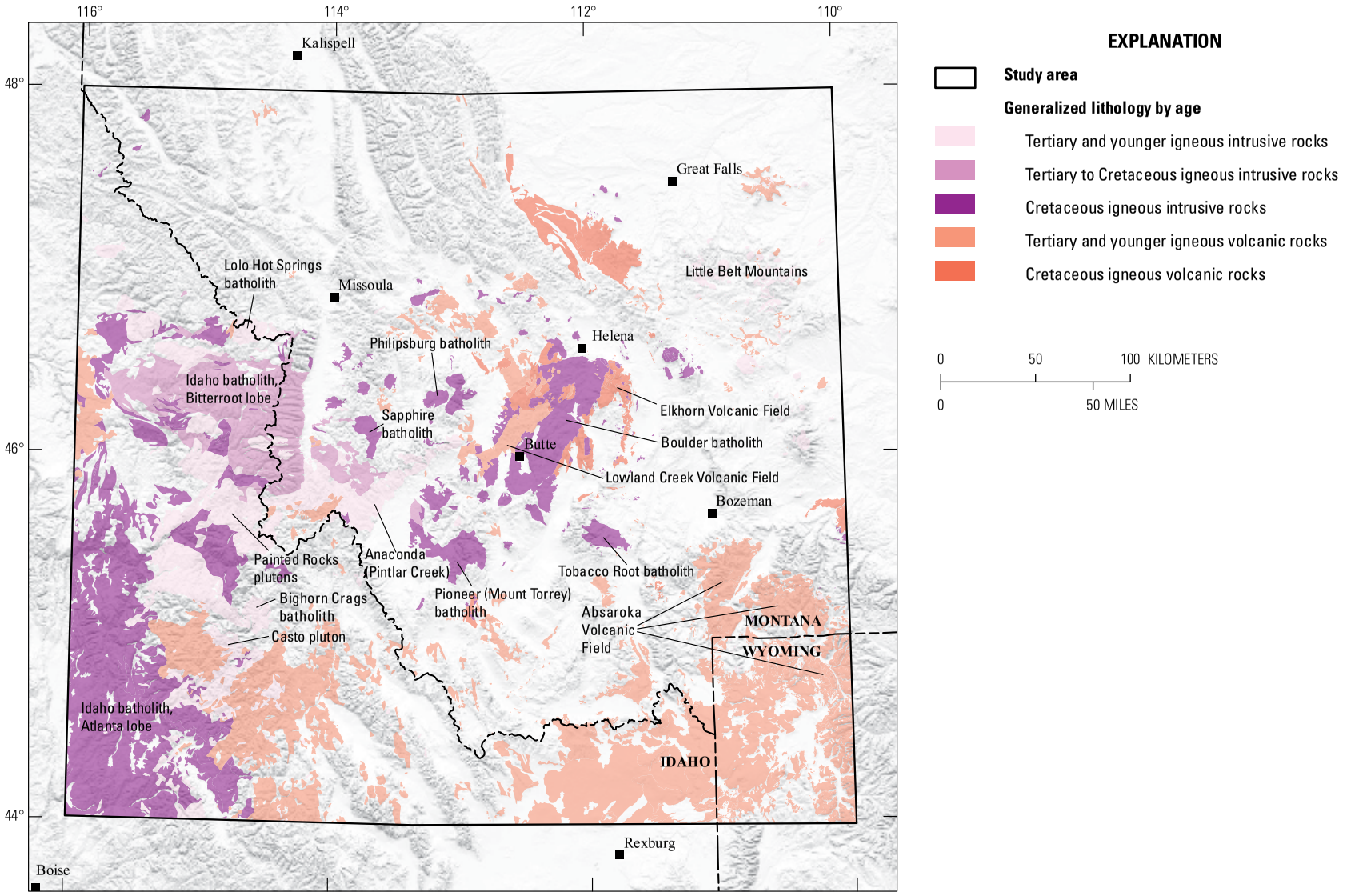


Political boundaries from U.S. Department of State (2009); Shaded relief from U.S. Geological Survey, National Geospatial Program; USA contiguous Albers Equal Area Conic Projection, central meridian 113° W. latitude of origin, 0°; North American Datum of 1983

**Figure 7.** Map showing Cretaceous to Tertiary intrusive and volcanic rocks of the northern Rocky Mountains tungsten skarn study area. Constructed from the geologic map databases of Zientek and others (2005) and Horton (2017).

Flathead Quartzite, which sits unconformably on crystalline basement or middle Proterozoic strata in the eastern front of the thrust belt, to the Phosphoria Formation and related Permian rocks (Ruppel and Lopez, 1984; Pearson and others, 1992a). The lower part of the Paleozoic section is mainly dolostone and limestone, whereas Carboniferous to Permian clastic rocks and phosphatic beds dominate in the upper part of the sequence. Mesozoic clastic and carbonate sedimentary rocks (preserved sequences of up to at least 6,700 m in the study area) were deposited east of the fold-and-thrust belt in a foreland basin, the thickest of which are Cretaceous age (Elliott and others, 1992b; Ruppel and Lopez, 1984).

Cordilleran arc magmatism during the Cretaceous included composite batholiths as well as smaller stocks and plutons emplaced at mesozonal and epizonal depths and volcanism above the eastward-dipping subduction zone and

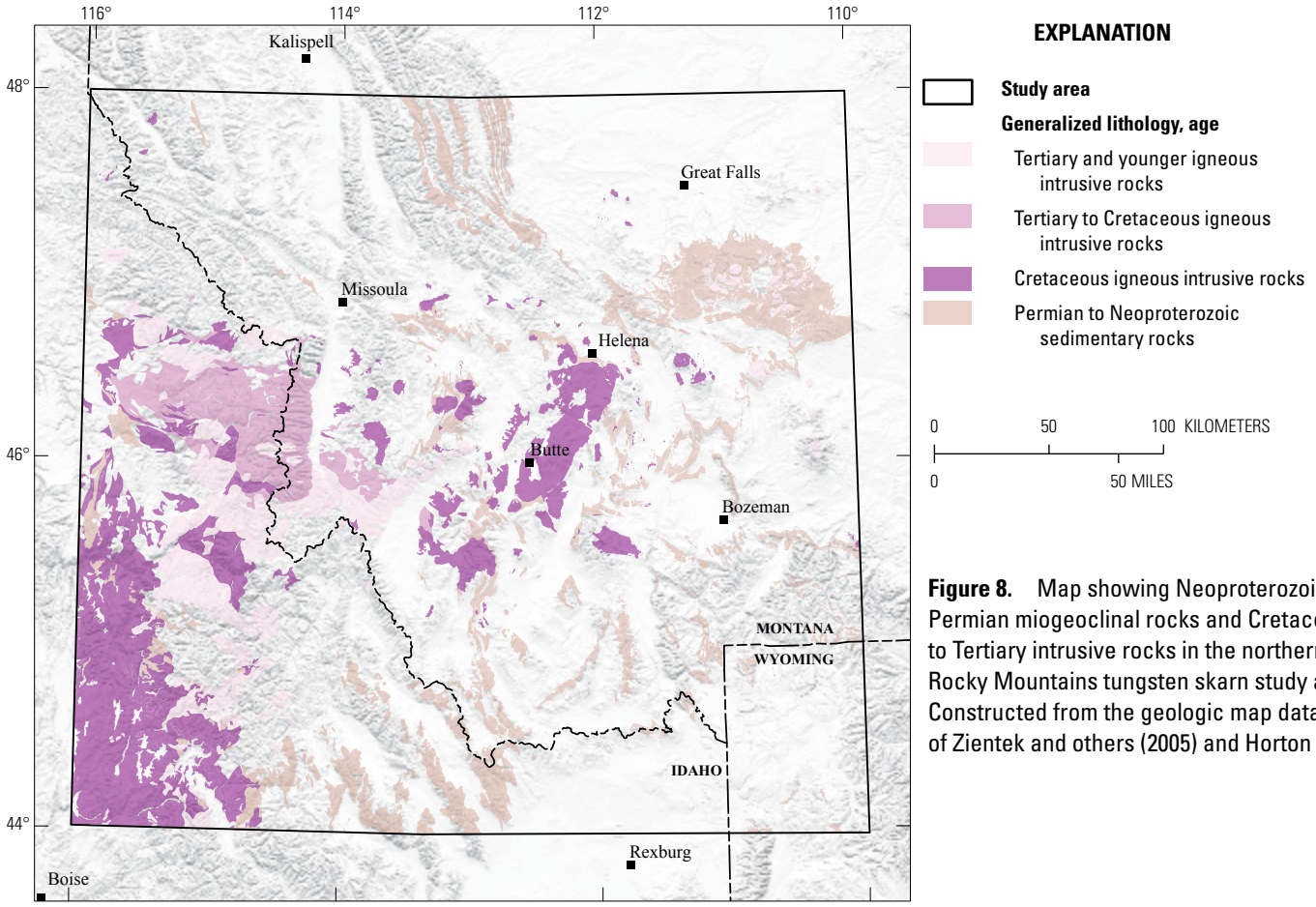


Political boundaries from U.S. Department of State (2009); Shaded relief from U.S. Geological Survey, National Geospatial Program; USA contiguous Albers Equal Area Conic Projection, central meridian 113° W. latitude of origin, 0°; North American Datum of 1983

**Figure 8.** Map showing Neoproterozoic to Permian miogeoclinal rocks and Cretaceous to Tertiary intrusive rocks in the northern Rocky Mountains tungsten skarn study area. Constructed from the geologic map databases of Zientek and others (2005) and Horton (2017).

foundering Farallon plate (Elliott and others, 1992b; DeCelles, 2004). Major batholithic suites of the study area include the Idaho, Boulder, Pioneer (Mount Torrey), Anaconda (Pintlar Creek), Philipsburg, Sapphire, and Tobacco Root batholiths (figs. 4 and 7). These plutons are mostly metaluminous to weakly peraluminous, calcic to alkali-calcic, and range in composition from tonalite to granite (predominately monzogranite and granodiorite). Chemically and temporally distinct intrusive phases are recognized in many of the plutons including the two largest: the Idaho batholith and Boulder batholith. The Boulder batholith is divided into a main, potassic suite which composes the central portion of the batholith and a sodic suite which comprises smaller peripheral plutons (Hyndman, 1983; du Bray and others, 2012). The bilobate Idaho batholith includes the southern Atlanta lobe and northern Bitterroot lobe. Temporally and chemically distinct pulses include (1) an early metaluminous and border zone suite of the Atlanta lobe (98–85 Ma), (2) a main peraluminous suite of the Atlanta lobe (83–67 Ma), (3) a late metaluminous suite of the Bitterroot lobe (75–68 Ma), and (4) a peraluminous suite of the Bitterroot lobe (66–53 Ma; Gaschnig and others, 2010; 2011; 2013).

Tertiary magmatism (~52–39 Ma) was less voluminous, resulting in the Challis Volcanic Group and associated plutons in Idaho (Bighorn Crags and Lolo Hot Springs batholiths, Casto pluton, and Painted Rocks plutons), most of which intruded along the eastern margin of the Idaho batholith and between the Atlanta and Bitterroot lobes (fig. 7). In Montana, Tertiary volcanic and intrusive rocks of the study area include the Lowland Creek Volcanic Field, shallow intrusions in the Little Belt Mountains, the Absaroka Volcanic Field, and other small plutons (fig. 7).

A major structural feature of the study area is the Sevier fold-and-thrust belt (fig. 5*A*), which extends ~200 km from the Idaho batholith to cratonic rocks of the Archean Wyoming province. Orogenesis occurred during subduction of the Farallon plate beneath North America with accretion of volcanogenic terranes along the Cordilleran margin and intrusion of Cretaceous batholiths causing overthickening of crust to the east and development of the fold-and-thrust belt in Paleozoic passive margin strata (Link and DeGrey, 2020). In Idaho and Montana, Sevier deformation (~130–60 Ma) consisted of east-vergent, thin-skinned thrusting prominent in Paleozoic platform sequences, whereas Laramide deformation (~70–55 Ma) was manifested by thick-skinned thrusting and basement-cored uplifts. The location of the thrust belt in southwest Montana and east-central Idaho was likely influenced by the geometry of the Belt-Purcell basin, Great Falls tectonic zone, northwest Archean Wyoming craton, and Lewis and Clark strike-slip fault system (Foster and others, 2006). Deformation was most intense during the Late Cretaceous, when laterally extensive thrust sheets, imbricate thrusts, and tight and overturned folds were formed (Ruppel and Lopez, 1984; Elliott and others, 1992b). Major thrust plates include the Medicine Lodge, Grasshopper, and Sapphire-Georgetown plates at the west edge of the belt, whereas the frontal fold-and-thrust zone developed to the east (fig. 5*A*; Ruppel and Lopez, 1984). An extensive foreland basin developed east of the thrust belt as a result of regional compression during the Mesozoic.

In the east-central part of the study area, the thrust belt forms the eastward-convex Helena salient, bounded to the north and south by northwest-southeast and east-striking strike-slip faults and is dominated by a thick succession of allochthonous Proterozoic clastic strata of the Belt-Purcell basin (DeCelles, 2004; Sears, 2007). Extension during the Cenozoic exhumed metamorphic core complexes along shallowly dipping normal faults, including the Anaconda, Bitterroot, Clearwater, and Pioneer complexes. Prominent Basin and Range normal faulting occurs in the southwest quadrant of the study area, separating the Beaverhead, Lemhi, Lost River, and Pioneer Mountain Ranges (fig. 5*B*; Kuntz and others, 1992; Foster and others, 2006).

This area of the Northern Rocky Mountains hosts a variety of identified epigenetic mineral resources, many of which are the result of magmatic-hydrothermal activity during the waning stages of Cretaceous and Tertiary magmatism (fig. 9). Several of the more significant mineral deposits occur within a copper-molybdenum-tungsten metallogenic belt which transects the study area from southwest to northeast, roughly coincident with the Great Falls tectonic zone. The mineralized belt previously referred to as the "transverse porphyry belt," "Idaho-Montana porphyry belt," and "White Cloud-Cannivan porphyry molybdenum belt of Idaho and Montana" (Jerome and Cook, 1967; Armstrong and others, 1978; Rostad, 1978) extends from the Cumo deposit just north of the Boise basin to the Big Ben molybdenum deposit of the Little Belt Mountains in north-central Montana (Pearson and others, 1992a). Endako-type porphyry molybdenum-copper or porphyry copper-molybdenum and Climax-type porphyry molybdenum deposits, some with associated tungsten resources, are centered on Cretaceous and Tertiary intrusions. Skarn-style tungsten mineralization is generally associated with Late Cretaceous mesozonal calc-alkaline plutons of granodiorite and quartz monzonite composition (Einaudi and others, 1981; Dawson, 1995). Tungsten mineralization in the form of wolframite-quartz-pyrite veins is generally associated with epizonal rhyolite or granite porphyry intrusions in this region that range in age from 50 to 40 Ma (Mutschler and others, 1981), but may also be associated with Cretaceous calc-alkaline plutons.

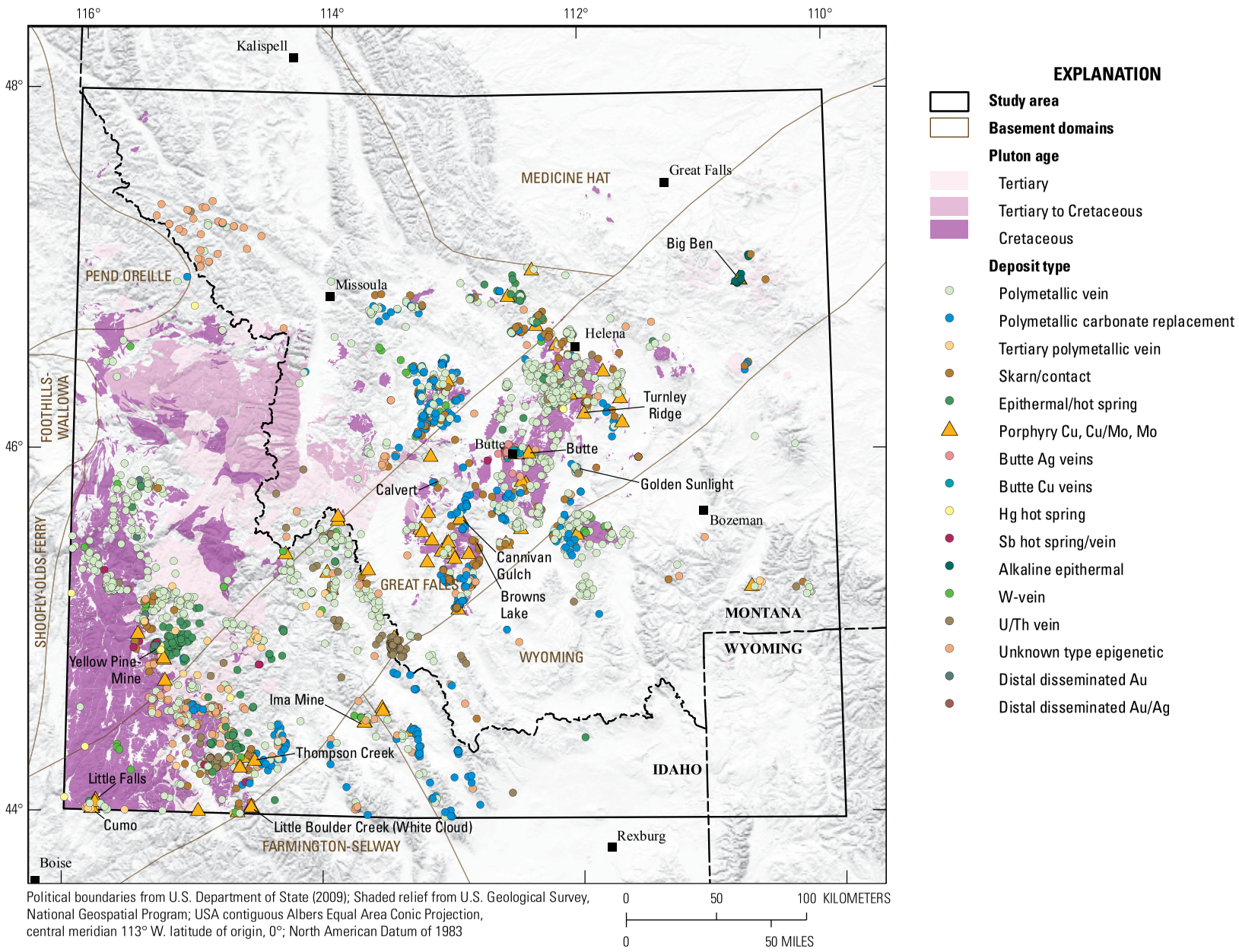


**Figure 9.** Map showing locations of epigenetic mineral deposits in the northern Rocky Mountains tungsten skarn study area. Mineral deposit types and locations are from Klein (2004). Plutons are from the geologic map databases of Zientek and others (2005) and Horton (2017). Basement domain boundaries are from Lund and others (2015). Cu, copper; Mo, molybdenum; Ag, silver; Hg, mercury; Sb, antimony; W, tungsten; U, uranium; Th, thorium; Au, gold.

# Descriptive Models and Orebody Characteristics of Tungsten in the Study Area

Tungsten is associated with many different deposit types and mineralization styles including strata-bound, disseminated, placer, brine or evaporite, granitoid- and porphyry-related quartz-molybdenite-scheelite and wolframite-quartz vein stockworks, skarn, and greisen (Hobbs and Elliott, 1973; Werner and others, 2014). In the North American Cordillera, most tungsten-bearing mineral deposits and prospects are related to Cretaceous or Tertiary granitoid plutons, border phases, or late-stage aplitic phases. The following sections are general descriptions of the tungsten-bearing deposit types pertinent to the study area. The section on tungsten skarn deposits describes the salient characteristics used in our model to delineate permissive tracts in the northern Rocky Mountains study area.

## Tungsten Skarn Deposits

Skarns form by metasomatism of calcareous and argillaceous sedimentary rocks in contact with an intruding igneous body, although they can form in nearly any rock type (Meinert and others, 2005). Skarn is synonymous with the terms tactite, contact-metamorphic, hydrothermal metamorphic, pyrometasomatic, and contact metasomatic (Burt, 1982; Elliott and others, 1992b). Classifications are based on proximity to intrusion-wall rock contacts or composition of the protolith, with endoskarn originating from replacement of the igneous intrusion and exoskarn resulting from replacement of carbonate wall rocks (Meinert and others, 2005). Protolith composition strongly influences skarn mineralogy and permits classification based on the calc-silicate mineral content of altered host rocks, such that calcic skarns comprise iron- and calcium-rich silicates owing to their formation in limestone and magnesian skarns primarily consist of magnesium silicates due to the replacement of dolostone.

Skarn deposits hosting economic concentrations of minerals may also be classified according to their primary metallic commodities of interest—Fe, Au, Cu, Zn-Pb-Ag, Mo, Sn, and W (Meinert, 1992). Metal endowment is influenced by several factors, including composition of the causative intrusion, composition of the wall rock, depth of formation, temperature, and oxidation state. Skarn deposits, including tungsten-rich variants, are reviewed in detail by Einaudi and others (1981), Newberry and Einaudi (1981), Einaudi and Burt (1982), Newberry and Swanson (1986), Kwak (1987), Meinert (1992), and Meinert and others (2005). For the purposes of this assessment, the essential characteristics of tungsten skarn deposits are best described by Cox (1986), Dawson (1995), Hammarstrom and others (1995), and Ray (1995), and are summarized below.

Tungsten-rich skarns contain abundant scheelite ($CaWO_4$) and are hosted in metasomatized pure and impure limestones and calcareous to carbonaceous pelitic rocks near the contacts of intrusive granitoids in broadly arc-related, syn- to late-orogenic environments (Einaudi and others, 1981; Newberry and Einaudi, 1981; Cox, 1986). Tungsten enrichment is strongly influenced by the oxidation state of both sedimentary and intrusive host rocks, with carbonaceous wall rocks hosting higher-grade deposits that exhibit a more reduced suite of metasomatic minerals incorporating ferrous iron, including hedenbergitic pyroxene, almandine garnet, iron-rich biotite, hornblende, and magnetite (Einaudi and others, 1981). Deposits hosted in hematitic or non-carbonaceous rocks typically contain more oxidized gangue mineralogies with an affinity for ferric iron, including low-hedenbergite pyroxene, grossular-andradite garnet, and epidote (Einaudi and others, 1981). The predominance of calcium-bearing gangue minerals in oxidized tungsten skarns lowers the availability of calcium needed to crystallize scheelite, contributing to the low scheelite grades of these deposits when compared to reduced tungsten skarns (Newberry, 1982). Similarly, limestone constitutes a better host rock for tungsten skarns compared to magnesian dolomite, which inhibits the formation of scheelite (Ray, 2013).

The size, morphology, and alteration assemblages of skarn deposits are predominantly controlled by their depth of formation (Meinert and others, 2005). Prominent spatial-alteration zoning reflects the stages of skarn development and distribution of reactive host rocks. Emplacement of the causative pluton into reactive limestone units and interbedded shales produces marble interlayered with calc-silicate reaction skarns and hornfels consisting of fine-grained aluminum-rich garnet, pyroxenes, and wollastonite (Meinert, 1992). Development of the scheelite exoskarn is restricted to a narrow but vertically extensive zone that forms a shell around the pluton, extending from 10s to 100s of meters away into the surrounding host rocks (Meinert, 1992; Dawson, 1995). Endoskarn development is typically minimal in mineralized tungsten deposits. Early contact metamorphic assemblages are overprinted by prograde hydrothermal alteration minerals including hedenbergite-diopside pyroxene, grossularite-andradite-almandine garnet, calcite, dolomite, quartz, vesuvianite, and wollastonite (Dawson, 1995). Prograde alteration is crosscut and overprinted by more hydrous minerals formed at lower temperatures (retrograde conditions), including hornblende, plagioclase, biotite, epidote, sphene, chlorite, actinolite, apatite, sulfides, and scheelite (Meinert and others, 2005). Massive quartz may be present in the interior of the skarn, alongside ore and gangue minerals. Retrograde alteration—typically the most strongly developed assemblage in scheelite-mineralized skarns—occurs as early calcium-rich silicate assemblages are replaced by calcium-depleted silicates, iron oxides, carbonates, and plagioclase accompanied by deposition or recrystallization of scheelite and sulfides (Meinert, 1992; Dawson, 1995).

Tungsten skarn deposits commonly contain variable amounts of Mo, Zn, Cu, Sn, and Bi hosted in subordinate ore minerals molybdenite, sphalerite, chalcopyrite, bornite, cassiterite, bismuthinite, and native bismuth.

Most known tungsten skarn deposits of the North American Cordillera are localized in the thermal aureoles of Cretaceous plutons that have intruded passive margin shelf limestone-pelite assemblages and more reduced slope and basin sequences (Newberry and Einaudi, 1981; Dawson, 1995). The associated plutons are typically coarse grained, porphyritic, metaluminous to peraluminous, calc-alkaline dioritic to granitic rocks and are most commonly granodiorite or quartz monzonite in composition. Following the classification of Chappell and White (1974), tungsten skarn deposits typically form in association with I-type granitoids, but may also be associated with S-type granitoids. Newberry and Swanson (1986) noted that causative plutons of the western United States are typically I-type granitoids, whereas those of the northern Canadian Cordillera are both S-type and I-type. Strontium isotopic signatures suggest variable degrees of crustal contamination in most intrusions, but a correlation between the degree of contamination and the quality of deposits has not been observed (Anderson, 1983; Sawkins, 1984; Newberry and Swanson, 1986). Granitoids associated with tungsten skarns tend to be more contaminated with sedimentary material, more differentiated, and have crystallized at greater depths compared to those associated with copper skarns (Ray, 1995).

Although granites associated with tungsten skarns have relatively low water and tungsten contents, they are thought to be the source of tungsten and hydrothermal fluid required to form the deposits (Newberry and Swanson, 1986). Tungsten is concentrated during the late stages of crystallization of the causative pluton, during which high degrees of fractional crystallization result in exsolution of high-salinity hydrothermal fluids that scavenge metals from the melt (Newberry and Swanson, 1986). In deep plutonic environments with pressures at ~2 kilobars (kbars), 59 percent crystallization is necessary to achieve water saturation in typical granitic magmas. However, fluids exsolved at these conditions will have a salinity of 53.4 weight percent sodium chloride (NaCl) equivalent (Cline and Bodnar, 1991).

These conditions are reflected by the fact that tungsten skarns form at greater depths than other types of skarn deposits, favoring deep environments with pressures exceeding 1 kbar, with most deposits forming at pressures >1.3 kbars (Einaudi and others, 1981; Newberry and Einaudi, 1981; Newberry and Swanson, 1986). Indeed, ore-stage fluid inclusions measured in a number of tungsten skarns show variable carbon dioxide ($CO_2$) contents and range in salinity from approximately 10 to 60 weight percent NaCl equivalent (Roedder, 1984). These ranges reflect the varying degrees of dilution from influxes of meteoric water, volatile loss to the vapor phase during boiling, and the progression of decarbonation reactions that occur during formation of the skarn deposit.

## Porphyry-Type Systems

Tungsten mineralization occurs in a variety of porphyry-type systems that include stockwork tungsten-molybdenum, porphyry molybdenum, vein tin-tungsten deposits, and, to a lesser extent, porphyry copper-molybdenum deposits. “Porphyry tungsten deposit,” has no consistent definition because these types of magmatic systems may form subordinate deposits and different mineralization or alteration types that include skarns, greisens, quartz-tungstate vein stockworks, and crackle breccias. In porphyry systems, the morphology and mineralogy of tungsten occurrences are highly dependent on wall-rock lithologies: tungsten skarns dominate in carbonate rocks, whereas quartz+tungstate±molybdenite vein stockworks are prevalent in more silicic or highly metamorphosed wall-rock (fig. 10). For example, the Logtung deposit in the Yukon Territory, Canada, has been considered a porphyry tungsten-molybdenum deposit with quartz-molybdoscheelite, quartz-pyrite-scheelite, and quartz-molybdenite veins in crackle breccia as the principal ore styles within a broad zone of unmineralized reaction skarns around a polyphase felsic stock (Noble and others, 1984). Quartz-diopside-garnet, biotite-quartzite, and wollastonite-vesuvianite reaction skarn assemblages were derived from thermal metamorphism of calcareous shales and graphitic quartzites by intrusion of an early monzogranite phase. Permeability in the more competent and carbonate-poor calc-silicate wall rocks was created by hydraulic fracturing, producing vein-controlled tungsten-molybdenum mineralization rather than replacement horizons at lithologic contacts (Noble and others, 1984).

Tungsten is a potential byproduct commodity of porphyry molybdenum deposits formed in different tectonic settings with variable magma compositions and degrees of crustal contamination. Deposits are subdivided into three types (Dabie, Endako, and Climax) on the basis of magma composition, gas contents, and tectonic setting. The Dabie-type porphyry molybdenum systems of China host substantial tungsten skarn and greisen deposits associated with unique silica-rich S-type granites generated through continental collision (Mi and others, 2015; Chen and others, 2016; Chen and others, 2017a; Chen and others, 2017b). These types of systems are not considered in this study, because a tectonic event of this nature has not occurred on the North American continent since the middle Paleozoic (Audétat and Li, 2017). However, the potential for tungsten resources in the study area related to both arc-related Endako-type and conventional rift-related Climax-type porphyry molybdenum systems is comparatively high, particularly in areas distal to these types of deposits. Endako- and Climax-type deposits are related to the intrusion of highly evolved calc-alkaline I-type plutons and of high-silica, fluorine-rich rhyolites associated with A-type granites, respectively (Audétat and Li, 2017).

Endako-type or arc-related porphyry molybdenum systems are $CO_2$-rich, fluorine-poor composite intrusions that range in composition from tonalite to granite, and most

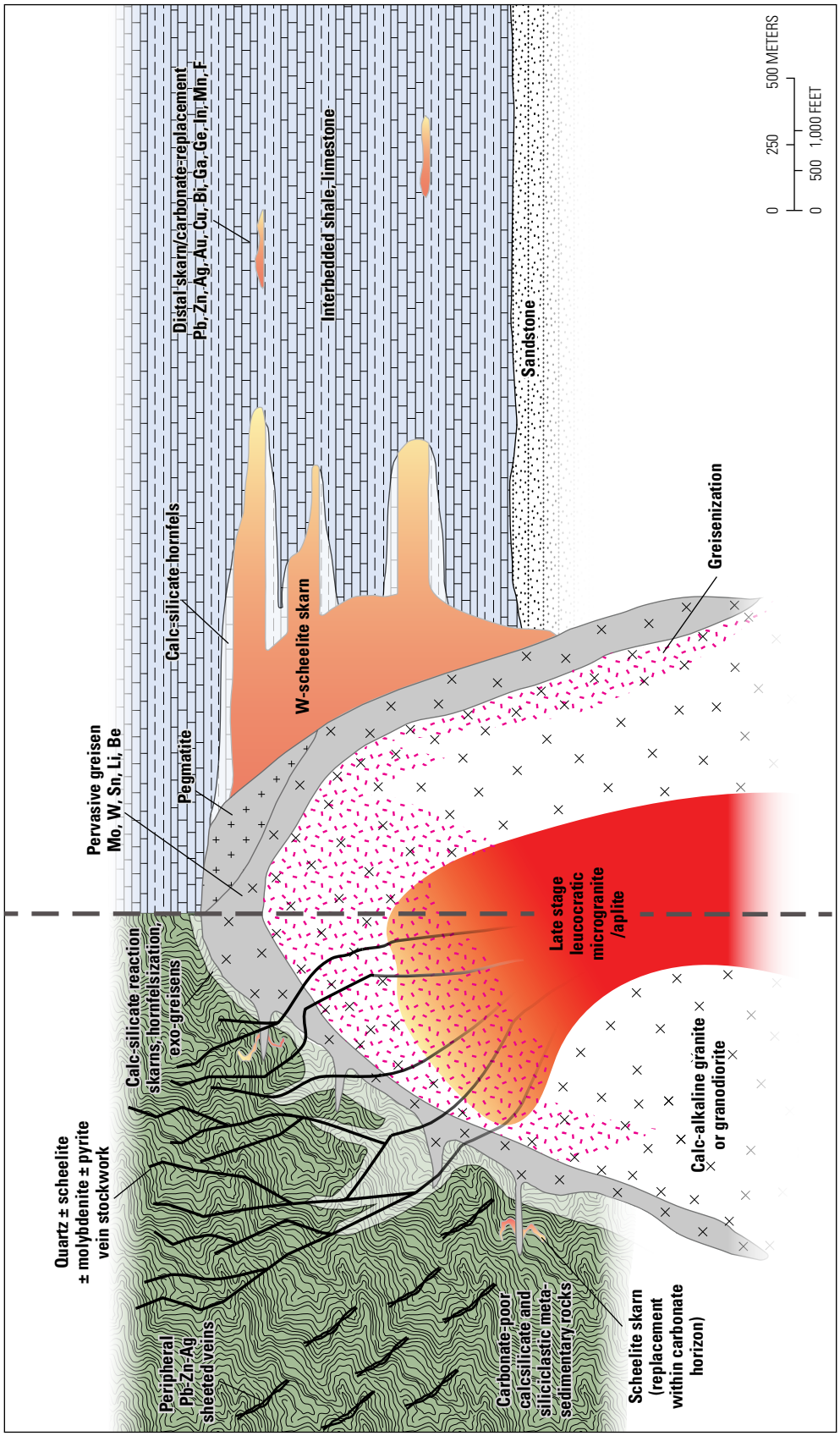


**Figure 10.** Schematic cross section of a calc-alkaline, intrusion-related, tungsten-rich mineralizing system. Left of the vertical dashed line, granitic magma intrudes carbonate-poor metasedimentary rocks, which are partially converted to hornfels and calc-silicate assemblages by early thermal metamorphism. Right of the vertical dashed line, a granitic magma under similar pressure-temperature-composition conditions intrudes a platform carbonate sequence of alternating limestone and calcareous shale. Constructed from elements of figures by Noble and others (1984), Strong (1988), Blevin (1998), Meinert and others (2005), and Mair and others (2006). Ag, silver; Au, gold; Be, beryllium; Bi, bismuth; Cu, copper; F, fluorine; Ga, gallium; Ge, germanium; In, indium; Li, lithium; Mn, manganese; Mo, molybdenum; Pb, lead; Sn, tin; W, tungsten; Zn, zinc.

productive intrusions are classified as granodiorite or quartz monzonite (Westra and Keith, 1981; Taylor and others, 2010). Granitoid-related stockwork molybdenum deposits and prospects of the study area (Thompson Creek, Little Boulder Creek, and Cannivan Gulch) are classified as Endako-type porphyry molybdenum deposits. These deposits host peripheral tungsten skarn mineralization and were emplaced at deeper levels than the classic porphyry copper systems of the southwest United States. Deposit-scale zoning is also observed at the MAX arc-related deposit near Trout Lake in British Columbia, where tungsten-bearing skarns, marginal to molybdenum mineralization, are cut by lead-zinc-silver veins within the contact metamorphic aureole of the Trout Lake stock (Boyle and Leitch, 1983; Lawley and others, 2010; Taylor and others, 2010). Scheelite skarn mineralization associated with these plutons is presumably favored by the deeper level of emplacement, reactive carbonate-rich wall-rock lithologies, and more reducing conditions.

Climax-type molybdenum deposits may be spatially associated with late-stage mafic magmatism in an intraplate rift environment or may form in response to crustal relaxation following continental collision (Audétat and Li, 2017). They occur in shallow polyphase intrusions with distinct but sometimes overlapping orebodies related to separate intrusive pulses accompanied by magmatic-hydrothermal activity. Host rocks have porphyritic textures, and unidirectional solidification textures may be present in the roof zones of causative plutons. Ore mineralization occurs as semispherical cupola-conforming shells that can be divided into three zones outward of the porphyry plug: (1) a molybdenite zone consisting of a stockwork of quartz+molybdenite+fluorite veins, (2) a tungsten zone generally containing hübnerite in quartz+pyrite±molybdenite veins, and (3) a distal pyrite and base metal sulfide zone (Mutschler and others, 1981). Tungsten-rich zones may overlap with molybdenum-rich zones, and ore shells temporally related to specific magmatic phases may be superimposed. Compared to Cretaceous plutons, Tertiary plutons of the study area are more likely to have been emplaced into a post-Laramide extensional regime and are therefore more favorable for Climax-type mineralization. The Big Ben molybdenum deposit in the Little Belt Mountains, Montana, is a sub-economic Climax-type molybdenum system (Olmore, 1991). Significant tungsten (~1,800 metric tons $WO_3$) was produced from hübnerite-quartz veins peripheral to molybdenite mineralization in the Tertiary pluton underlying the Ima Mine in eastern Idaho (Mitchell, 1999; Gentor Resources Inc., 2008).

Alteration zones associated with Climax-type deposits consist of potassic K-feldspar±biotite zones, greisen zones with coarse-grained muscovite+pyrite±topaz, and hydrolytic quartz+sericite+pyrite veins that are common in other types of porphyry deposits (Seedorff and others, 2005). Sericitic and greisen alteration zones may be interrelated in some porphyry molybdenum deposits, as at Turnley Ridge, Montana, where both are related to late-stage quartz-sericite veins (Steefel and Atkinson, 1984). Consequently, it is difficult to draw a clear line separating deep greisen alteration zones encountered in porphyry molybdenum systems and those in vein tin-tungsten systems (discussed in the following "Vein Tin-Tungsten Deposits" section) from more shallow sericitic veins and alteration in less evolved porphyry copper-molybdenum systems (Roedder, 1984), which are commonly referred to as D veins in the porphyry literature (Gustafson and Hunt, 1975; Monecke and others, 2018).

Tungsten±molybdenum±tin greisen-type deposits are an important source of global tungsten and rare metals. Large Paleozoic- to Mesozoic-age deposits occur in Russia, Kazakhstan, China, Canada, and Mongolia; Proterozoic deposits occur in northern and southeastern Europe; and other significant occurrences are reported in Australia, Austria, Argentina, Finland, France, Italy, Norway, Portugal, and Ukraine (Blevin, 1998; Kotlyar and others, 1995). Deposits of this type with significant tonnage are comparatively rare in North America and only occur in the study area as low-grade alteration zones associated with Tertiary plutons. These narrow, cupola-shaped alteration zones and vein stockworks are formed along the periphery of the host pluton via exsolution and discharge of highly saline magmatic-hydrothermal fluids, and consist of quartz, topaz, fluorite, sericite, chlorite, and lithium- and fluorine-bearing micas. Manganese and iron tungstate minerals of the wolframite group (hübnerite and ferberite) or calcium tungstate (scheelite) are the main tungsten-bearing minerals formed; the specific species depending on the calcium content of the surrounding country rocks. Subordinate ore minerals include molybdenite, bismuth, bismuthinite, and cassiterite.

## Vein Tin-Tungsten Deposits

Vein tin-tungsten deposits may contain minor to significant amounts of tungsten as wolframite or scheelite, along with cassiterite and lesser molybdenite, bismuth, and bismuthinite (for example, Panasqueira Mine in Portugal; Polya and others, 2000). Like tungsten skarns, deposits exhibiting these styles of mineralization are associated with highly evolved granitic intrusions and are spatially associated with the apical portion of plutons in the roof zones of batholiths. These highly evolved granitic intrusions include fractionated high potassium calc-alkaline granitoids and I-type ilmenite series granites with intermediate to reduced oxidation states. Alteration and mineralization are typically centered on later stage metaluminous to peraluminous fluorine-rich felsic intrusions. Porphyritic host rocks and unidirectional solidification textures are prevalent in tin-tungsten deposits, similar to Climax-type molybdenum systems. District-scale metal zonation reflects decreasing temperatures away from the parent batholith, with a central core of tungsten-dominant mineralization grading outward into tin- and finally lead-zinc-copper-dominant deposits. This classic zonation pattern is apparent in deposits of the Mole Granite tungsten-tin vein system of the New England batholith in eastern Australia, where wolframite veins and greisen deposits grade outward into cassiterite deposits to sulfide-dominant polymetallic deposits in the surrounding sediments (Schaltegger and others, 2005).

## Other Deposit Types

Although scheelite is a common mineral in calc-silicate skarns, its presence near pluton-carbonate contacts does not necessitate skarn-forming conditions, particularly in the absence of other calc-silicate minerals like garnet and clinopyroxene. For example, the Yellow Pine Mine (historically known as the Bradley Mine) in east-central Idaho was a major domestic producer of tungsten from silicified, scheelite-mineralized irregular ore shoots within heavily fractured granodiorite of the Idaho batholith (U.S. Bureau of Mines, 1945). Thermal metamorphism (113–99 Ma) is indicated by the presence of marble and calc-silicate metasedimentary rocks of Neoproterozoic and early Paleozoic age in nearby roof pendants within the Idaho batholith, Atlanta lobe. However, scheelite mineralization at 57.5 Ma and 47 Ma postdates emplacement of Atlanta lobe granitoids (99–82 Ma) by at least 24.5 million years (Wintzer, 2019). Scheelite ore lacks the garnet and pyroxene typical of skarns and is chiefly fault-controlled rather than controlled by lithological contacts. Scheelite ore is associated with pervasive brecciation and silicification of the host rock. Ore mineralogy of the combined Yellow Pine-Stibnite mining area reflects multiple styles of deposition that shifted with progressive uplift of the region, beginning at 64 Ma with early gold mineralization that predates scheelite mineralization. The area was overprinted at 47 Ma by significant stibnite and epithermal-style gold-silver mineralization (Wintzer, 2019).

Fault-controlled quartz-scheelite vein systems, breccia-fill deposits, and low-grade disseminated scheelite prospects and occurrences near pluton-carbonate contacts are reported throughout much of the study area in Montana and Idaho (Walker, 1960; Walker, 1963; Cookro, 1985; Cookro and others, 1995b). Some of these deposits, prospects, and occurrences have previously been described as tungsten vein and replacement deposits (Elliott and others, 1992a; Cookro and others, 1995b; Klein, 2004). Many of these sites are associated with broad areas of marble and hornfels that represent initial isochemical thermal metamorphism of limestone and pelite. To date, none of these sites have been shown to contain tungsten ore tonnages comparable to the Yellow Pine Mine.

# Exploration History and Significant Tungsten Mineral Sites

The study area has been explored extensively for Au, Ag, Cu, Mo, Pb, Zn, W, and other commodities, with some significant discoveries and major producers including the Butte porphyry copper-molybdenum deposit, Thompson Creek stockwork molybdenum deposit, and Golden Sunlight gold-silver telluride deposit (fig. 9). Records of mineral exploration date back to at least the 1860s. Until World War II, tungsten production in the study area was insignificant. Through the 1930s and 1940s, substantial tungsten production in Idaho came from scheelite ore at the Yellow Pine Mine (also known as the Bradley Mine) and hübnerite at the Ima Mine (U.S. Bureau of Mines, 1945; Bradshaw, 1981; fig. 9). In 1952, exploration for tungsten resources increased because of the Defense Minerals Exploration Administration (DMEA), a government program responsible for issuing contracts and providing financial aid for exploration of critical and strategic minerals. The DMEA focused solely on mineral exploration, while its predecessor, the Defense Minerals Administration (DMA), had been concerned with broader aspects of the minerals industry including minerals supply expansion and allocation of metals and mineral concentrates in short supply (Frank, 2016).

Many of the Montana and Idaho tungsten-bearing mineral sites compiled during this study were discovered or initially developed because of World War II- and 1950s-era exploration. There are 14 DMEA contracts that mention tungsten among 12 sites listed within the study area. Between 1954 and 1957, tungsten production in Montana totaled 2,057 metric tons of $WO_3$, making it the fourth largest tungsten-producing State (U.S. Tungsten Corporation, 2013; 2014). Production dropped rapidly at the termination of the domestic stockpiling program in 1956 and ceased in 1958 with the end of the DMEA, when federally supported mineral exploration under the Defense Production Act of 1950 was no longer considered justifiable (Frank, 2016; U.S. Tungsten Corporation, 2013; 2014).

Interest in mineral properties with tungsten as the principal commodity has been sporadic since the 1950s. In 2012, U.S. Tungsten Corporation acquired exploration rights at and near the Calvert Mine (fig. 9) with intentions of (1) verifying the historical in-place reserves and their potential extension to depth and down plunge to the east and (2) exploring the contact of the Amsden Formation with the Late Cretaceous intrusive rocks for tungsten mineralization long strike (U.S. Tungsten Corporation, 2013; 2014). The Ima Mine, once a major tungsten producer described as a sub-Climax-type porphyry molybdenum system, has recently been a site of interest for its molybdenum potential (Gentor Resources Inc., 2008). In 2007, Gentor Resources acquired rights to explore the Ima Mine property and followed with a diamond drill program. The Yellow Pine-Stibnite mining area is a site of renewed interest for gold and antimony with the development of the Stibnite Gold Project by Perpetua Resources and funding through the U.S. Department of Defense's Defense Production Act Investments Program to ensure the timely development of a domestic source of antimony trisulfide (U.S. Department of Defense, 2022). Remaining tungsten resources there are unknown.

The following sections summarize information about some of the more significant tungsten mineral sites and those that have seen greater historical development efforts or production, their associated plutons, and the mineralogy of these sites throughout the study area. The region is divided into five focus areas of greatest tungsten skarn potential, primarily on the basis of mineral-site density (fig. 11). The focus areas are for illustrative purposes and were not assessed individually in this report.

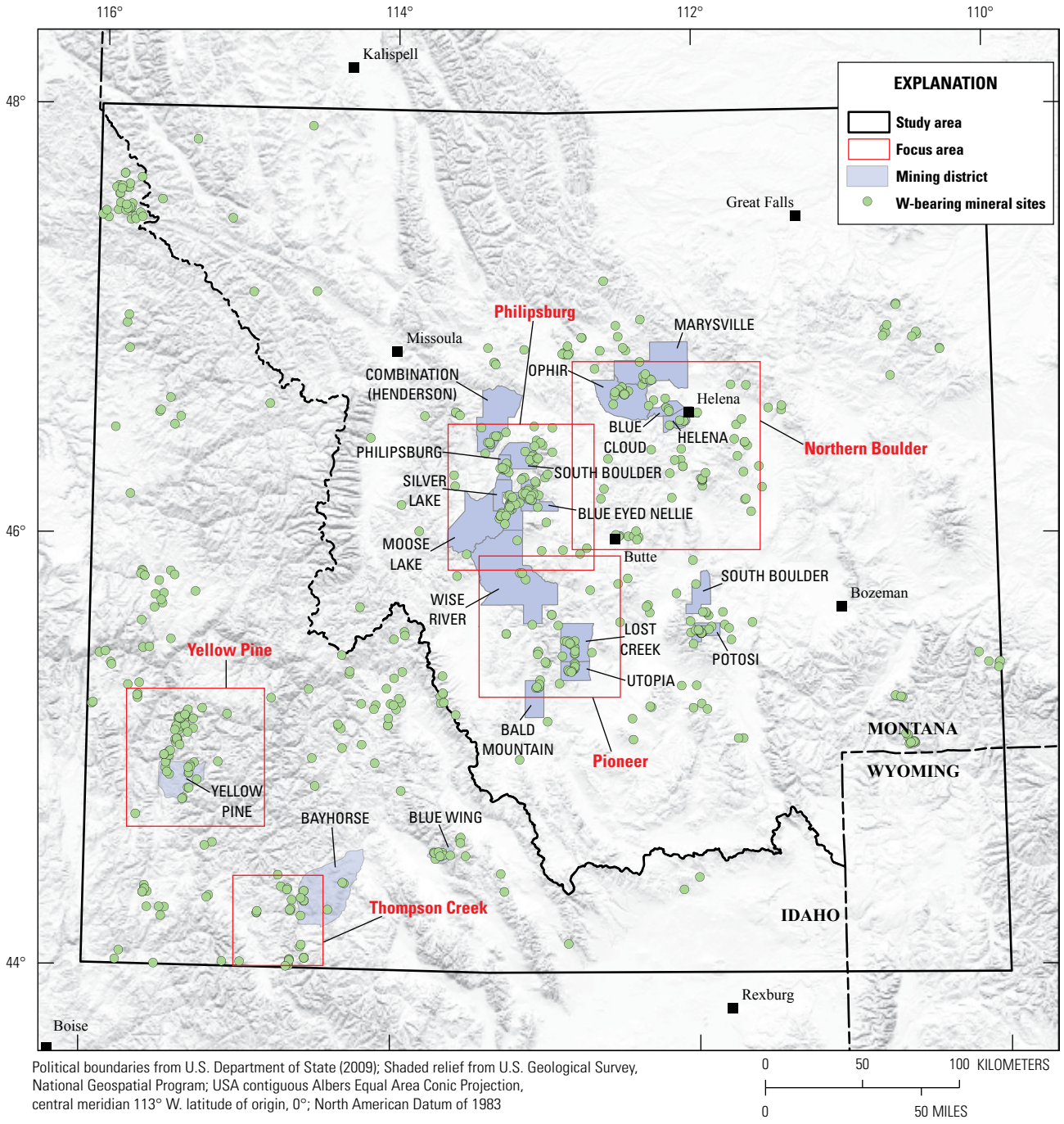


**Figure 11.** Map showing five focus areas, mining districts with historical tungsten exploration or production, and mineral deposits or prospects with some reference to tungsten (W) in the northern Rocky Mountains tungsten skarn study area.

## Pioneer Focus Area

Centered on the Pioneer Mountains in Montana, the Pioneer focus area (figs. 11 and 12) has historically produced the most tungsten from skarn-hosted ores in the study area. Most deposits and prospects occur along the eastern and southern margins of the Pioneer batholith in the Lost Creek, Utopia, and Bald Mountain Mining Districts. Metamorphism of Upper Mississippian and Lower Pennsylvanian carbonate rocks on the east side of the batholith extends 1.6–2.4 km beyond the intrusive contact (Pattee, 1960). Relatively oxidized skarn assemblages consist of andradite, quartz, calcite, with lesser epidote, diopside, hedenbergite, chlorite, tremolite, magnetite, hematite, limonite, copper-zinc-iron sulfides, and tungsten ore minerals, scheelite and powellite (Pattee, 1960).

Two deposits, Browns Lake and Calvert, contain sufficient grade and tonnage to be considered significant deposits in the most recent tungsten skarn global grade-tonnage model (Green

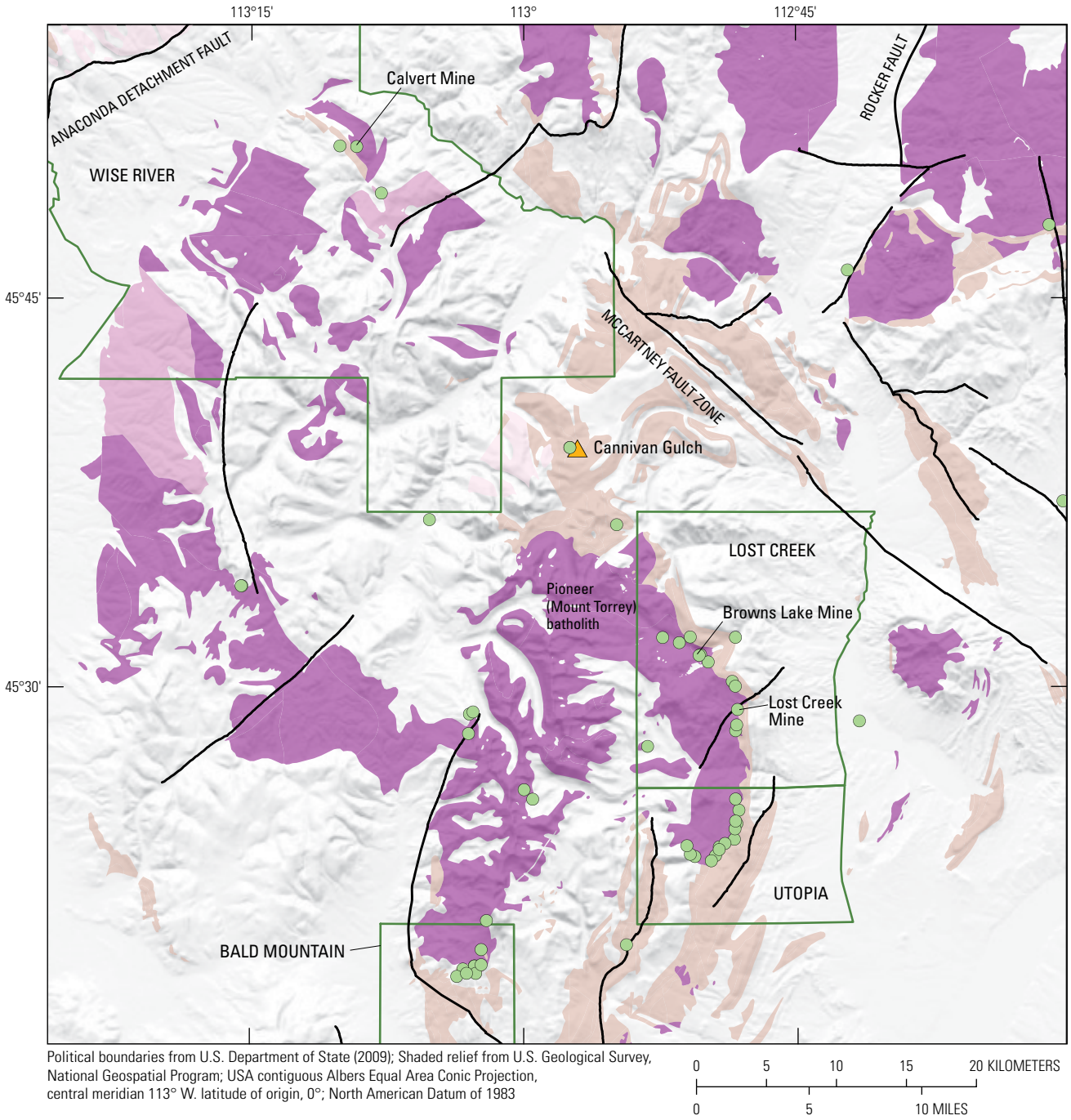


**Figure 12.** Map showing tungsten deposits and prospects, associated plutons, and carbonate strata of the Pioneer focus area in the northern Rocky Mountains tungsten skarn study area. Cu, copper; Mo, molybdenum; W, tungsten.

and others, 2020). A third deposit in the Pioneer focus area, Lost Creek, saw minor production. Historical resource estimates and production data for the Browns Lake and Calvert tungsten deposits are presented in table 1. The Browns Lake Mine (fig. 12) was one of the leading domestic tungsten producers during the mid-1950s. The main ore body was 18.3–24.4 m thick and probably at least 410 m in length. Granodiorite, quartz monzonite, and aplite sills are exposed at the surface, and skarn bodies are roughly conformable with bedding and intercalated with barren marble and scheelite-mineralized hornfels (Pattee, 1960). The main orebody has been referred to as the Ivanhoe tungsten deposit. In the late 1970s and early 1980s, exploration of the surrounding property revealed a marginally economic, moderate-grade resource (referred to as the Lentung resource) of substantial size (table 1).

The Calvert tungsten deposit is located on the northern edge of the Pioneer batholith among Cretaceous tonalite, quartz monzonite, and granite of the Foolhen intrusions that were emplaced into previously folded and faulted sedimentary rocks (figs. 12 and 13). The Foolhen thrust fault juxtaposed older Precambrian paragneiss over a package of younger Mississippian to Cretaceous sedimentary rocks, whose lower contact with quartzites of the Belt Supergroup is the Calvert thrust fault (U.S. Tungsten Corporation, 2013). The open pit of the Calvert Mine is centered on a brecciated contact between the Foolhen granitoids and limestones and mudstones of the Mississippian Amsden Formation. The irregular orebody is approximately 60 m in diameter and plunges to the southeast at 55° (U.S. Tungsten Corporation, 2013). Mined and in-ground ore grades at the Calvert Mine (1.1 percent $WO_3$) are approximately two times those of the Browns Lake Mine and other deposits and prospects along the east side of the Pioneer batholith (table 1).

Scheelite ore at the Calvert tungsten deposit occurs as metasomatic replacement zones in the Amsden Formation with zonation from high-temperature assemblages (red garnet-epidote-pyroxene) at the center of the deposit to lower temperature assemblages (green garnet-epidote-chlorite) near the margins (U.S. Tungsten Corporation, 2013). The presence of cassiterite, wolframite, and beryl within the deposit is indicative of a high-temperature, highly fractionated magmatic-hydrothermal system. Scheelite occurs in both altered and unaltered quartz monzonite and reaches ore grade in some places (U.S. Tungsten Corporation, 2013). The Mississippian Amsden Formation is an exceptional host of skarn-style mineralization in the Pioneer focus area. Contacts between the Amsden Formation and Cretaceous plutons have not been thoroughly explored using modern approaches, and these contacts are permissive for additional tungsten skarn discoveries or expansions from existing deposits and prospects.

**Table 1.** Summary of historical tungsten production and resource estimates for deposits of the Pioneer focus area in the northern Rocky Mountains tungsten skarn study area.

[Tonnage is reported here in metric tons of ore. Grades for total production and sum of production and resources are calculated as a weighted average. The sum of production and resources from known deposits is a maximum estimate because it includes resources not sufficiently delineated and those considered marginally economic or subeconomic. $WO_3$, tungsten trioxide; %, percent]

| Status | Period | Tonnage | $WO_3$ grade (%) | Source |
|---|---|---|---|---|
| Calvert tungsten deposit | | | | |
| Production-mined | 1956–1957 | 84,220 | 1.09 | Aro, 1966; U.S. Tungsten Corporation, 2013 |
| Production-mined | 1960–1962 | 113,400 | 1.10 | Aro, 1966; U.S. Tungsten Corporation, 2013 |
| Historical reserve estimate; 1967 proven, still in ground | 1967 | 116,300 | 1.10 | Ebbley, 1966; U.S. Tungsten Corporation, 2013 |
| **Total production** | **1956–1962** | **197,710** | **1.10** | Aro, 1966; U.S. Tungsten Corporation, 2013 |
| Browns Lake—Ivanhoe tungsten deposit | | | | |
| Production-mined | 1953–1958 | 567,477 | 0.35 | Pattee, 1960; Werner and others, 2014 |
| Production-mined | 1952–1956 | 19,200 | 0.18 | Pattee, 1960; Werner and others, 2014 |
| **Total production** | **1952–1958** | **586,677** | **0.34** | |
| Browns Lake—Lentung tungsten resource | | | | |
| Marginally economic; reliable estimate | 1971–1976; 1986 | 3,175,000 | 0.57 | Werner and others, 2014 |
| Subeconomic; preliminary estimate | 1971–1976; 1986 | 2,268,000 | 0.57 | Werner and others, 2014 |
| **Total historical resource estimate** | **1971–1976; 1986** | **5,443,000** | **0.57** | |
| Sum of production and resources from known deposits | | 6,343,687 | 0.57 | |

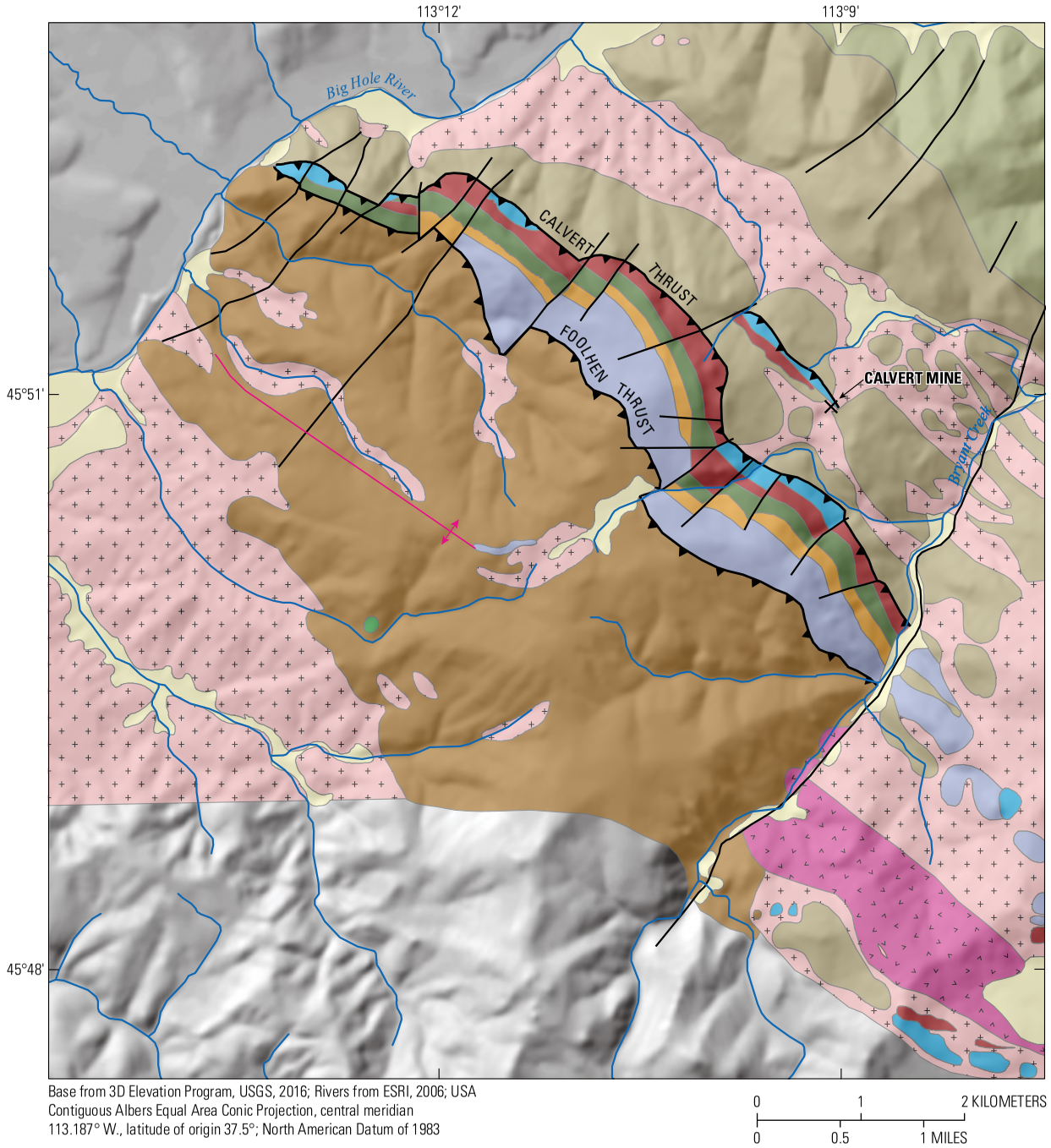


**Figure 13.** Geologic map of the area surrounding the Calvert tungsten deposit in Montana. Reconstructed from Truckle (1988) and U.S. Tungsten Corporation (2013). Scale 1:24,000.

## Philipsburg Focus Area

Tungsten mineralization in the Philipsburg focus area (figs. 11 and 14) formed structurally controlled vein and replacement deposits (in limestones altered to marble) at various distances from Cretaceous and Tertiary plutons. Although many of the sites were at one time classified as skarn, classic garnet-bearing skarns at the carbonate-pluton contacts are developed in only a few places (Walker, 1960). The skarns contain variable amounts of garnet, amphibole, epidote, pyroxene, vesuvianite, calcite, and fine-grained disseminated scheelite (Walker, 1960). Scheelite-mineralized zones are present in the Moose Lake, Silver Lake, and Blue Eyed Nellie Mining Districts south of Philipsburg, Montana, among the Cable, Owens Gulch, and Lost Creek stocks (fig. 14).

Northeast of Philipsburg, Montana, contacts along the southern exposed margin of the Royal stock host several tungsten skarn or scheelite occurrences. The most prominent of these occurrences, Finlay Basin, was discovered by Union Carbide Corporation during exploration drilling in the 1970s (Erickson and others, 1981; Elliott and others, 1992b). The skarn deposit occurs between limestones of the Madison and Snowcrest Range Groups and granodiorite of the Royal stock, and it contains an estimated 850,000 tons at 0.68 percent $WO_3$ (Elliott and others, 1992b). Past tungsten producers in this area include the Pay Day Prospect, Smith Prospect, Sunshine Mine and prospect, and Trigger Mine (sites 6–9; fig. 14), all of which are scheelite-bearing, but may or may not be skarn occurrences. Tungsten skarn sites between the Cable stock and Storm Lake stock occur in Cambrian through Carboniferous units, but principally in the Devonian Jefferson Formation. Most occur in carbonate beds that dip 20°–45° northwest in the eastern limb of a gentle syncline striking northeast (Walker, 1960).

Ore bodies at the Trigger Mine are described as replacement deposits and lenses in limestone of the Jefferson Formation that has been metamorphosed to white marble with scheelite along shear zones and fractures and minor amounts along bedding planes (Walker, 1960). Mineralized zones at the Sunshine Mine and prospect are described as fine-grained scheelite and tetrahedrite in quartz lenses along the N50°–70° E-trending Tarlach Fault. On a broad scale, the "skarn" classification is understandable: scheelite mineralization near carbonate-pluton contacts and associated marble formations. However, much of the mineralization was structurally controlled and lacks the calc-silicate mineralogy typical of skarn deposits. Additional studies could reveal details about the mineralizing processes and whether a "skarn" classification is appropriate for these sites within the Philipsburg focus area.

## Northern Boulder Focus Area

The Northern Boulder focus area (figs. 11 and 15) has produced very little tungsten from scheelite-bearing skarn. Tungsten is found in three major districts: (1) the Marysville Mining District centered on the Marysville stock, (2) the Helena and White Cloud Mining Districts near northern protrusions of the Boulder batholith, and (3) the Ophir Mining District centered on the Blackfoot City stock (fig. 15). In the Marysville District, quartz diorite intrudes limestones and shales of the Belt Supergroup which have been converted to hornfels within ~3.2 km of the stock (Walker, 1963). Scheelite is mainly confined to lenticular skarns that consist of garnet, epidote, quartz, actinolite, and lesser chalcopyrite and pyrite.

Tungsten mineral sites in the Helena Mining District occur near the northern margin of the Unionville Granodiorite, whereas sites in the White Cloud Mining District occur along the eastern margin of an intrusive outlier of similar age and granodiorite composition (McDonald and others, 2020; fig. 15). Sedimentary rocks ranging from Mesoproterozoic through Cretaceous were uplifted by the granodiorite dome, and skarn mineralization reportedly occurred near granodiorite- and monzonite-limestone contacts (Walker, 1963). The pluton is in intrusive contact with rocks of the Mississippian Madison Group and Devonian Jefferson Formation, with Cambrian to Devonian limestone and shale and rocks of the Belt Supergroup located farther from the contact (McDonald and others, 2020). Only minor tungsten has been reported at sites described as skarn, vein and replacement, wolframite-quartz veins, disseminated scheelite, and placer occurrences (Walker, 1963).

The Spring Hill Gold Mine is located along a contact between granodiorite and limestone of the Madison Group. Gold is hosted by endoskarn, which consists of tremolite and (or) actinolite, augite, calcite, quartz, epidote, zoisite, chlorite, phlogopite, scapolite, serpentine, monticellite, apatite, titanite, and sulfides. Associated exoskarn consists of calcite, diopside, dolomite, and garnet (Jones, 1934; Elliott and others, 1992b). The Helena Mining District and surrounding area has also produced significant gold from early placer mining in the numerous gulches, some of which also contained scheelite (Pardee and Schrader, 1933; Walker, 1963). Several skarn mineral sites occur at quartz monzonite-limestone contacts around the Blackfoot City stock (fig. 15). The Boulder Ores prospects (Snowshoe-Arnold, Flagstaff, and Strategic sites) include skarn bodies as much as 213 m in length and ~55 m wide, which consist of garnet, epidote, quartz, calcite, scheelite, magnetite, and chalcopyrite (Walker, 1963).

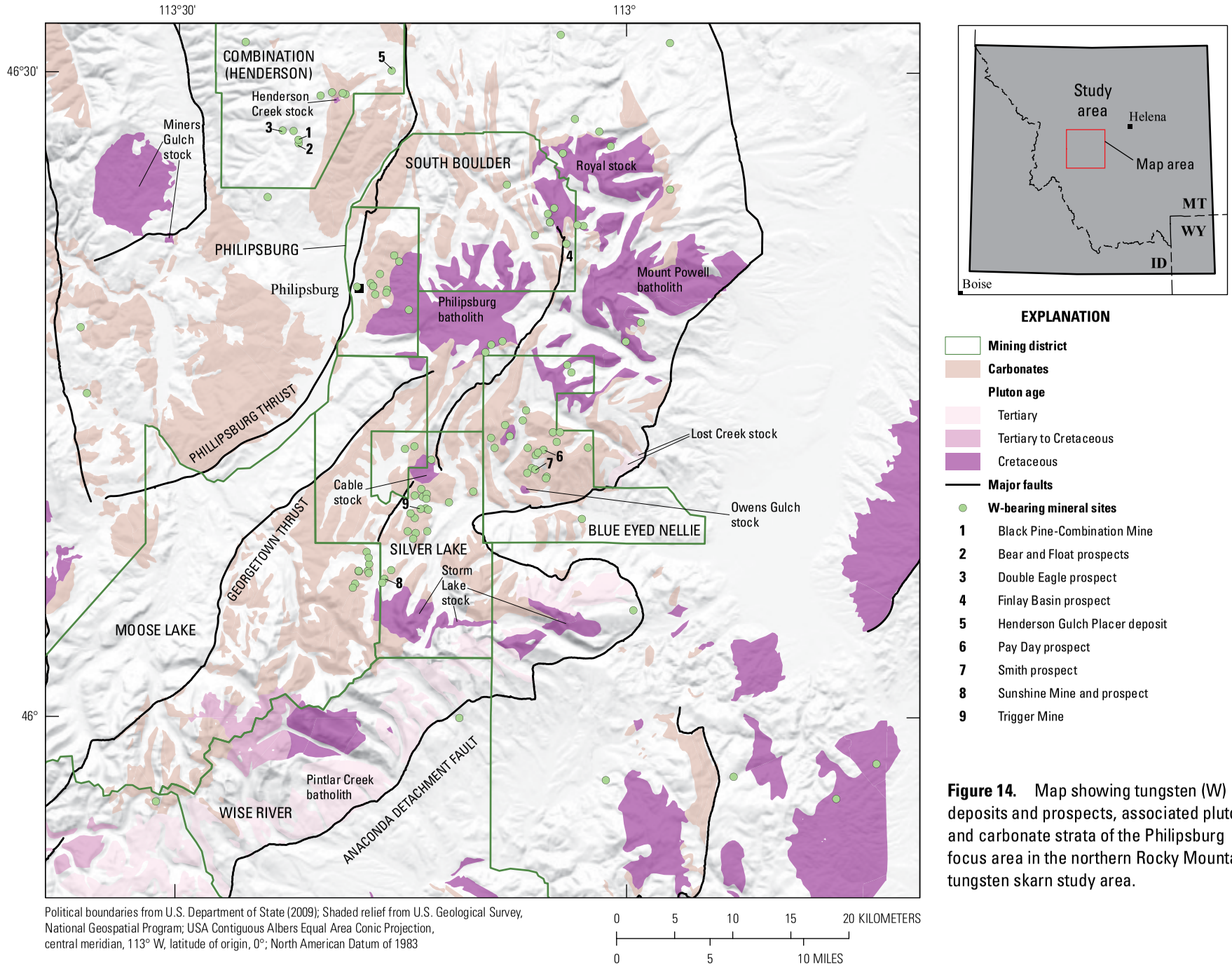


Political boundaries from U.S. Department of State (2009); Shaded relief from U.S. Geological Survey, National Geospatial Program; USA Contiguous Albers Equal Area Conic Projection, central meridian, 113° W, latitude of origin, 0°; North American Datum of 1983

**Figure 14.** Map showing tungsten (W) deposits and prospects, associated plutons, and carbonate strata of the Philipsburg focus area in the northern Rocky Mountains tungsten skarn study area.

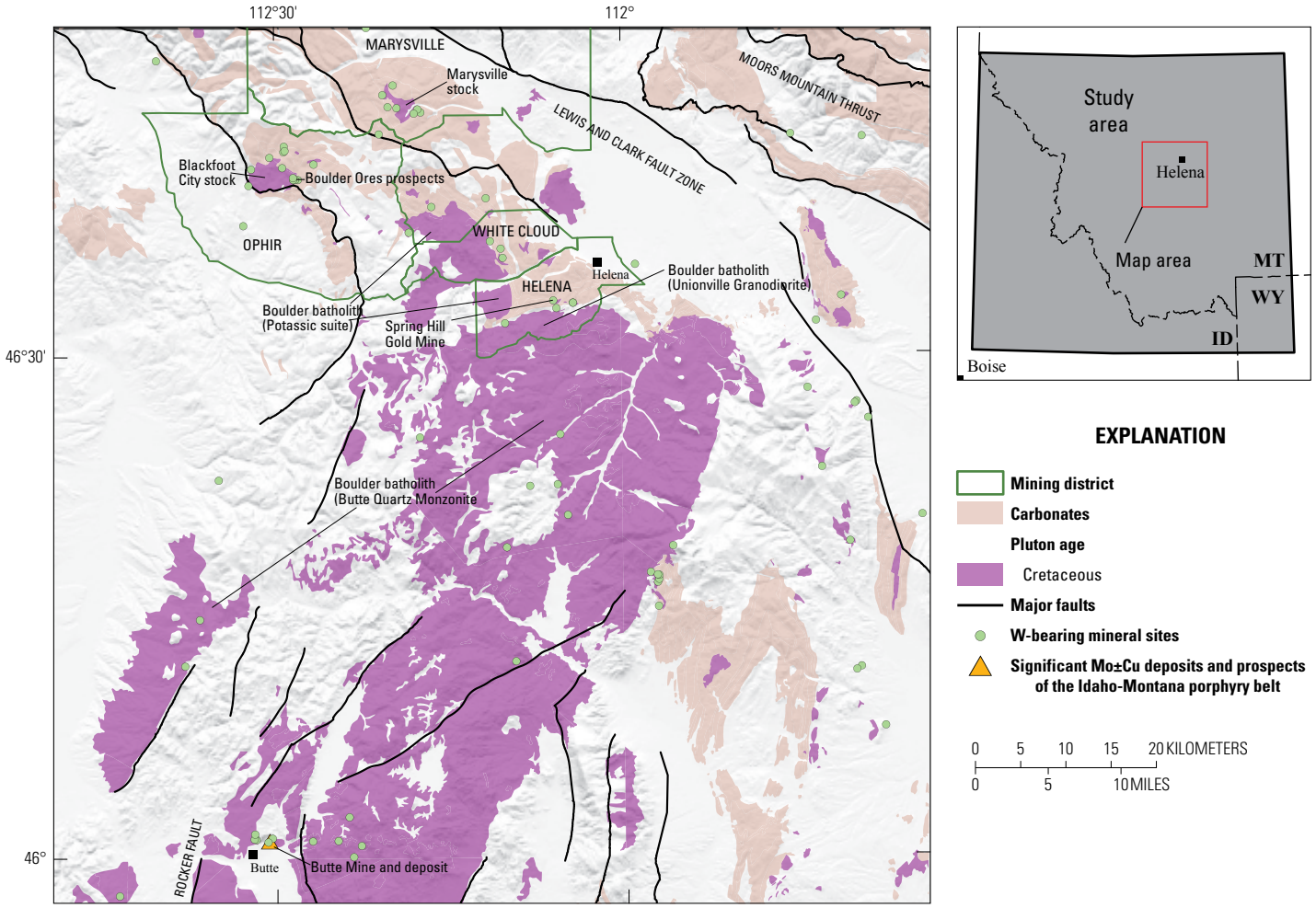


Political boundaries from U.S. Department of State (2009); Shaded relief from U.S. Geological Survey, National Geospatial Program; USA Contiguous Albers Equal Area Conic Projection, central meridian, 113° W, latitude of origin, 0°; North American Datum of 1983

**Figure 15.** Map showing tungsten deposits and prospects, associated plutons, and carbonate strata of the Northern Boulder focus area in the northern Rocky Mountains tungsten skarn study area. Cu, copper; Mo, molybdenum; W, tungsten.

## Yellow Pine Focus Area

The Yellow Pine Mine was the largest past producer of tungsten within the Yellow Pine focus area, having produced 7,694 metric tons of $WO_3$; 38,241 metric tons of antimony; 310,237 ounces of gold; and 1,741,524 ounces of silver between 1932 and 1957 (Vitz, 1964). During World War II, the Yellow Pine Mine was the chief producer of both tungsten and antimony in the United States, and the tungsten orebody was largely exhausted by 1945.

Scheelite in the Yellow Pine Mine area occurs in breccia-fill or tungsten vein and replacement bodies (Cookro, 1985; Cookro and others, 1995b). Mineralization was localized along major north- to northeast-trending shear zones that include the Meadow Creek and West End Faults (Jayne, 1984; fig. 16), with the primary deposits (Yellow Pine and Meadow Creek Mines) located along the Meadow Creek Fault. Pervasive silicification and scheelite-mineralized fault breccias are concentrated in dilational zones created by local intersecting N. 30°–60° E. faults (Cookro and others, 1995b). Along the structures, scheelite occurs within fissure-filling quartz veins and breccias with quartz+scheelite+calcite matrix and associated silicification and sericitization. According to Cookro (1985) and Cookro and others (1995b), calcite was remobilized from large inclusions of Neoproterozoic and early Paleozoic metasedimentary rocks within granitic rocks of the Idaho batholith forming veins and broken blocks in the breccias. Scheelite replaced this remobilized or recrystallized calcite. Most of the mineralization was confined to sheared quartz monzonite or granodiorite, as opposed to skarn deposits, in which most of the scheelite occurs in exoskarn and adjacent carbonates. The Golden Gate prospect hosts similar quartz+scheelite matrix breccias in dilational zones along the N. 10° E. trending Johnson Creek shear zone (Galli, 1964; fig. 16).

The Stibnite and Missouri Ridge-Sugar Mountain roof pendants are the two major blocks of Neoproterozoic and early Paleozoic carbonate-bearing metasedimentary rocks within the Yellow Pine focus area (Stewart and others, 2016; fig. 16). The blocks consist of mixed calc-silicate rock, dolomitic marble,

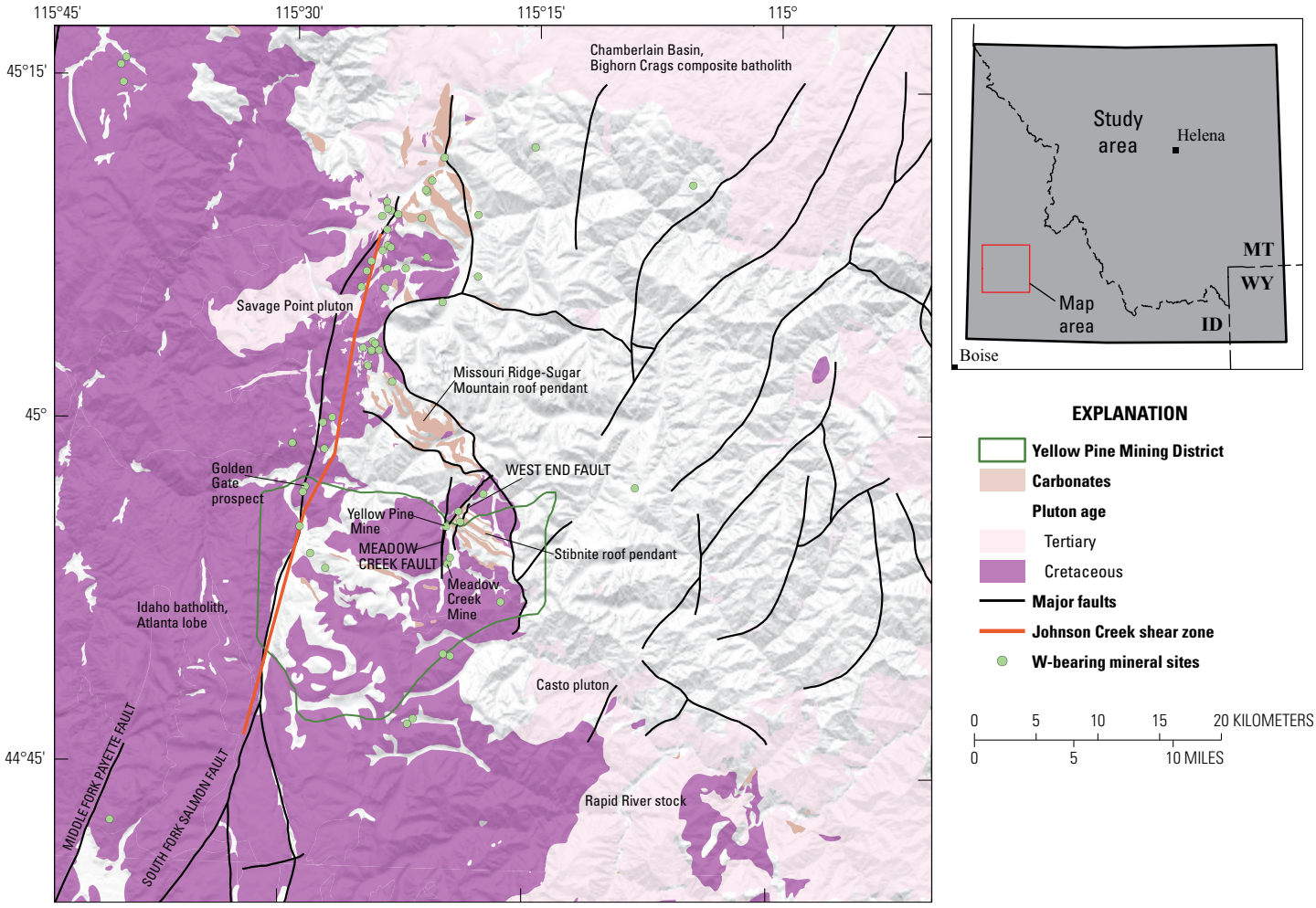


Political boundaries from U.S. Department of State (2009); Shaded relief from U.S. Geological Survey, National Geospatial Program; USA Contiguous Albers Equal Area Conic Projection, central meridian, 113° W, latitude of origin, 0°; North American Datum of 1983

**Figure 16.** Map showing tungsten (W) deposits and prospects, associated plutons, and carbonate strata of the Yellow Pine focus area in the northern Rocky Mountains tungsten skarn study area.

quartzite, schist, and phyllite. This sequence is more favorable for scheelite-bearing skarn than the dominantly siliciclastic metasedimentary rocks of the Belt Supergroup. Small areas of skarn mineralization are noted within the calc-silicate roof pendants. These types of barren, iron-poor calc-silicates and bleached, impure marbles are characteristic of tungsten skarn districts (Einaudi and others, 1981), although formation of skarns in the Yellow Pine Mine area likely preceded scheelite mineralization by ≥ 20 million years (see "Other Deposit Types" section). The juxtaposition of carbonate units, known scheelite-mineralized granitoids, and areas of skarn-style mineralization make the Yellow Pine area permissive for tungsten skarns despite most past production coming from younger Eocene non-skarn scheelite ore at the Yellow Pine Mine.

## Thompson Creek Focus Area

The most significant past tungsten producer of the Thompson Creek focus area (figs. 11 and 17) is the Tungsten Jim Mine (also known as the Salmon River Scheelite Mine or Thompson Creek Tungsten Mine). Between 1954 and 1980, the Tungsten Jim Mine produced 20,936 metrics tons of ore with a production grade of 0.84 percent $WO_3$. Studies from the 1960s report reserves of 61,000 to 72,000 tons at 1.72–1.80 percent $WO_3$ (Larson and others, 1971; U.S. Bureau of Mines, 1960). An estimate of 189,000 metric tons at 0.93 percent $WO_3$, reported by Benjamin (1981), is more conservative in terms of grade and consistent with the past production grade.

Tungsten-bearing skarns of this area are medium to coarse grained; granoblastic; and slightly foliated with associated Mo, Zn, Pb, Cu, Bi, and As geochemical anomalies (Cookro, 1985; Cookro and others, 1987; Cookro and others, 1995a). Minerals include diopside-hedenbergite, plagioclase, quartz, potassium feldspar, biotite, titanite, calcite, garnet, wollastonite, chlorite, epidote, vesuvianite, sericite, scheelite, magnetite, ilmenite, and sulfides. Scheelite is the primary ore mineral, although significant ferberite is reported in ore from the Tungsten Jim Mine. Cook (1956) describes skarn formation along discordant solution channelways, replacing both argillite and limestone and additional bedding

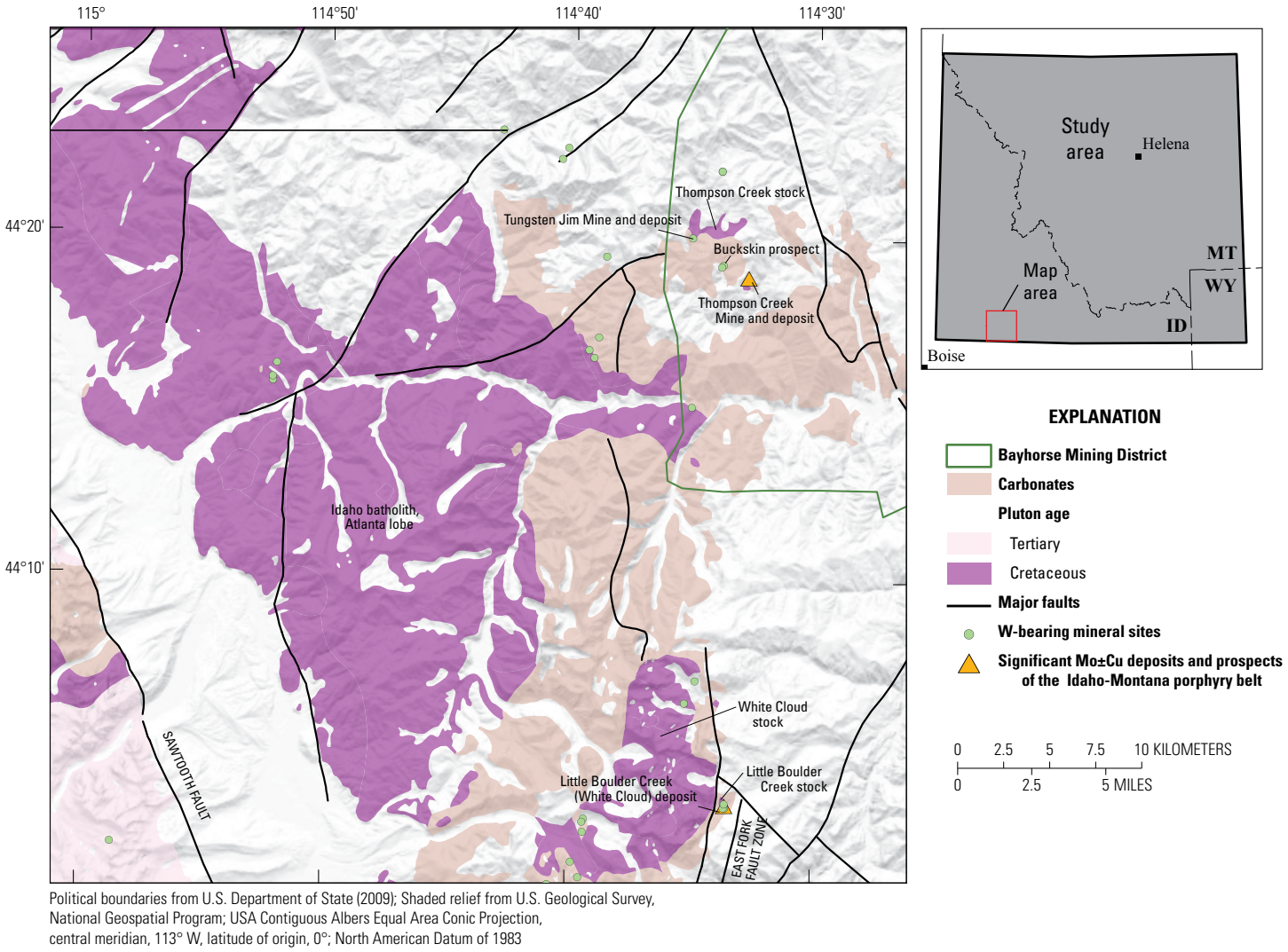


Political boundaries from U.S. Department of State (2009); Shaded relief from U.S. Geological Survey, National Geospatial Program; USA Contiguous Albers Equal Area Conic Projection, central meridian, 113° W, latitude of origin, 0°; North American Datum of 1983

**Figure 17.** Map showing tungsten deposits and prospects, associated plutons, and carbonate strata of the Thompson Creek focus area in the northern Rocky Mountains tungsten skarn study area. Cu, copper; Mo, molybdenum; W, tungsten.

plane-controlled mineralization due to chemical favorability and differential permeability. Unlike the oxidized skarn deposits of the Pioneer focus area, the Tungsten Jim Mine site consists of a reduced skarn, which may be partly related to the relatively reduced, carbonaceous argillite host rocks.

Similar styles of mineralization were described at the Buckskin prospect, which was considered by Union Carbide Corporation to be the best skarn-hosted tungsten prospect of the area, after the Tungsten Jim Mine (J.S. Hollingsworth, Union Carbide, written commun., 1983). The prospect is now buried under the Buckskin waste rock dump of the Thompson Creek Mine to the southeast (U.S. Environmental Protection Agency, 1992).

## Regional Non-Skarn Tungsten Resources

The 12-quadrangle study area includes 561 tungsten-bearing sites (89 percent of total tungsten sites) that are not skarn or cannot be classified as such based on available data. Many of these sites contain scheelite in veins or replacement bodies; they may very well be skarns, but do not have descriptions of calc-silicate mineral assemblages that are characteristic of skarn deposits. Other tungsten-bearing sites include quartz-tungstate stockwork veins related to: (1) existing structures acting as fluid pathways; (2) hydrofracturing facilitated by shallower levels of magma emplacement; (3) more well-indurated, competent, and carbonate-poor wall-rock lithologies; or combinations of these factors. Sites described as wolframite-quartz vein stockworks compose a substantial proportion of non-skarn sites, and some were past tungsten and silver producers. Three are discussed below: the Combination (Henderson) Mining District, the Potosi Mining District, and the Ima Mine (figs. 9, 14, and 18).

The Combination Mining District, located approximately 15 km northwest of the Philipsburg batholith, includes 10 tungsten-bearing sites located along a NE–SW corridor between the Henderson Creek and Miners Gulch stocks (fig. 14). Occurrences are predominantly wolframite-quartz

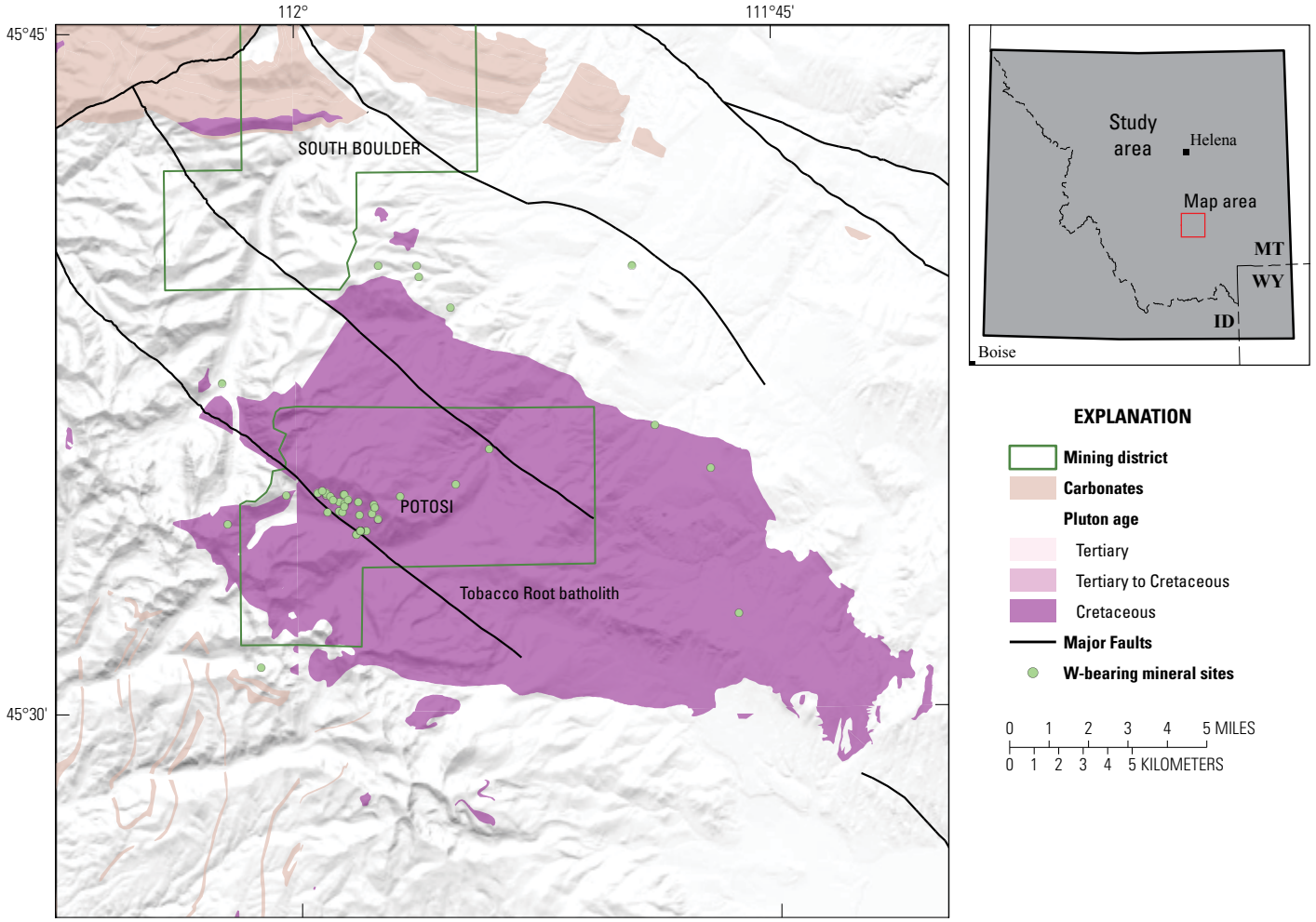


**Figure 18.** Map showing tungsten (W) prospects, associated plutons of the Tobacco Root batholith, and carbonate strata in the the Potosi Mining District, Montana.

veins with lesser scheelite-skarn within the Mesoproterozoic Helena, Mount Shields, Spokane, and Newland Formations of the Belt Supergroup. A greater siliciclastic component and metamorphism of the Belt Supergroup in this region may have imparted some control on the style of tungsten mineralization, which is skarn or scheelite vein and replacement elsewhere in the Philipsburg focus area. The Black Pine-Combination Mine, Bear and Float prospects, and Double Eagle prospect (sites 1–3; fig. 14) contain fissure veins composed of quartz, hübnerite, tetrahedrite-tennantite, pyrite, and galena in quartzite of the Spokane Formation (Walker, 1960). The Black Pine Mine produced more than 2.3 million ounces of silver, mainly prior to 1900, and saw some tungsten exploration by the U.S. Bureau of Mines which disclosed a large-tonnage, submarginal hübnerite resource (Volin and others, 1952; Walker, 1960).

Mining at the Henderson Gulch placer deposit, just 5 km northeast of the Black Pine-Combination Mine, produced gold and tungsten periodically from its discovery in 1866 until about 1950. Scheelite is the principle tungsten mineral in the placer and also occurs within granodiorite of the Henderson Creek stock and in the adjacent impure limestones, argillites, and calcareous shales of the Newland Formation (Walker, 1960). The source of placer scheelite is unknown but could be related to unrecognized tungsten- and gold-bearing skarns.

The Potosi Mining District, located in the Late Cretaceous Tobacco Root batholith (fig. 18), includes several historic claim blocks, prospect pits, and shallow shafts centered on groupings of tungsten- and silver-bearing quartz veins. Quartz veins from subdecimeter to 4.5 m in width and as much as 90 m in length occur in quartz monzonite, leucogranite, or aplite throughout an approximately 0.8×1.6 km area with a vertical extent of more than 550 m (Walker, 1963). The veins contain irregularly distributed bands of hübnerite with lesser tetrahedrite, galena, chalcopyrite, molybdenite, pyrite, anglesite, fluorite, feldspar, rhodocrosite (Eyde, 1958). Alteration minerals include sericite, kaolinite, tungstite, miargyrite or pyrargyrite,

chlorargyrite, pyrolusite, and copper carbonates. Average grades of samples are ~0.5 percent $WO_3$ with maximum values around 3.5 percent $WO_3$ (Walker, 1963). Silver and tungsten ores were recovered and milled in the late 1800s and early 1900s, but the narrow veins had low spatial density and inconsistent metal content, which kept the Potosi Mining District from being developed further.

The Ima Mine is one of the most significant past tungsten producers in the United States and is associated with a shallow biotite quartz monzonite intrusion approximately 73 km east-northeast of the Thompson Creek molybdenum deposit in the Blue Wing Mining District (figs. 9 and 11), beyond the eastern margin of the Idaho batholith, Atlanta lobe. The Eocene monzonite stock intrudes the thrusted and folded Mesoproterozoic quartzites of the Big Creek, the siltites of the Apple Creek, and the youngest quartzites of the Gunsight Formations of the Lemhi Group on the west flank of the Lemhi Range (Mitchell, 1999; Gentor Resources Inc., 2008). The property has recently been described as a sub-Climax-type molybdenum porphyry system with a peripheral quartz-hübnerite vein stockwork and greisen system (Gentor Resources Inc., 2008). Features characterstic of Climax-type deposits found at the Ima Mine site include (1) tungsten- and manganese-enriched zones with elevated Cu, Pb, Zn, and Ag peripheral to the main Mo ore zones; (2) abundant fluorite; (3) aplitic dikes emanating from the main cupola; and (4) high molybdenum:copper grades within the intrusion. Molybdenite, chalcopyrite, pyrite, scheelite, fluorite, and apatite are disseminated in potassically altered parts of the intrusion and molybdenite also occurs in coarse veins containing quartz, orthoclase, muscovite, chalcopyrite, and pyrite near monzonite-quartzite contacts (Bradshaw, 1981; Gentor Resources Inc., 2008). Bradshaw (1981) describes an early molybdenum-stage, transitional molybdenum/tungsten-stage, and later tungsten-stage, in which hübnerite to molybdenite ratios generally increased outward from potassically altered stock.

Silver in tetrahedrite was recovered from the stockwork veins in the early 1900s, and most commercial tungsten production occurred between 1931 and 1958. Until its closure in 1958, 655,352 metric tons of ore were recovered at Ima, and this ore produced 2,351 metric tons of $WO_3$ and 20,607 metric tons of sulfide concentrate that contained unknown quantities of Mo, Ag, Cu, Zn, Pb, and Au (Gentor Resources Inc., 2008). Historical resource estimates for exisiting mine workings prepared by the Inspiration Development Company in 1980 include 312,616 metric tons of ore grading 0.53 percent $WO_3$, 0.043 percent molybdenum disulfide ($MoS_2$), 2.26 ounces per ton silver, 0.16 percent copper, 0.31 percent lead, and 0.23 percent zinc (Gentor Resources Inc., 2008). Tungsten resources contained within mine tailings were estimated to be 140,000 tons grading 0.171 percent $WO_3$ in the upper tailings and 280,000 tons grading 0.09 percent $WO_3$ in the lower tailings (Gentor Resources Inc., 2008).

# Assessment Data and Tract Delineation

The reviews of deposit models, geologic settings, and known mineral sites in the preceding sections of this report demonstrate that skarn-type deposits have the potential to be primary tungsten producers in the study area. Subsequent sections of this report focus on the quantitative assessment of undiscovered tungsten skarn deposits using a three-part assessment form (Singer and Menzie, 2010). Adopting this methodology, we generated a map of mineral potential based on various geologic criteria. For areas with elevated mineral potential, estimates of the number of undiscovered deposits were made by a panel of geoscientists. Deposit estimates, together with the global grade and tonnage model for tungsten skarn, were used as inputs to a Monte Carlo simulation and an economic filter to forecast (1) how much undiscovered metal may be present and (2) how much of that may be economic. Areas with lower mineral potential or with insufficient data for a quantitative assessment are discussed qualitatively.

Models that describe the geologic setting, formation, and orebody characteristics of tungsten skarn deposits (see the "Tungsten Skarn Deposits" section) present mappable criteria that can be used to identify areas of greatest tungsten mineral potential. The key mappable feature of tungsten skarns in the North American Cordillera is their occurrence in the thermal aureole of Mesozoic plutons where they have intruded Paleozoic shelf carbonate-pelite sequences (Dawson, 1995). Because the degree of fractionation, composition, water content, and oxidation state are known to be important controls on metal endowment in the source plutons, the following attributes can be used to identify plutons that are most favorable for associated tungsten skarn mineralization: (1) rock classification (for example, quartz monzonite, granodiorite, granite), (2) varietal accessory mineralogy (muscovite, muscovite-biotite, biotite, biotite-hornblende), (3) rock chemistry (indices of alkalinity, aluminum saturation, modified alkali-lime, and iron), (4) age (Cretaceous and Tertiary), (5) potassium-thorium-uranium enrichment as indicated by airborne radiometric surveys, and (6) relative ilmenite and magnetite contents indicated by magnetic surveys.

Tungsten skarns form at (or near) the contact between intruding magmas of calc-alkaline affinity and reactive carbonate or intercalated carbonate-pelite host rock, and some lithologies may be more favorable hosts than others. In the study area, skarn formation is favored in limestones relative to dolostones and in rocks that are only weakly metamorphosed with higher porosity at the time of formation. Existing geologic maps (see the "Geologic Maps" section) were imported into ArcGIS 10.7 (Esri, Redlands, CA) and used to map the pluton-carbonate contacts. Permissive host rocks were identified using the following mappable criteria: (1) lithology (carbonate or calcareous sedimentary rock), (2) age (Jurassic and older), and (3) proximity to pluton of appropriate criteria (within 2 km of contact).

Additional datasets were used to generate or modify permissive tracts. Mineral site locations are an important factor in the delineation of permissive tracts because they show where the mineralized skarn-forming process has taken place, independent from model predictions. Crustal architecture can affect the ascension of metal-bearing magmas and ancient crustal terranes may contribute to metal endowment. We therefore considered the proximity of tungsten skarn sites and their causative plutons to deep crustal structures, specific Archean and Paleoproterozoic terrane boundaries, and Paleoproterozoic terranes that were possibly more susceptible to partial melting (Foster and others, 2006). Geophysical surveys (magnetic and gravity) can help to map the extent of plutons under cover and were used to modify tract boundaries in some locations. Finally, although they cannot be considered diagnostic of a specific tungsten mineralization style or deposit type, stream-sediment anomalies indicate if tungsten occurrences are present upgradient, in domains identified using criteria other than geophysical surveys, tungsten skarn proximity, and crustal architecture. The following sections describe the datasets used for delineation of permissive tracts, the tract delineation procedure, and other datasets reviewed in support of tract area design.

## Geologic Maps

Data from all sources were combined in a single GIS database. Two principal digital geologic map sources were used: (1) the "State Geologic Map Compilation (SGMC) geodatabase of the conterminous United States" (ver. 1.1, Horton, 2017), which represents a seamless spatial database of geologic maps across state boundaries ranging from 1:50,000 to 1:1,000,000 in scale, and (2) "Spatial databases for the geology of the Northern Rocky Mountains—Idaho, Montana, and Washington" (Zientek and others, 2005), which provides a regionally consistent and integrated geologic spatial database for these areas combining forty-three 1:100,000–1:250,000-scale maps with added attribute information on igneous rock composition, classification, and age. Regional geologic maps in Hyndman (1983) and Gaschnig and others (2010; 2011) and state geologic maps of Idaho (Lewis and others, 2012) and Montana (Vuke and others, 2007) were used to evaluate Cretaceous and Tertiary pluton chemistry. Several maps from reports by the U.S. Bureau of Mines (Pattee, 1960; Walker, 1960; Walker, 1963) and Montana Bureau of Mines and Geology (Eyde, 1958; Roby and others, 1960) were georeferenced to confirm mineral-site locations in historic claim blocks and mining districts. Major tectonic domains, including Great Falls, were added from the "Basement domain map of the conterminous United States and Alaska" (Lund and others, 2015). Important data packages including mineral resource datasets, the National Uranium Resource Evaluation (NURE) stream sediment geochemistry dataset, and a national compilation of airborne radiometric survey data collected under the NURE program were used in the GIS and are discussed in greater detail in the following sections.

Geologic map units and lithologic descriptions were obtained from the Zientek and others (2005) and Horton (2017) compilations. The Northern Rocky Mountains compilation of Zientek and others (2005) includes geologic maps at the 1:100,000–1:250,000 scales; the Montana map included in the SGMC (Horton, 2017) is at the 1:500,000 scale (Ludington and others, 2007; Stoeser and others, 2007). Throughout this report, the Northern Rocky Mountains map data of Zientek and others (2005) was used within the extent of this dataset, and the SGMC of Horton (2017) was only used to fill gaps in coverage of the Northern Rocky Mountains compilation: namely, the northeast and southeast corners of the study area.

## Permissive Lithologies

### Plutonic Rocks

Source plutons favorable for tungsten skarn resources in the North American Cordillera have the following characteristics: (1) Cretaceous pre- and syn-Laramide, (2) mesozonal (deeper than rhyolite porphyries that host Climax-type molybdenum deposits or wolframite-quartz stockworks), and (3) calc-alkaline composition, typically coarse-grained porphyritic granodiorite to quartz monzonite (Einaudi and others, 1981). Tungsten mineral sites are concentrated near the margins of specific plutons with the above characteristics. For example, 17 tungsten-mineralized skarn sites (out of 27 total sites) occur within 2 km of the eastern margin of the Pioneer batholith (fig. 12), which consists of one major intrusive phase; the Uphill Creek Granodiorite; and smaller plutons of melanogabbro, tonalite, quartz monzonite, and granite (Foster and others, 2012, and references therein). Metaluminous hornblende-biotite quartz diorite and granodiorite of the main intrusive phase is cut by younger Cretaceous to Paleocene two-mica leucogranites. Although a significant part of the batholith's eastern margin is dominated by granodiorite, tungsten skarns are commonly spatially associated with smaller bodies of quartz monzonite.

Western Montana's largest composite pluton, the Boulder batholith (figs. 7 and 15), is divided into (1) a main (potassic) suite which includes the voluminous Butte Quartz Monzonite and Unionville Granodiorite and (2) a sodic suite which includes smaller peripheral plutons referred to here by compositional names following the convention of du Bray and others (2012): Rader Creek Granodiorite, Hell Canyon monzogranite, Climax Gulch granodiorite, Donald granodiorite, Moose Creek monzogranite, and Moosetown monzogranite. Tungsten skarn and vein and replacements are associated with plutons of the northern Boulder batholith and northern outliers, including the Unionville Granodiorite, Colorado Gulch granodiorite (du Bray and others, 2012), the Blackfoot City (quartz monzonite) stock, and Marysville (granodiorite) stock (fig. 15).

Six main intrusive rock types are recognized in the Idaho batholith, Atlanta lobe: tonalite, hornblende-biotite granodiorite, porphyritic granodiorite, biotite granodiorite,

muscovite-biotite granite, and leucocratic granite (Kiilsgaard and Lewis, 1985; King and Valley, 2001). Several metal deposits and occurrences are associated with granitoids near the eastern margin of the Atlanta lobe, including the Thompson Creek and Little Boulder Creek (White Cloud) stockwork molybdenum deposits and Tungsten Jim Mine skarn deposit (fig. 17). The Thompson Creek host pluton is a complexly zoned stock with biotite granodiorite forming a border zone around a core of quartz monzonite (Schmidt and others, 1982), whereas samples from the Tungsten Jim Mine dumps are granite (Van Gosen and others, 2000).

Tungsten sites are associated with several smaller plutons of granodiorite to quartz monzonite composition including the Philipsburg batholith, Mount Powell batholith, Royal stock, and Storm Lake stock (fig. 14). Hyndman (1983) describes the Philipsburg batholith as I-type and the Mount Powell batholith and Royal stock as S-type granitoids. Although most composite plutons in western Montana are granodiorite in composition, it appears that tungsten skarn mineralization at many sites was related to intrusive phases of quartz monzonite and granite.

## Pluton Petrochemistry

The correlation between specific ore metal associations (for example, copper-gold, copper-molybdenum, molybdenum-tungsten, and tin-tungsten) and the compositional character of causative granitoids is supported by empirical and theoretical evidence (Blevin and Chappell, 1992; Blevin and Chappell, 1995; Blevin, 2004). Previous studies classify the large Cretaceous and Tertiary plutons of the study area as metaluminous, peraluminous, and peralkaline on the basis of alumina saturation (Gaschnig and others, 2010; 2011) and as I-type (mafic, metaigneous source) and S-type (metasedimentary source) (Hyndman, 1983) on the basis of the scheme first introduced by Chappell and White (1974).

Additional petrochemical parameters such as the indices of alkalinity [Al(Na+K)], aluminum saturation [Al/(Na+K+Ca)], modified alkali-lime [$Na_2O+K_2O-CaO$], and iron [$FeO^{total}/(FeO^{total}/MgO)$] (Shand, 1943; Shand, 1947; Frost and others, 2001; Frost and Frost, 2008) were used to further investigate the broad compositional character of granitoids in the study area. Major element geochemical data for a total of 2,375 samples were evaluated for the following categories: Idaho batholith, Atlanta lobe; Idaho batholith, Bitterroot lobe; Cretaceous western Montana plutons; and Tertiary plutons (Idaho and Montana, but mainly of the Challis magmatic belt). Data were compiled from EarthChem PetDB (Lehnert and others, 2000), a comprehensive, searchable Web-based repository of published geochemical data for igneous and metamorphic rocks (available at https://search.earthchem.org). Additional data were added from du Bray and others (2012) and the National Geochemical Database (available at https://mrdata.usgs.gov/#geochemistry) for the Boulder and Pioneer batholiths, respectively. Unfortunately, the spatial density of samples included in the database is highly inconsistent, and less than 10 samples are reported for many plutons. A simplified dataset is available in the GIS data release accompanying this report (Goldman and others, 2022); however, these data were not used to delineate tracts. Pluton age and proximity to the Great Falls domain proved to be more useful for tract delineation.

The Fe-number or Fe-index [$FeO^{total}/(FeO^{total}/MgO)$] is particularly useful in distinguishing Cordilleran-type granitoids from those that form in anorogenic (A-type) environments, because the latter are typically more iron-enriched (Frost and others, 2001). The plot of iron-index versus silicon dioxide ($SiO_2$; fig. 19) shows that most granitoid samples of the Idaho batholith and western Montana are magnesian, whereas a greater proportion of Tertiary rocks in the Challis magmatic belt are ferroan, as expected for post-Laramide plutons. Correlative maps showing sample locations classified according to the various indices discussed here are presented in appendix 1. We classify only the individual samples according to the indices and do not classify entire plutons because of the inconsistent sample density.

Most granitoid samples from the four categories are metaluminous or weakly peraluminous ($Al_2O_3/(CaO+Na_2O+K_2O) \leq 1.1$; left of dashed line in fig. 20). This is consistent with the major lithological suites recognized in the Idaho batholith: early metaluminous suite and border zone, Atlanta lobe peraluminous suite, Bitterroot lobe peraluminous suite, and late metaluminous suite (Gaschnig and others, 2010; 2011). Although there is substantial overlap, many Cretaceous plutons in western Montana are metaluminous, whereas a greater percentage of Tertiary plutons are peraluminous.

The modified alkali-lime index plot (MALI: $Na_2O+K_2O-CaO$ versus $SiO_2$ ) introduced by Frost and others (2001) illustrates compositional trends for comagmatic igneous suites. Granitoid samples of the study area range from calcic to alkalic, with the largest number of samples classified as calc-alkalic (fig. 21). Most samples from the Bitterroot lobe are calc-alkalic to alkali-calcic, although a subset roughly parallels the calcic reference curve representing samples of diorite to tonalite and trondjhemite of the late metaluminous suite. Granodiorite and granite samples from the Atlanta lobe plot within the same fields, with a small subset of mafic samples classified as calcic. Samples from Cretaceous western Montana plutons plot as a distinct array within the calc-alkalic field but at lower $SiO_2$ concentrations (quartz diorite, tonalite, granodiorite) relative to Idaho batholith samples, with some highly alkaline outliers. The high-silica Tertiary plutons are alkali-calcic or calc-alkalic (fig. 21).

The ratio of ferric to ferrous iron oxide ($Fe_2O_3$:FeO) is commonly used to evaluate redox conditions but is indeterminable for many samples in this dataset because both ferric and ferrous forms are not consistently reported. Samples for which both oxides were reported are plotted as

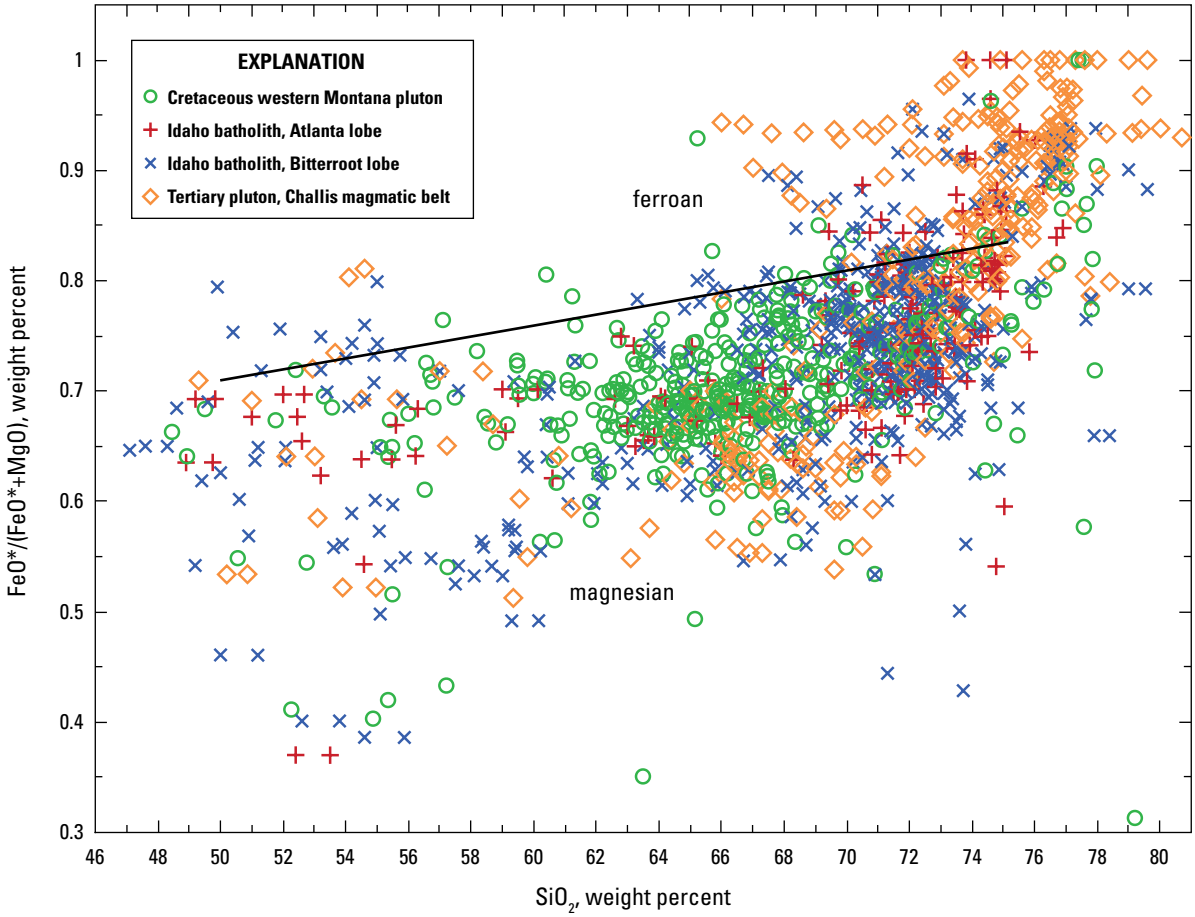


**Figure 19.** Variation diagram showing the iron-index classification of granitoid samples from Idaho and Montana plutons. Ferroan versus magnesian boundary (black line) from (Frost and Frost, 2008). FeO*, total iron expressed as ferrous iron; MgO, magnesium oxide; $SiO_2$, silicon dioxide.

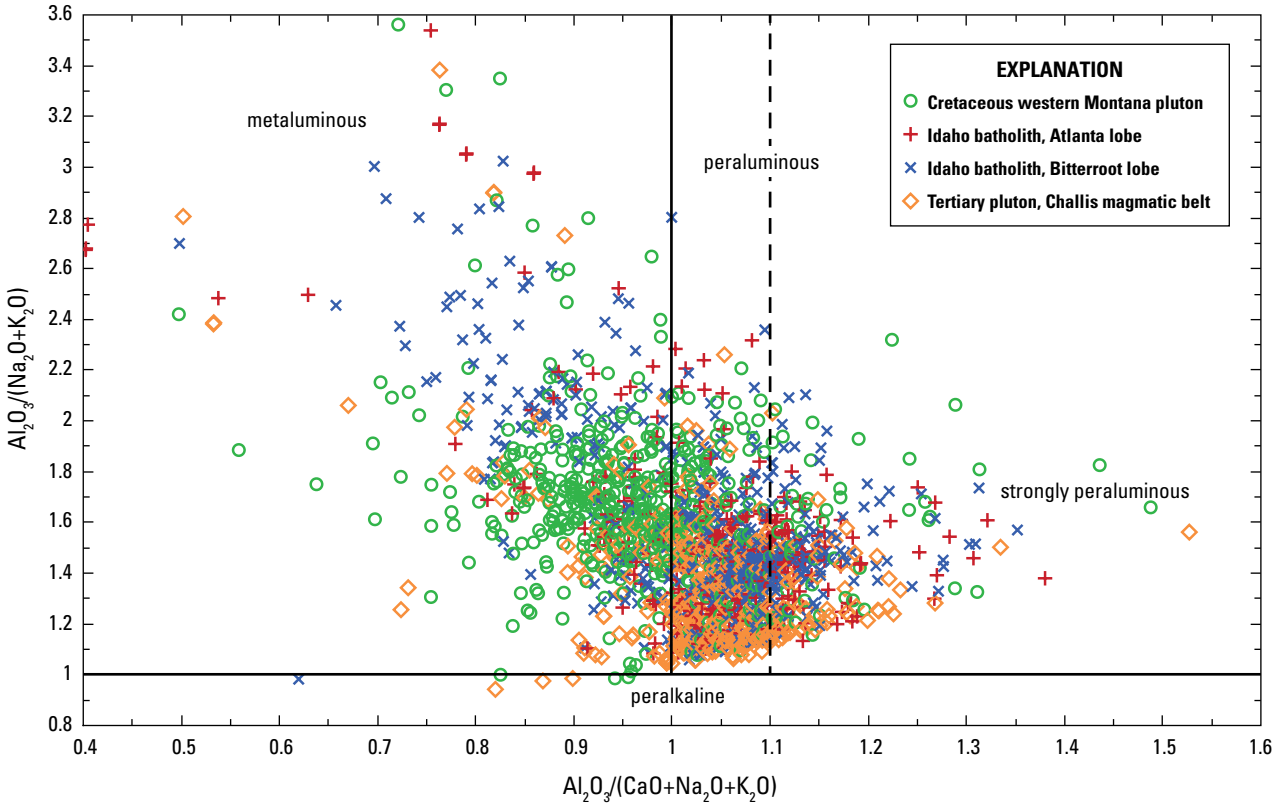


**Figure 20.** Variation diagram showing molar major oxide iron-index classification of granitoid samples from Idaho and Montana plutons as a function of alkalinity index [$Al_2O_3/(Na_2O+K_2O)$] and aluminum saturation index [$Al_2O_3/(CaO+Na_2O+K_2O)$]. $Al_2O_3$, aluminium oxide; CaO, calcium oxide; $Na_2O$, sodium oxide; $K_2O$, potassium oxide.

histograms for each of the four categories in figure 22. Median $Fe_2O_3$:FeO values for Tertiary plutons of the Challis magmatic belt, Bitterroot lobe, and Atlanta lobe are 0.87, 0.77, and 0.71, respectively. Western Montana plutons have a distinctly higher median $Fe_2O_3$:FeO value of 1.0.

The results presented in figure 22 are consistent with the broad geochemical character of Cordilleran granitoids in the compilation by Frost and others (2001). There is significant overlap on the chemical variation diagrams, but the samples from each category tend to form broad compositional arrays

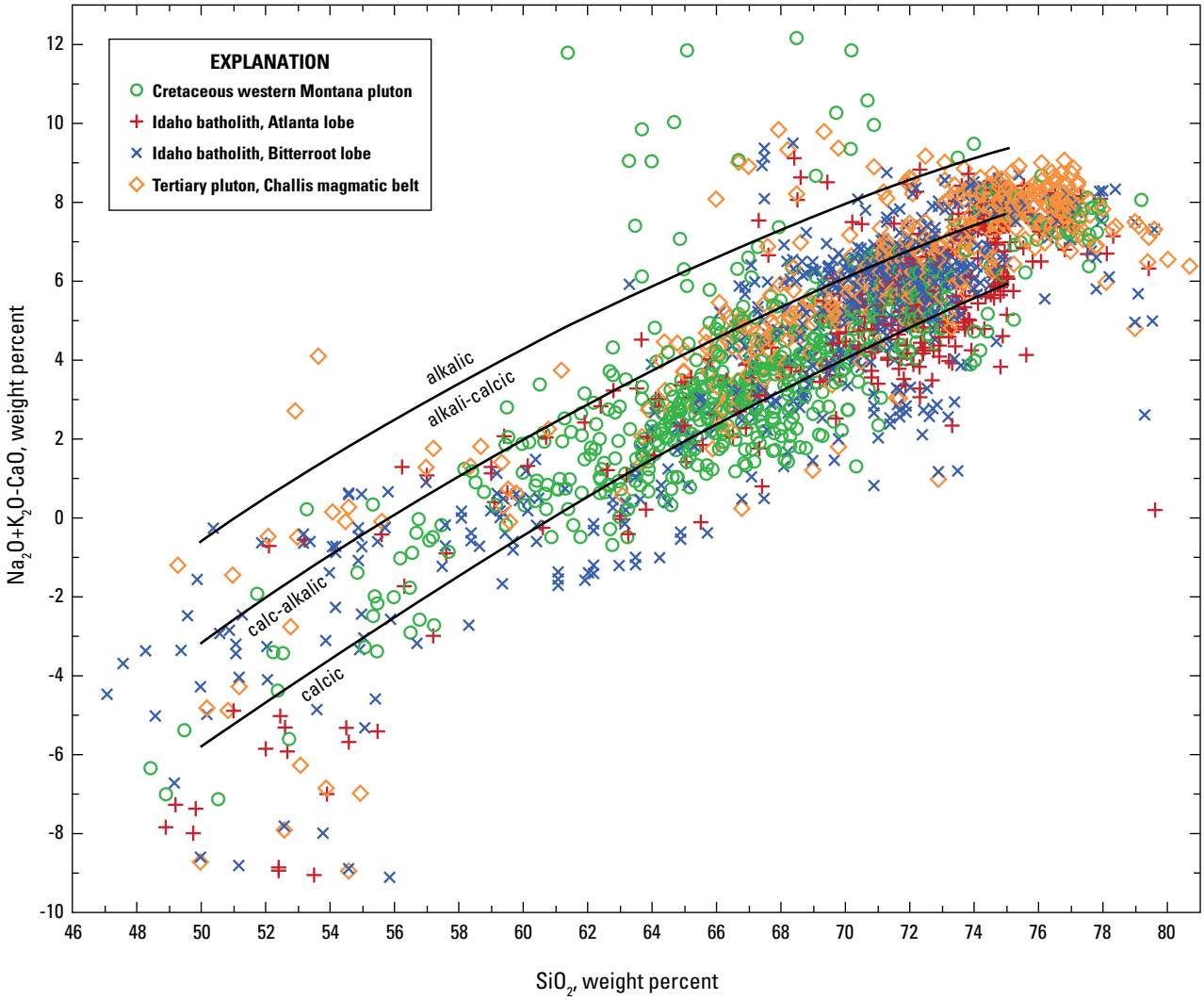


**Figure 21.** Variation diagram showing the compositions of granitoid samples from Idaho and Montana plutons as a function of modified alkali-lime index ($Na_2O+K_2O–CaO$) and $SiO_2$ in weight percent. Boundaries between various rock series from Frost and others (2001). CaO, calcium oxide; $Na_2O$, sodium oxide; $K_2O$, potassium oxide; $SiO_2$, silicon dioxide.

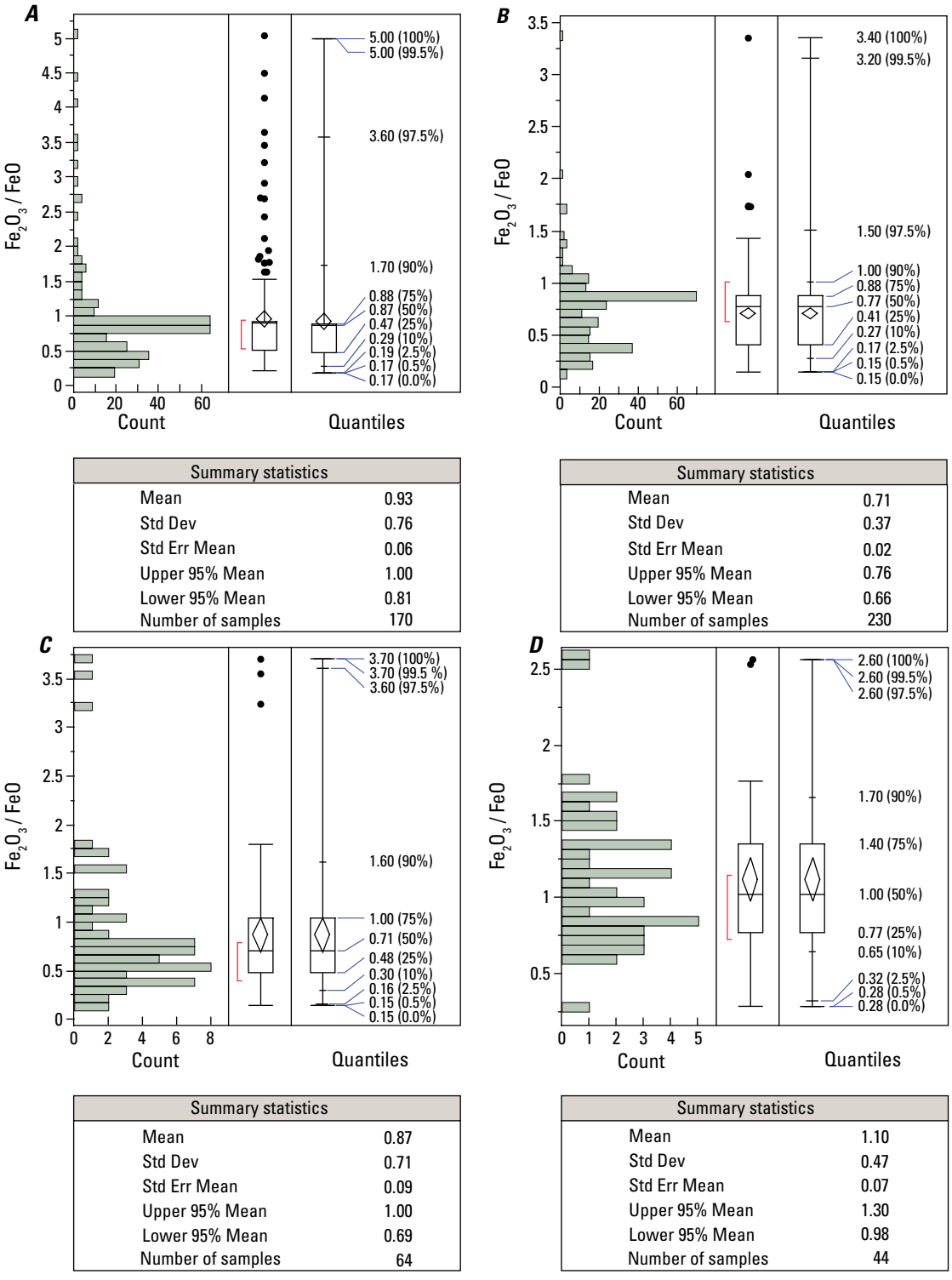


**Figure 22.** Ferric to ferrous iron oxide ratio ($Fe_2O_3$:FeO) of whole-rock samples displayed as a histogram, quantile box plot, and outlier box plot with summary statistics below for Tertiary plutons, Challis magmatic belt (*A*); Idaho batholith, Bitterroot lobe (*B*); Cretaceous Idaho batholith, Atlanta lobe (*C*); and Cretaceous western Montana plutons (*D*). Components of the histogram, quantile box plot, and outlier box plot are further explained in figure 2.1 of appendix 2.

(figs. 19–21). Based on the whole-rock geochemical data reviewed here, most plutons associated with tungsten skarn sites in western Montana are Cretaceous in age, magnesian, metaluminous, and calc-alkalic or alkali-calcic.

## Sedimentary Rocks

Skarns are generally found in carbonate-bearing lithologies, although they also occur in calcareous siltstone, sandstone, granite, and other rock types (Meinert and others, 2005). Thin bedding and intercalated carbonate and non-carbonate rocks increase permeability, which enhances fluid flow, making such sequences favorable skarn host rocks (Elliott, 1981; Pearson and others, 1992a). Paleozoic carbonates of the Montana fold-and-thrust belt contain several favorable sequences that are potential hosts for tungsten skarn mineralization. The principal sedimentary host rock sequences in each of the five focus areas (fig. 11) are shown in figures 23 and 24. Known deposits and prospects throughout the Dillon quadrangle occur at the contact between granodiorite and quartz monzonite of the Pioneer batholith and the Upper Mississippian or Lower Pennsylvanian carbonate rocks of the Amsden Formation or Snowcrest Range Group (figs. 12 and 23). These rocks consist of red shale; gray, thin-bedded limestone; siltstone; silty limestone; mudstone; and dolomite (Vuke and others, 2007). Calcareous rocks of the Permian Phosphoria Formation and Mississippian Madison Group also represent potential host rocks as they occur in proximity to the granitoids of the eastern Pioneer batholith (fig. 23).

Cambrian through Permian carbonate strata occur in proximity to the Philipsburg batholith and associated satellite plutons (figs. 14 and 23). The Mississippian Madison Group, Devonian Jefferson Formation, and Cambrian Hasmark Formation are the most favorable host rocks for scheelite-bearing tungsten mineralization (Walker, 1960).

In the Northern Boulder focus area (fig. 15), Cambrian through Mississippian carbonates are permissive for scheelite-bearing skarn in the Ophir Mining District. In the Helena Mining District, scheelite-bearing skarn is associated with Cambrian carbonates or the Mississippian Madison Group in proximity to quartz monzonite of the Boulder batholith. Reactive carbonate units in proximity to the Marysville diorite stock include the limestones of the Helena Formation and calcareous shales of the Empire Formation of the Belt Supergroup.

Some tungsten mineral sites in the Yellow Pine focus area are associated with pendants or screens of sedimentary and metasedimentary rock within granite of the Idaho batholith (fig. 16). Permissive rocks include calcareous units of the Belt Supergroup and a sequence of marbles and calc-silicate rocks of Neoproterozoic through Ordovician age (fig. 24). Stewart and others (2016) suggest that much of this sequence belongs to the Windermere Group with younger units that may correlate with Cambrian to Ordovician quartzites and marbles in the Bayhorse area west of the Salmon River lineament (Hobbs and Hays, 1990). Detrital zircon geochronology supports a Neoproterozoic to early Paleozoic age for roof pendants in the Yellow Pine area (Stewart and others, 2016).

Tungsten skarns in the Thompson Creek focus area (fig. 17) occur at the contact between granodiorite of the Cretaceous Thompson Creek stock and sedimentary rocks of the Idaho black shale mineral belt of Hall (1985). The belt of allochthonous Cambrian to Permian rocks, 145 km long in a north-northwest direction and 15–45 km wide, crops out along the eastern margin of the Idaho batholith, Atlanta lobe where rocks occur in imbricated structural plates separated by east-directed thrust faults (Hall, 1985). The rocks are predominantly black, siliceous-facies argillite, siltite, limey sandstone, shale, and siltstone. Permissive units of the Idaho black shale mineral belt include the Pennsylvanian to Permian Sun Valley Group (Grand Prize and Wood River Formations) and the Cambrian to Devonian Salmon River assemblage (Milligen Formation; fig. 24; Cook, 1956; Cookro, 1985; Link and Janecke, 1999). The Thompson Creek stock intruded rocks of the Salmon River assemblage, while the White Cloud and Little Boulder Creek stocks were emplaced near a major thrust fault that placed rocks of the Grand Prize Formation above rocks of the Salmon River assemblage and Wood River Formation (Hall, 1985). Host rocks of the Tungsten Jim deposit (Thompson Creek Tungsten Mine) are a sequence of dark, carbonaceous bedded argillite and thin interbedded limestone (Van Gosen and others, 2000) that may belong to the Grand Prize Formation or the Salmon River assemblage. A small thrust slice of the Grand Prize Formation is mapped near the Tungsten Jim deposit that is otherwise surrounded by the lower Salmon River assemblage block (Hall, 1985).

# Mineral Occurrence Data and Classification

Mineral site data were compiled from seven sources: (1) USGS Mineral Resources Data System (MRDS; McFaul and others, 2005), (2) U.S. Mineral Deposit Database (USMIN) Tungsten Deposits in the United States (Carroll and others, 2018), (3) U.S. Geological Survey Open-File Report 2004–1005 (Klein, 2004), (4) U.S. Geological Survey Open-File Report 2004–1038 (Spanski, 2004), (5) Idaho Geological Survey (IGS) Database of Mines and Prospects of Idaho (Tate and others, 2018), (6) Montana Bureau of Mines and Geology (MBMG) Abandoned and Inactive Mines Database (Montana Bureau of Mines and Geology, 2006), and (7) Defense Minerals Exploration Administration contracts (Kiilsgaard, 1996; 1997). Tungsten-bearing mineral sites or those that reference tungsten were extracted from each dataset, a unique ID referencing the data source was assigned to each record, and the datasets were combined. Records with information pertaining to the same site were identified based on matching MRDS identification numbers, similarity of site names, and proximity. In most instances, duplicate records were within 500–1,000 m of each other. Where it could be demonstrated that records with different site names represent the same site, records were combined, and one location was chosen.

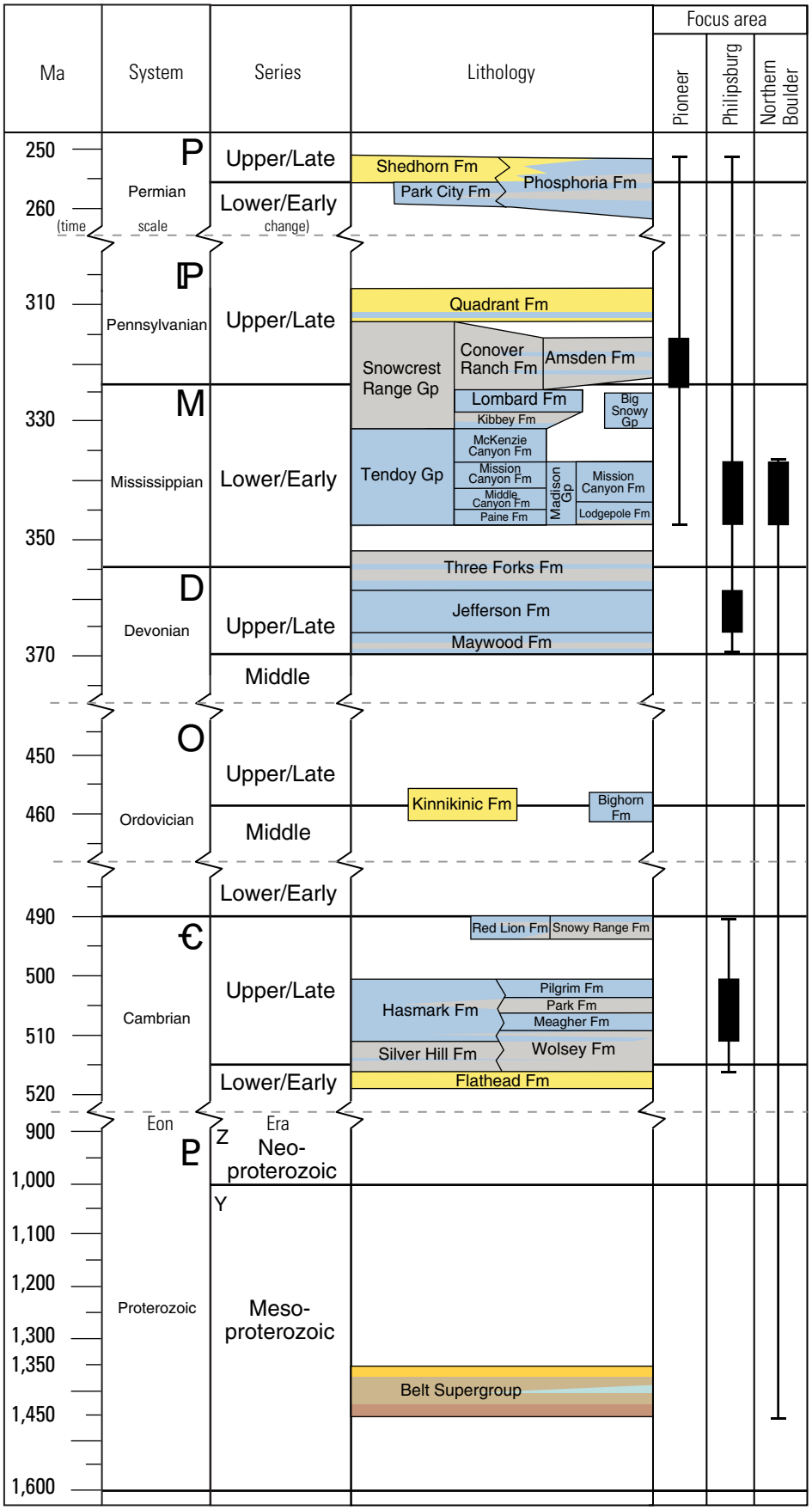


**EXPLANATION**

**Sediment and sedimentary rock**

**Marine**

- Sandstone and conglomerate
- Siltstone, mudstone, claystone, and shale
- Carbonate

**Nonmarine**

- Gravel, conglomerate, and breccia
- Sand, sandstone, and quartzite
- Silt, mud, and clay; siltstone, mudstone, claystone, siltite, and argillite
- Carbonate

**Focus area features**

- Range of possible reactive host rocks in the focus area indicated
- Range of probable or known reactive host rocks in the focus area indicated

**Figure 23.** Stratigraphic section showing Proterozoic and Paleozoic rocks in southwest Montana. The range of possible or known reactive host rock units for tungsten skarn mineralization in given focus areas is indicated by a vertical line and a bold black box, respectively. Geologic timescale and stratigraphic classification from Vuke and others (2007). Although rocks of the Belt Supergroup are shown here as non-marine, they have also been interpreted as partly marine or marine-influenced. Ma, mega-annum; Fm, formation; Gp, group.

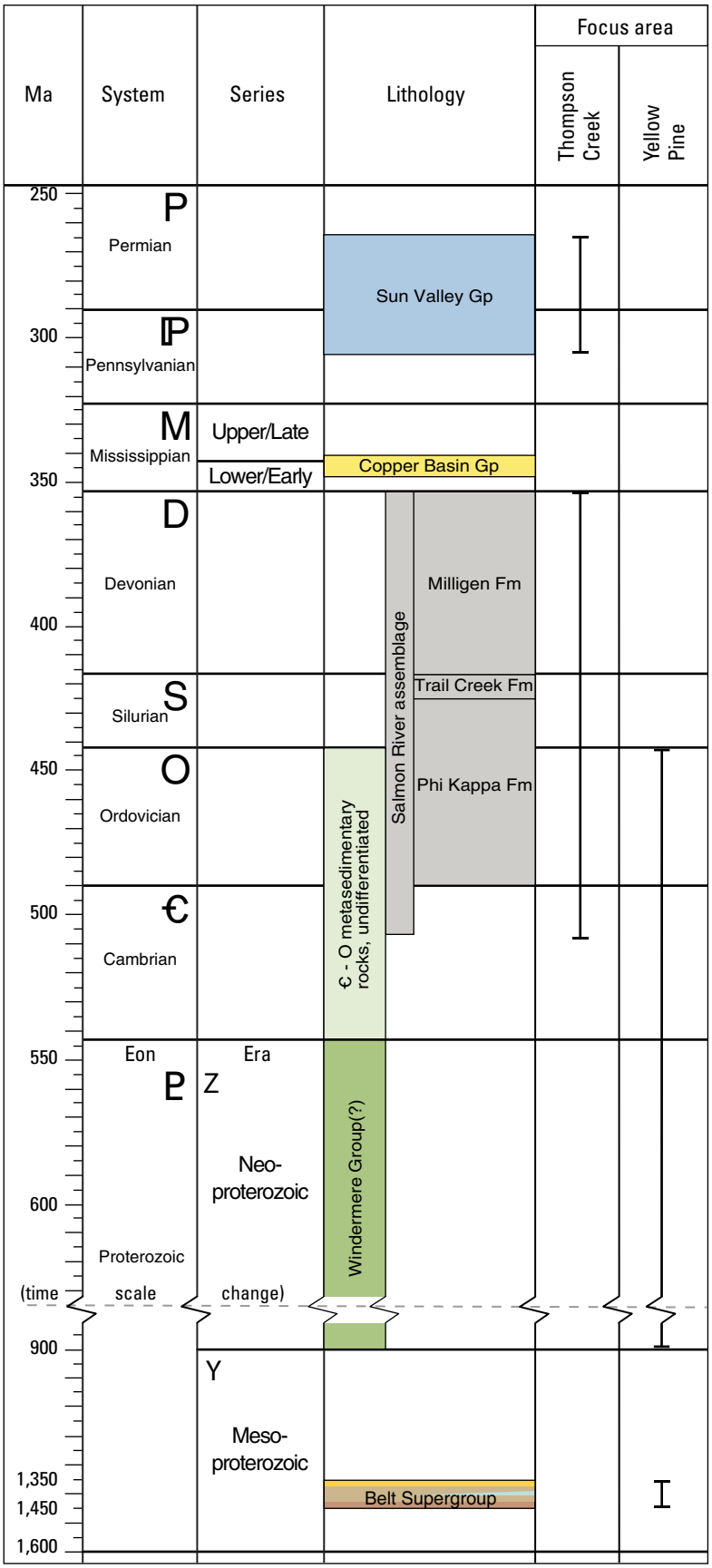


**EXPLANATION**

**Sediment and sedimentary rock**

**Marine**

- Sandstone and conglomerate
- Siltstone, mudstone, claystone, and shale
- Carbonate

**Nonmarine**

- Gravel, conglomerate, and breccia
- Sand, sandstone, and quartzite
- Silt, mud, and clay; siltstone, mudstone, claystone, siltite, and argillite
- Carbonate

**Metasedimentary rocks**

- Quartzite, marbles, and calc-silicate rocks
- Quartzite, schist, marble, and calc-silicate rocks

**Focus area features**

- Range of possible reactive host rocks in the focus area indicated

**Figure 24.** Stratigraphic section showing Proterozoic and Paleozoic rocks in east-central Idaho. The diagram is not a complete sedimentary section of this area or a specific site. It does show the range of possible reactive host rock units for tungsten skarn mineralization in given focus areas as indicated by a vertical line. Geologic timescale from Vuke and others (2007). Stratigraphic classification modified from Ballard and others, 1983; Link and Janecke, 1999; Stewart and others, 2016; and Vuke and others, 2007. Although rocks of the Belt Supergroup are shown here as non-marine, they have also been interpreted as partly marine or marine-influenced. Ma, mega-annum; Gp, group; Fm, formation.

A "best" location was selected for each set of duplicate records based on the source of the data and on observation of surface workings in satellite imagery. Spatial information reported with mineral sites is highly variable because many records are located based on published reports containing imprecise or insufficient information on the specific geographic location (McFaul and others, 2005). USMIN is considered the most current and reliable source of positional information, so if a site had a record in USMIN, the location recorded in USMIN was used. For the remaining sites, the location recorded in Klein (2004) was typically considered the best location, followed by locations recorded in MRDS, IGS, and MBMG.

Sites were ranked (see table 2) to identify those tungsten-bearing sites that were likely to be skarn-related, and thus should be expected to fall within permissive tracts. An important distinction for this study is that sites ranked 3 and above have some mention of skarn-style mineralization (12 percent of total sites), while sites ranked 1 or 2 have only a brief description of tungsten or scheelite which may or may not be skarn-hosted. The ranking also reflects the amount of production and resource information available for mineral sites. Table 3 shows the name, location, source, and ranking of known tungsten skarn deposits (rank 10) and past producers or prospects with reported tungsten resource or production data (rank 5), respectively.

## Tract Delineation

Target lithologies for tungsten skarns are based on the descriptive model customized for the known geology of the northern Rocky Mountains study area. Calcium-rich

**Table 2.** Mineral site ranking criteria.

[W, tungsten; Cu, copper; Ag, silver; Mo, molybdenum]

| Rank | General classification | Criteria |
|---|---|---|
| 10 | Site described as skarn or tactite | Known deposit with reliable identified W resources; consistent with grade and tonnage model |
| 5 | Site described as skarn or tactite | Producer (at time data was entered), past producer, or explored prospect of W with some W resource or production data |
| 4 | Site described as skarn or tactite | Producer (at time data was entered), past producer, or prospect with no W resource or production data or data suggests low grade or too small. May have been mined for something other than W (for example: Cu-Ag skarn). Many sites will have resource or production data for commodities other than W |
| 3 | Site described as skarn or tactite | "Skarn" or "tactite" mentioned in compiled site record, typically classified as an occurrence; no resource or production data available (possibly Cu skarn or W skarn) |
| 2 | Other W deposit type, possibly skarn related. Examples: porphyry, replacement, vein/replacement, Cu-W unknown, Mo-W unknown, W unknown, placer (W) | "Scheelite" mentioned among minerals present; typically classified as a prospect or occurrence |
| 1 | Other W deposit type, possibly skarn related. Examples: porphyry, replacement, vein/replacement, Cu-W unknown, Mo-W unknown, W unknown, placer (W) | Prospect or occurrence with W; if carbonate-hosted, could be skarn. Placer could be related to an upstream W skarn site. May include notable W production, but not from skarn-type mineralization |

**Table 3.** Known tungsten skarn deposits and significant tungsten skarn prospects and occurrences.

| Name | Latitude | Longitude | Source | Focus Area | Rank |
|---|---|---|---|---|---|
| Browns Lake | 45.5209 | −112.8383 | (Kiilsgaard, 1996; Klein, 2004; McFaul and others, 2005; Montana Bureau of Mines and Geology, 2006; Carroll and others, 2018) | Pioneer | 10 |
| Calvert | 45.8481 | −113.1522 | (Klein, 2004; McFaul and others, 2005; Montana Bureau of Mines and Geology, 2006; Carroll and others, 2018) | Pioneer | 10 |
| Finley Basin | 46.3674 | −113.0673 | (Klein, 2004; McFaul and others, 2005) | Philipsburg | 5 |
| Pay Day | 46.2077 | −113.0926 | (Klein, 2004; McFaul and others, 2005; Montana Bureau of Mines and Geology, 2006) | Philipsburg | 5 |
| Tungsten Jim | 44.3339 | −114.5861 | (Kiilsgaard, 1997; Klein, 2004; Spanski, 2004; McFaul and others, 2005; Carroll and others, 2018; Tate and others, 2018) | Thompson Creek | 5 |

carbonaceous and mixed sedimentary rock units (figs. 8, 23, and 24) proximal to Cretaceous granitoids within or adjacent to the Great Falls domain (fig. 6) have the greatest potential to host tungsten skarn resources. A more detailed description of the steps used in the generation of permissive tracts, including specific query statements, is presented in appendix 3.

Cretaceous and Tertiary intrusive igneous units were selected from the Northern Rocky Mountains and SGMC maps (Zientek and others, 2005; Horton, 2017), excluding volcanic and ultramafic igneous rocks (fig. 7). Next, sedimentary rock units Jurassic and older with some mention of carbonate were selected. These criteria eliminated (1) Cretaceous and younger rocks within the northern Rocky Mountains map area and (2) most lithologies of the Belt Supergroup, which are predominantly siliciclastic. The carbonate and igneous units were buffered to 2 km, and the intersections of the buffered carbonate and igneous units were extracted as a polygon feature class. Unselected areas smaller than 1 square kilometer (km$^2$) were removed from inside the polygons, and the resulting polygons defined our initial prototract. The prototract was then divided into separate tracts on the basis of major tectonic domains, age of intrusive rocks, and other available data. Areas in the southeast corner of the study area (the eastern half of the Ashton and Bozeman 1°×2° quadrangles; fig. 2) are omitted because of the relatively few reported tungsten skarn mineral sites and their proximity to the Absaroka-Beartooth Wilderness and Yellowstone National Park (fig. 3).

Two permissive tracts were identified in the study area (fig. 25). The Bitterroot tract in north-central Idaho incorporates pluton-carbonate contacts west of the Bitterroot mylonite zone (fig. 5*B*) and includes areas of the Idaho batholith, Bitterroot lobe, northern Atlanta lobe, and northern Challis magmatic belt (fig. 4). The GFTZ-Cretaceous tract

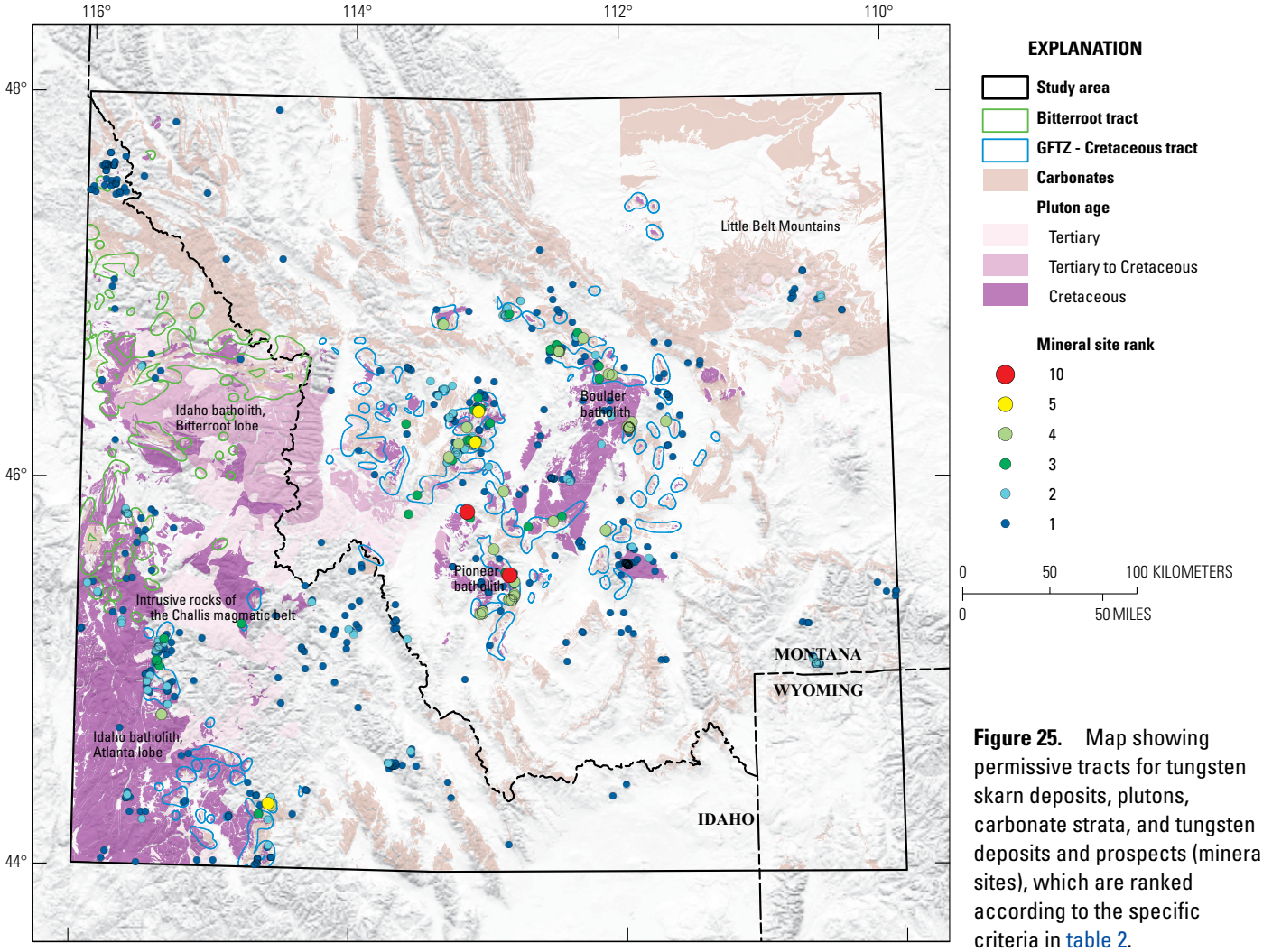


Political boundaries from U.S. Department of State (2009); Shaded relief from U.S. Geological Survey, National Geospatial Program; USA contiguous Albers Equal Area Conic Projection, central meridian 113° W. latitude of origin, 0°; North American Datum of 1983

**Figure 25.** Map showing permissive tracts for tungsten skarn deposits, plutons, carbonate strata, and tungsten deposits and prospects (mineral sites), which are ranked according to the specific criteria in table 2.

extends from parts of south-central Idaho into western Montana and includes appropriate carbonate strata intruded by Cretaceous intrusions within ~80 km of the Great Falls domain of Lund and others (2015). Areas adjacent to Tertiary plutons were excluded from the GFTZ-Cretaceous tract, because these areas are permissive for wolframite-quartz vein stockworks but less so for skarn. This procedure was justified as only two rank-3 sites fell within Tertiary pluton-carbonate tract boundaries in proximity to the Great Falls domain.

Final modifications to tract delineation included removing sedimentary formations less favorable for skarn development (but possibly hosts to wolframite-quartz veins) such as the Spokane and Newland Formations (Belt Supergroup) and adding permissive units classified as marble or metamorphosed calc-silicate rocks. Ninety-eight percent of tungsten mineral sites in the study area ranked 3 and above (skarn in table 2) are located within the GFTZ-Cretaceous tract. The abundance of data and the number of deposits, prospects, and occurrences permitted a quantitative assessment of the finalized GFTZ-Cretaceous tract. The lack of data permitted only a qualitative assessment of the apparently lesser-explored Bitterroot tract. Other styles of tungsten mineralization are discussed separately.

## Other Supporting Data

### Radiometric Data

Airborne gamma ray spectrometry (AGRS) measures the gamma rays that are emitted from naturally occurring radioactive isotopes found in rocks and soil, the most abundant of which are potassium-40, uranium-238, and thorium-232. Maps of estimated (e) Th, eU, and K concentrations and their derivatives (for example, dose rate, eTh:K ratio) created from AGRS data are an important and cost-effective tool for geologic mapping and mineral exploration (Minty and others, 2009). Relations between deposits of certain critical mineral resources and radiation can aid in exploration of these mineral deposits (Schulz and others, 2017).

Data from AGRS for the study area were extracted from the national compilation of airborne radiometric survey data collected under the NURE program. These data were collected over the period from 1974 to 1981 to provide a regional picture of natural radioactivity across parts of North America (Duval and others, 2005), with the primary purpose of identifying uranium resources in the United States (Hill and others, 2009). The NURE airborne surveys were flown at a nominal terrain clearance of 120 meters with a flightline spacing that ranges from 5 to 10 km over the study area. Each airborne data point samples an area of several thousand square meters to a depth of about 30 centimeters (Duval and others, 1971). Surfaces of predicted eTh, eU, and K derived from the flightline data for the conterminous United States were prepared using Bayesian kriging in R statistical software (R Core Team, 2019; Ellefsen and others, 2020).

Flightline data points were clipped to Cretaceous and Tertiary intrusive igneous units (IgneousUnits, NR_SG_UNIT from accompanying data release; Goldman and others, 2022) and element concentrations (eTh, eU, and K) were summarized by unit. Left-censored concentrations (values of zero) were excluded in data summaries. Maps of median concentration by map unit for each element are included in appendix 4 (figs. 4.1, 4.2, and 4.3). Maps of predictions surfaces for the study area are also included in appendix 4 (figs. 4.4, 4.5, and 4.6).

### Aeromagnetic and Other Geophysical Data

Geophysical data evaluated for this study include publicly available airborne magnetics, surface gravity, and magnetotelluric surveys. Airborne magnetic data included collections from the USGS (Phillips and others, 1993; U.S. Geological Survey, 1999; U.S. Geological Survey and National Geophysical Data Center, 2002; Hill and others, 2009; Johnson and others, 2019) and the National Oceanic and Atmospheric Administration (Meyer and others, 2017). Gravity data were compiled from the USGS (Phillips and others, 1993) and the International Gravimetric Bureau World Gravity Map (Bonvalot and others, 2012). Magnetotelluric data were retrieved from a study compiled by the EarthScope USArray project (Kelbert and others, 2012). Aeromagnetic data proved to be most useful in locating areas of tungsten mineral potential but were not used quantitatively in this assessment. We applied Analytic Signal and Local Wave Number algorithms (Nabighian, 1972; Phillips, 2002; Pilkington and Keating, 2006) to the total field Earth Magnetic Anomaly Grid North American Magnetic residual data (Bankey and others, 2002) to generate a map of filtered magnetic responses that envelope pluton edges, which are known to be permissive for tungsten skarns. This map and additional details on this procedure are presented in appendix 5.

### Stream Sediment Geochemistry and Watersheds

Stream sediment geochemistry was evaluated to confirm that rocks within permissive tracts have anomalous tungsten concentrations. Data were retrieved for samples that were initially collected in select areas of the western United States as part of the NURE Hydrogeochemical and Stream Sediment Reconnaissance project available at https://mrdata.usgs.gov/nure/sediment. Many of these samples have been reanalyzed for 51 elements, including tungsten, by four acid digestion and inductively coupled plasma mass spectrometry (ICP–MS; Smith and others, 2018). Stream sediment results for all NURE locations were retrieved, including the original 1980s-era data and the updated version 5 of Smith and others (2018), which includes 7,418 reanalyzed samples for the Montana-Idaho study area. Original 1980s-era data were considered only if there was no reanalysis of the respective sample. A comparison of old and new data shows poor correlation for analyses of tungsten concentrations at less

than 50 parts per million (ppm; fig. 26) and a bimodal log distribution (fig. 27*A*). Therefore, only older 1980s-era results with tungsten concentrations greater than 50 ppm were retained (fig. 27*B*).

Using the Esri ArcGIS Pro 2.2 watershed tool, a watershed polygon was generated for each stream sediment sample location from a point file. The output watershed features represent the complete upstream catchment areas that contribute to flow at each pour point. Resolution was determined using the highest quality digital elevation model available. Extraordinarily large watersheds (>500 km$^2$) that are of limited use in identifying specific source mineralization were omitted. Although the highlighted watersheds shown in figure 28 do not distinguish mineralization styles (for example, scheelite skarn, tungsten vein and replacement, and wolframite-quartz veins), they represent drainages with potential tungsten-enrichment upslope. Watersheds generated for those samples at the 90th percentile and higher (fig. 27*B*) were expected to correspond closely with our permissive tracts, except where skarns are not the dominant host of tungsten minerals. Highlighted watersheds generated from samples with tungsten concentrations at the 75th and 90th percentiles (figs. 27*B* and 28), equivalent to 2.2 ppm and 5.5 ppm tungsten respectively, were also treated as anomalous. Although the different mineral site rankings in figure 28 show that watershed areas with anomalous tungsten may host different styles of tungsten mineralization, a high number of these watersheds intersect the GFTZ-Cretaceous tract that is permissive specifically for skarn-style tungsten deposits. Watersheds were not used to delineate permissive tracts as discussed in the "Tract Delineation" section.

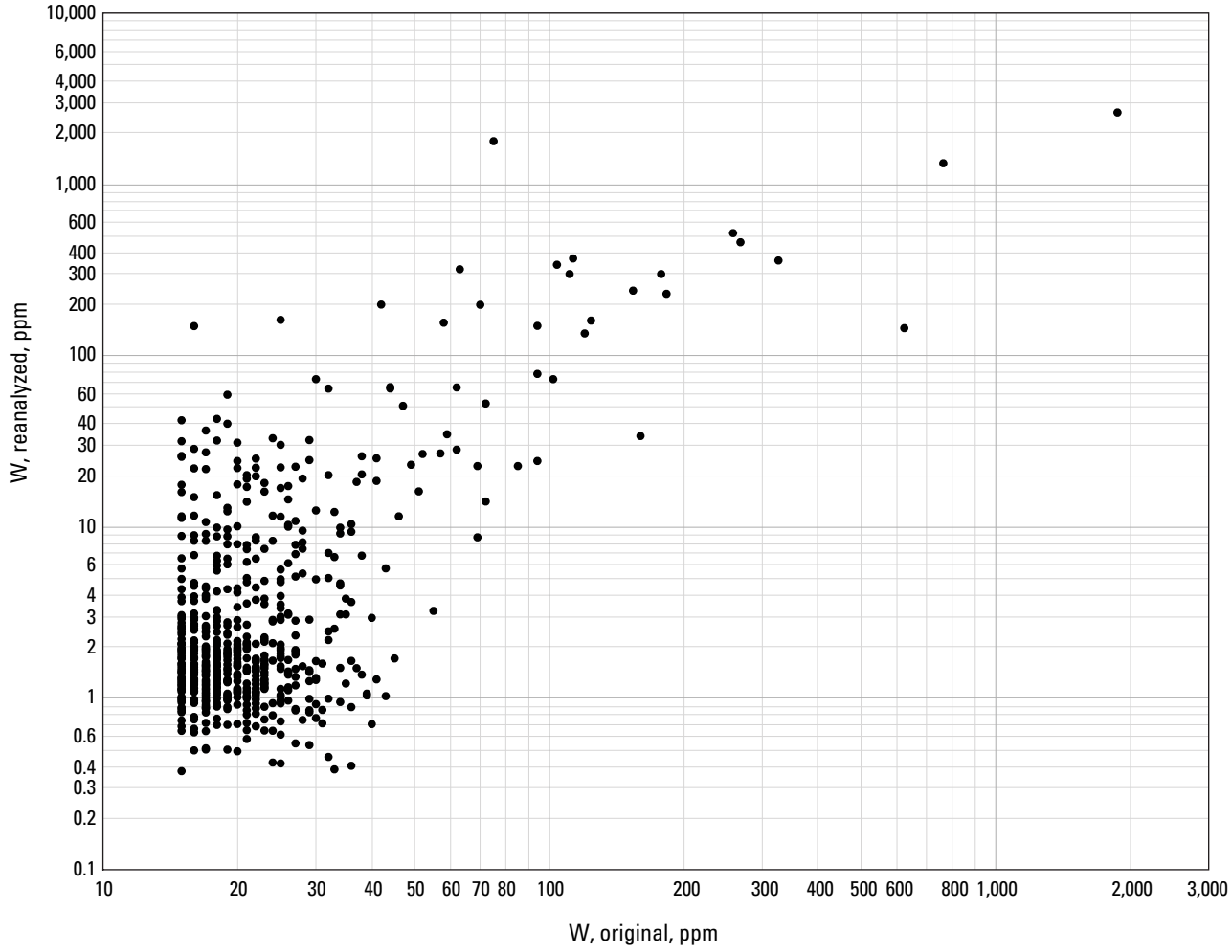


**Figure 26.** Graph showing the comparison of original 1980s-era (https://mrdata.usgs.gov/nure/sediment/) and reanalyzed (Smith and others, 2018) tungsten (W) concentration data from National Uranium Resource Evaluation stream sediment samples. ppm, parts per million.

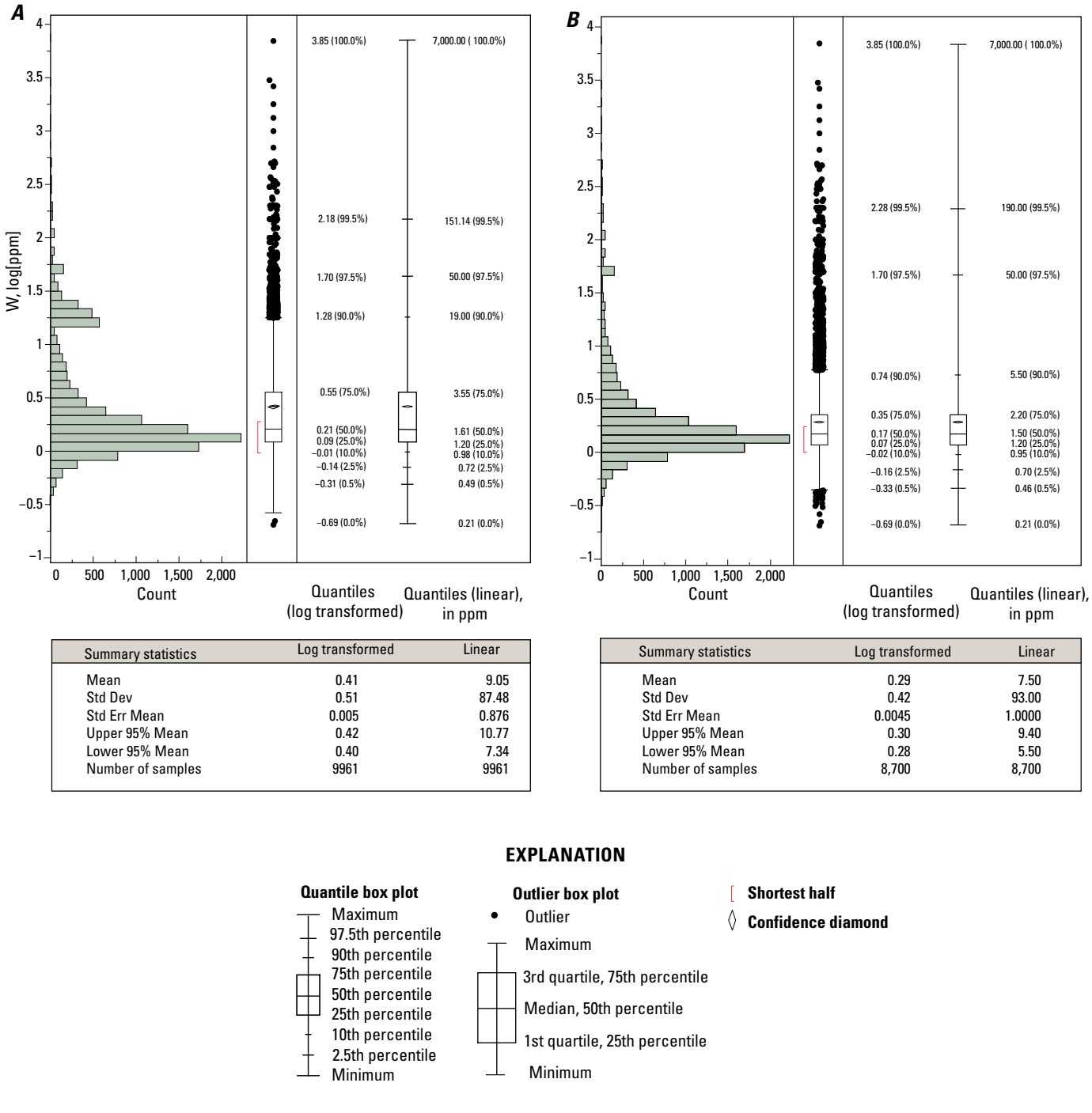


| Summary statistics | Log transformed | Linear |
|---|---|---|
| Mean | 0.41 | 9.05 |
| Std Dev | 0.51 | 87.48 |
| Std Err Mean | 0.005 | 0.876 |
| Upper 95% Mean | 0.42 | 10.77 |
| Lower 95% Mean | 0.40 | 7.34 |
| Number of samples | 9961 | 9961 |

| Summary statistics | Log transformed | Linear |
|---|---|---|
| Mean | 0.29 | 7.50 |
| Std Dev | 0.42 | 93.00 |
| Std Err Mean | 0.0045 | 1.0000 |
| Upper 95% Mean | 0.30 | 9.40 |
| Lower 95% Mean | 0.28 | 5.50 |
| Number of samples | 8,700 | 8,700 |




**Figure 27.** The log distribution of National Uranium Resource Evaluation stream sediment tungsten (W) concentrations from combined original and reanalyzed data (*A*) and original data greater than 50 parts per million (ppm) and all data from reanalysis (*B*) displayed as a historgram, quantile box plot, and outlier box plot with summary statistics below. Components of the histogram, quantile box plot, and outlier box plot are explained in figure 2.1 of appendix 2.

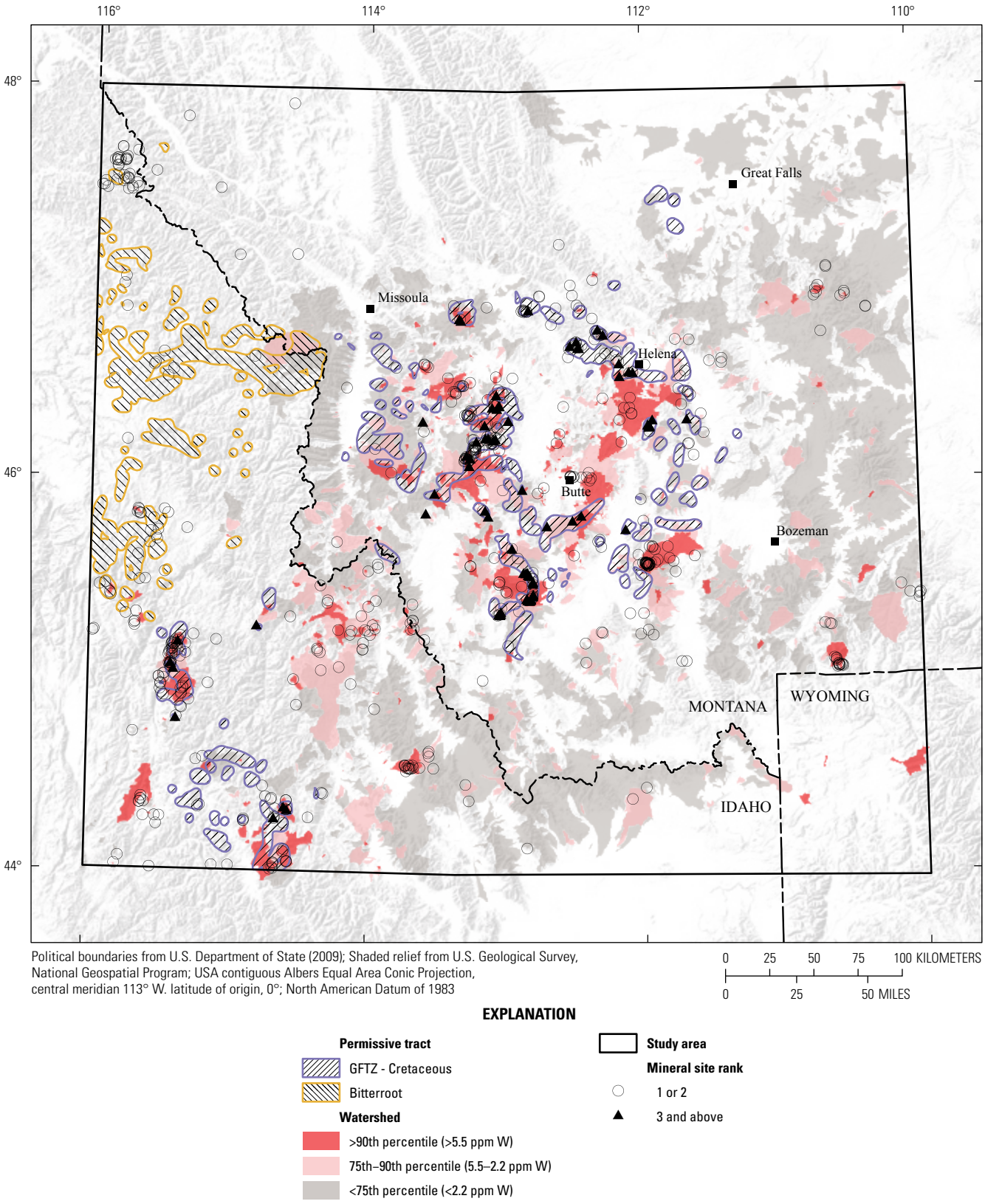


**Figure 28.** Map of watersheds constructed from National Uranium Resource Evaluation stream sediment data. Watersheds highlighted in red were generated from samples with tungsten (W) concentrations at the 75th and 90th percentiles. Highlighted watersheds with anomalous stream-sediment samples correlate with areas of known W mineral sites. ppm, parts per million.

# Mineral Potential Assessment of Undiscovered Tungsten Skarn Deposits

## Qualitative Assessment of the Bitterroot Tract

The Bitterroot tract crops out in a heavily forested region of the Payette National Forest. Although the geology of this region shares similarities to the areas of western Montana that host tungsten skarns, the Bitterroot tract has seen only limited historical exploration. This may partially explain the paucity of known tungsten skarn deposits and prospects, which precludes a quantitative assessment of the area. Pluton-carbonate contacts west of the Bitterroot mylonite zone (fig. 5*B*) define the tract that is confined mainly to the margins of the Bitterroot lobe and parts of the northern Atlanta lobe of the Idaho batholith (fig. 29). The core of the Bitterroot lobe consists of granodiorite and granite that is ~20 Ma younger (66–54 Ma) than granitoids of the southern Atlanta lobe (Lewis and others, 2012). Older (100–90 Ma) metaluminous plutons of tonalite, granodiorite, and quartz diorite compose the northern border zone of the Bitterroot lobe. Tertiary plutons of the Challis magmatic belt were emplaced along the northern margin (Bungalow pluton, Horseshoe Lake stock, and Lolo Hot Springs batholith) and southern margin (Whistling Pig pluton, Running Creek pluton, and Chamberlain Basin, Bighorn Crags composite batholith) of the Bitterroot lobe (fig. 29).

Bitterroot tract boundaries are not distinguished between those along Cretaceous versus Tertiary plutons, whereas the numerous tungsten sites to the south and east allowed refinement of the GFTZ-Cretaceous tract to only contacts along Cretaceous plutons. Estimates for the depth of crystallization for the Bitterroot lobe are 12–20 km (Hyndman, 1983; Barton, 1996). Younger Tertiary plutons of the study area, including subvolcanic rhyolite and granite with miarolitic cavities, probably crystallized at much shallower depths (2–3 km) during a period of regional extension beginning at ~54–52 Ma (Hyndman, 1983; Foster and others, 2010; Lewis

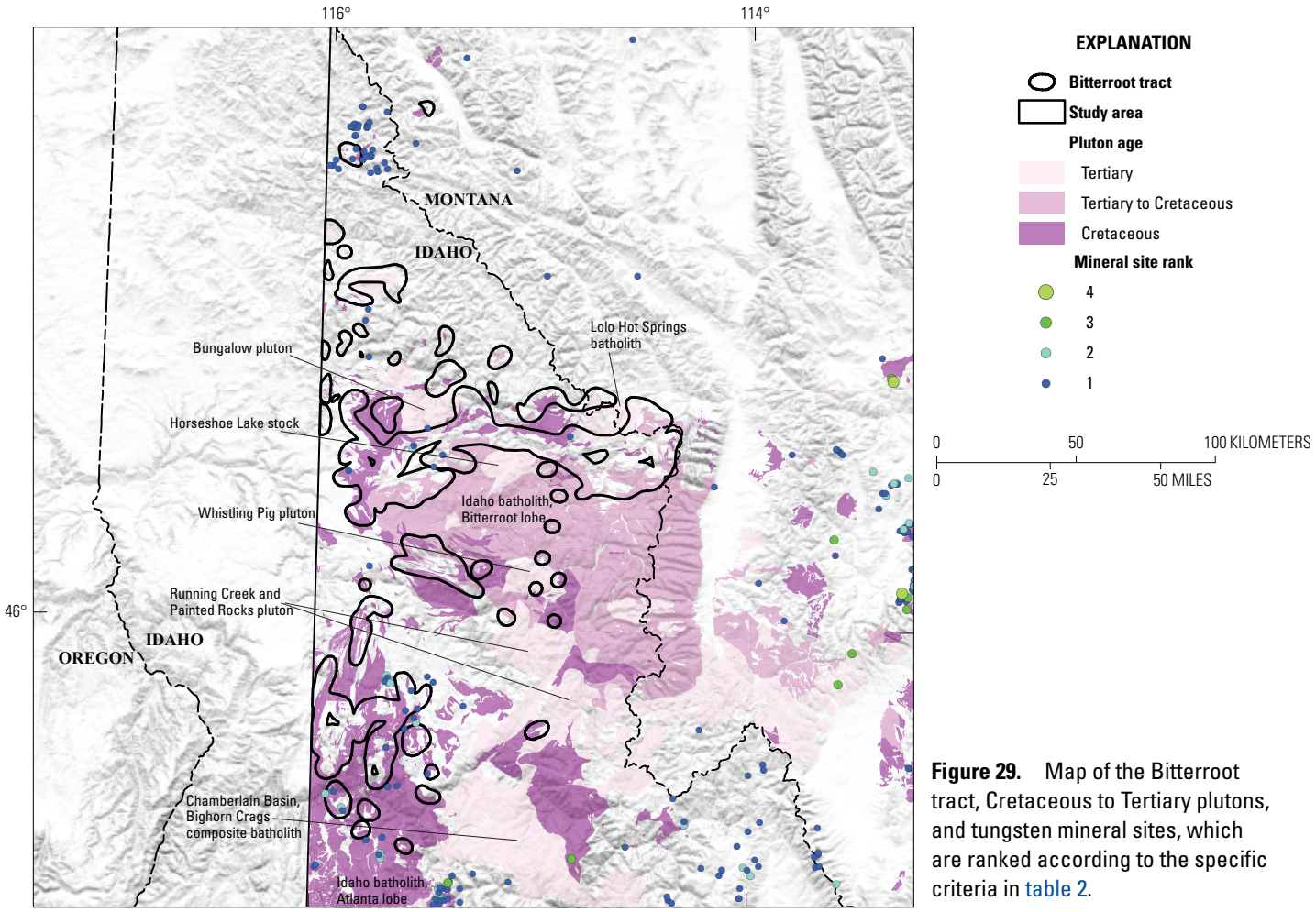


**Figure 29.** Map of the Bitterroot tract, Cretaceous to Tertiary plutons, and tungsten mineral sites, which are ranked according to the specific criteria in table 2.

Political boundaries from U.S. Department of State (2009); Shaded relief from U.S. Geological Survey, National Geospatial Program; USA contiguous Albers Equal Area Conic Projection, central meridian 113° W. latitude of origin, 0°; North American Datum of 1983

and others, 2012). Plutons of the Bitterroot lobe, emplaced at greater depths, are probably more favorable for skarn-type tungsten resources, while the shallower Tertiary intrusions of the Challis magmatic episode appear to be more favorable for wolframite-quartz vein stockworks associated with Climax-type molybdenum mineral systems (for example, the Ima Mine, Idaho, and Big Ben deposit, Montana). Based on the total length of pluton-carbonate contacts, the depth of emplacement, Cretaceous pluton chemistry, and a Proterozoic basement similar to that underlying western Montana plutons, the Bitterroot tract is permissive for tungsten skarn resources.

## Quantitative Assessment of the GFTZ-Cretaceous Tract

### Estimating Numbers of Undiscovered Deposits

An assessment panel of 21 people met in August 2019 to estimate the number of undiscovered tungsten skarn deposits in the GFTZ-Cretaceous tract. After an initial discussion of regional geology and criteria used to rank sites and define the GFTZ-Cretaceous tract, each panel member made a subjective estimate of the number of undiscovered deposits at specified levels of certainty (90 percent, 50 percent, and 10 percent). For example, a panel member might estimate that there is a 90-percent chance of 1 or more, a 50-percent chance of 5 or more, and 10-percent chance of 10 or more undiscovered deposits within a given tract. Uncertainty is expressed as the spread of estimated numbers of deposits at the 90, 50, and 10 percentiles, with a large spread among panel member estimates representing greater uncertainty (Singer, 2007; 2010).

Each member made initial estimates without sharing their results or strategy; then, the results were compiled and discussed before a second round of estimations. Average estimations at each confidence level were not significantly different between the first and second rounds, and the second-round results were selected for the quantitative simulation process (see "Probabilistic Assessment Results" section). The final estimates of undiscovered tungsten deposits reflect both the uncertainty in what may exist and the favorability of the tract (Singer, 1993). Final panel estimates for undiscovered deposits in the GFTZ-Cretaceous tract are summarized in table 4, along with statistics that describe the mean number of estimated undiscovered deposits, the variance within the estimate, and the information entropy. The assessment predicts a mean of 4 undiscovered deposits within 1,000 m of the surface for the GFTZ-Cretaceous tract, which is twice the number of known deposits. Panel members reported different levels of experience with the assessment process. The impact of experience level on estimates is evaluated graphically in appendix 6.

### Probabilistic Assessment Results

The probabilistic assessment requires inputs of (1) the estimated numbers of deposits (outlined in the "Estimating Numbers of Undiscovered Deposits" section) and (2) a grade and tonnage model. Probability calculations for this assessment were performed using MapMark4GUI (Shapiro, 2018), a graphical user interface version of MapMark4 (Ellefsen, 2017a; Ellefsen, 2017b), an open-source software package with functions written in the R statistical programming language (R Core Team, 2019). An updated grade and tonnage model for tungsten skarn deposits (Green and others, 2020) was used for this assessment. The new model includes 41 skarn-only deposits, up from the 36 sites in the previous tungsten skarn grade and tonnage model of Menzie and others (1992) and from 28 in the initial model by Menzie and Jones (1983; 1986). Data for the model include the average grade and tonnage of tungsten skarn deposits based on the total production, reserves, and resources at the lowest cutoff grade (Singer and others, 2008; Singer, 2010). The new model includes operations that have produced tungsten from skarn deposits since publication of the previous 1992 model and excludes deposits no longer considered "skarn" or those where tungsten ore zones are insufficiently delineated. From the grade and tonnage model, MapMark4 generates a separate probability density function that accounts for uncertainty for both grade and tonnage in an undiscovered deposit (fig. 30).

Estimates for the number of undiscovered tungsten deposits made by the assessment panel for the GFTZ-Cretaceous tract (appendix table 6.1) were used to generate a probability mass function (pmf) that accounts for uncertainty. Figure 31*A* shows the negative binomial pmf representing the number of undiscovered deposits in the GFTZ-Cretaceous tract. Figure 31*B* shows the estimates of undiscovered deposits made by panel members compared to the pmf recast as elicitation percentiles (for example, 90 percent confidence

**Table 4.** Undiscovered tungsten deposit estimates, tract area, and summary statistics for the GFTZ-Cretaceous tract.

[NXX, estimated number of deposits associated with the xxth percentile; $Mean_{und}$, mean number of expected undiscovered deposits; Variance, measures how far the randomly generated numbers deviate from their average value; Information entropy, the negative logarithm of the probability mass function; Total, total of expected number of deposits plus known deposits in the tract. $Mean_{und}$, Variance, and Information entropy are calculated using a negative binomial probability mass function. $km^2$, square kilometers]

| Tract Name | Tract Area ($km^2$) | Consensus undiscovered deposit panel estimates | | | | | Summary statistics from the probability mass function | | | | |
|---|---|---|---|---|---|---|---|---|---|---|---|
| | | N90 | N50 | N10 | N05 | N01 | $Mean_{und}$ | Variance | Information entropy | Known deposits | Total |
| GFTZ-Cretaceous | 7,933 | 2.2 | 4.2 | 7.1 | 8.4 | 11 | 4 | 3.9 | 2.1 | 2 | 6 |

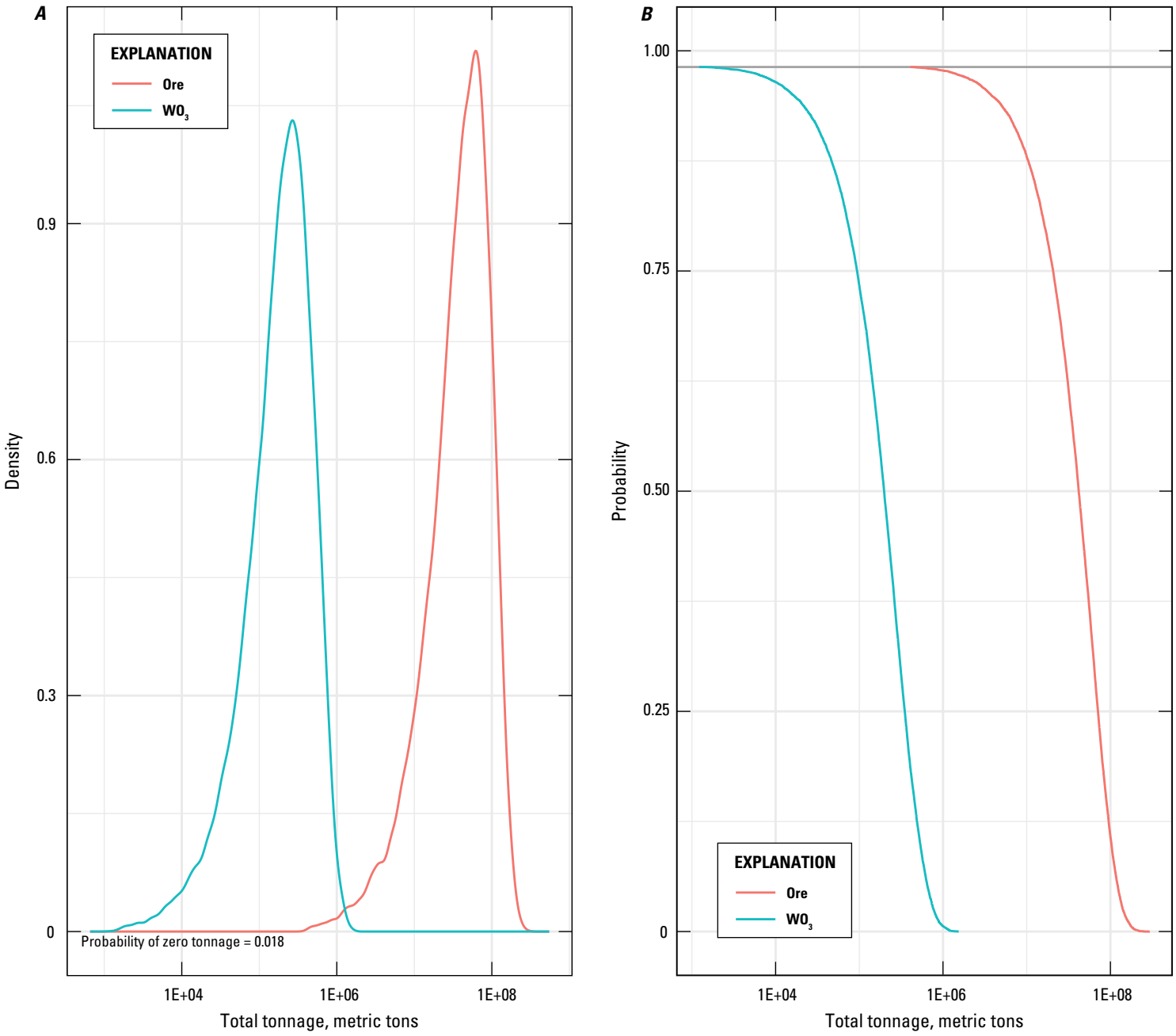


**Figure 30.** Graphs showing functions for total ore and tungsten trioxide ($WO_3$) tonnages in all undiscovered deposits within the GFTZ-Cretaceous tract. *A*, Univariate, marginal, probability density functions and *B*, univariate, marginal cumulative distribution functions for total ore and tungsten trioxide ($WO_3$) tonnages in all undiscovered deposits within the GFTZ-Cretaceous tract.

that two undiscovered deposits are present within the tract, 50 percent confidence that four undiscovered deposits are present). The estimated pmf is a relatively good fit with panel estimates. The greatest deviation between the pmf and panel estimates occurs at the 10th percentile where a higher level of uncertainty is expected.

To quantify potential tonnage of tungsten in skarn deposits of the GFTZ-Cretaceous tract, a Monte Carlo simulation was performed based on the probability density functions for grade and tonnage and the probability mass function for the estimates of undiscovered deposits. Simulation results are reported at selected quantile levels, with each quantile representing the least amount of metal expected. Results of the Monte Carlo simulation are shown on a histogram, quantile box plot, and outlier box plot with summary statistics in figure 32*A* and *B*. The mean (51,000,000 tonnes) and median (43,000,000 tonnes) ore tonnage estimates for undiscovered skarn-hosted tungsten deposits likely exceed the total amount of $WO_3$ ore from

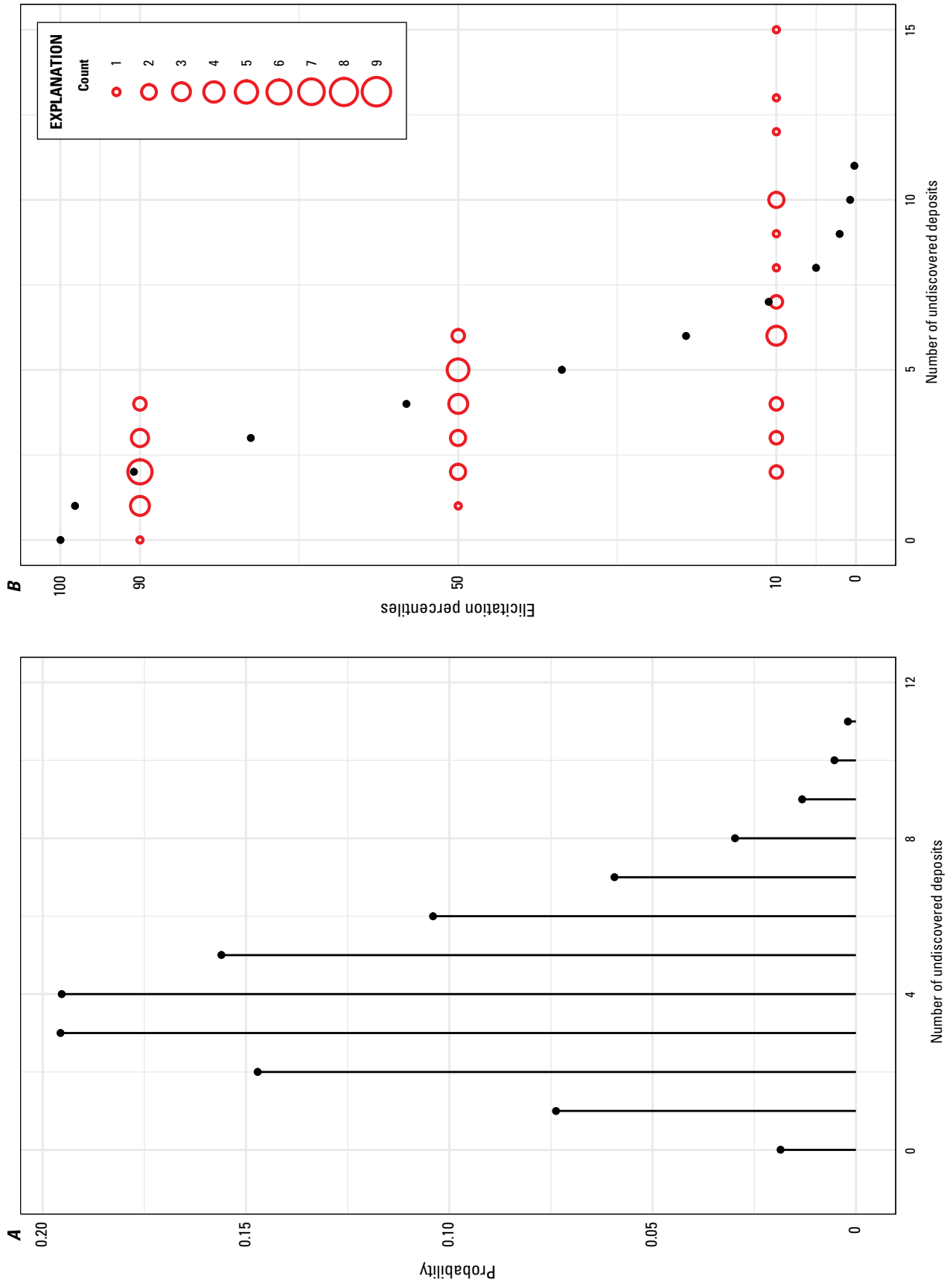


**Figure 31.** Graphs showing negative binomial probability mass function representing the number of undiscovered deposits in the GFTZ-Cretaceous tract (*A*) and estimates of undiscovered deposits made by panel members compared to the probability mass function recast as elicitation percentiles (*B*).

historical production and resource estimates of the study area because the combined tonnage of the Calvert and Browns Lake deposits (6,343,687 tonnes; table 1) is approximately one-sixth of these estimates.

## Economic Considerations

In this section, we provide an economic evaluation of undiscovered tungsten skarn resources from results of the quantitative three-part assessment. Economic filter analysis is used to determine whether some portion of an undiscovered mineral resource estimate might be economic to extract and to estimate its value, much like a prefeasibility study in the mineral exploration sector. The new Resource Assessment Economic Filter (RAEF), introduced by Shapiro and Robinson (2019), is applied to the results of the Monte Carlo simulation described in the "Probabilistic Assessment Results" section. The RAEF utilizes a set of economic filter parameters, including undiscovered deposit simulation results, cost-inflation factors, a depth profile of undiscovered deposits, mine and mill type selections appropriate for the deposit type, and engineering cost models for different mine and mill types (Shapiro and Robinson, 2019). Created using the open-source statistical programming language R (R Core Team, 2019), the RAEF allows the user to define specific input parameters

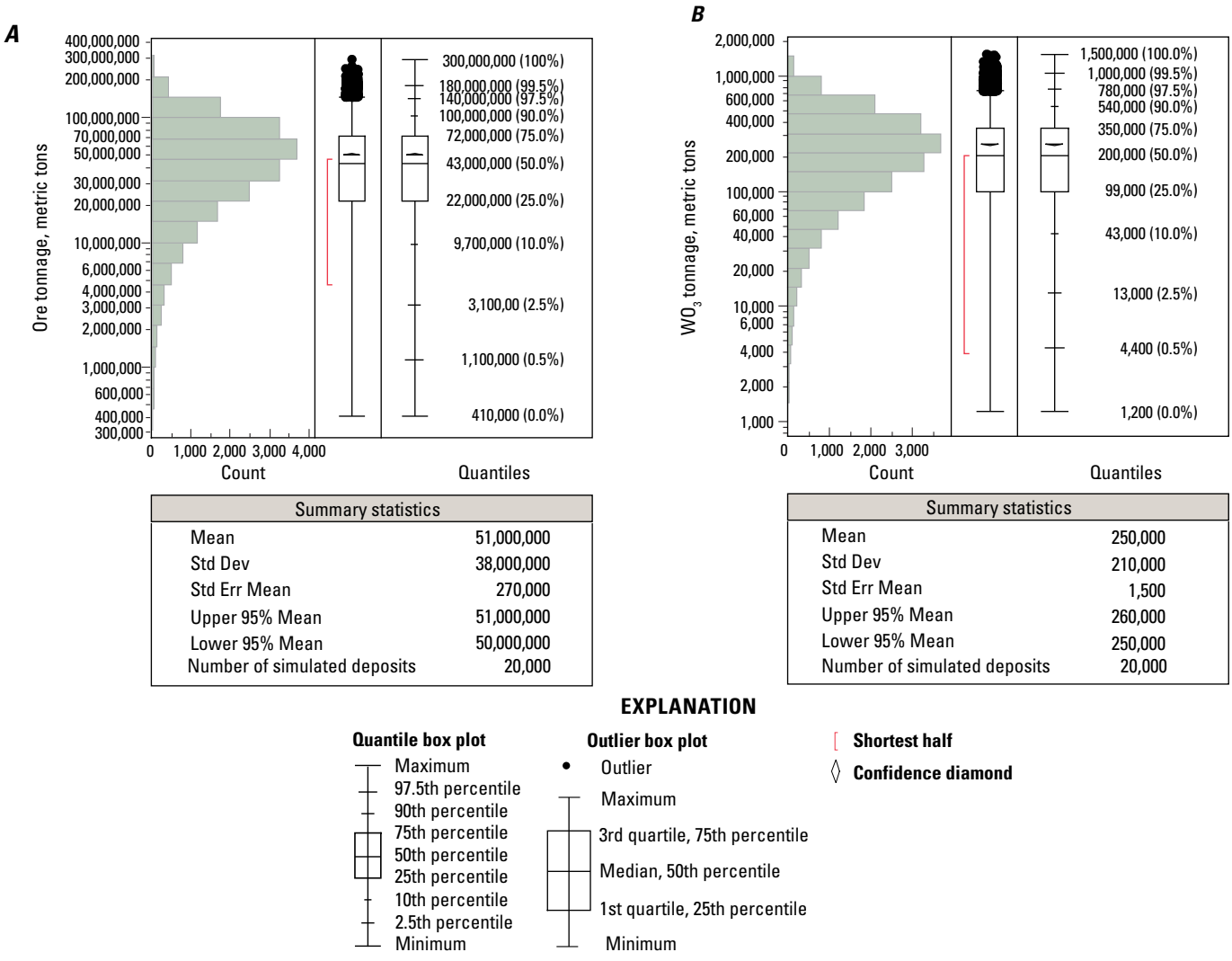


**Figure 32.** Simulated total ore tonnage (*A*) and simulated total tungsten trioxide ($WO_3$) produced (*B*) in metric tons (see text for discussion) displayed as a historgram, quantile box plot, and outlier box plot with summary statistics below. Quantiles are points in a distribution that relate to the rank order of values in that distribution. In this figure, the data are ranked from lowest to highest. Components of the histogram, quantile box plot and outlier box plot are explained in figure 2.1 of appendix 2.

through its graphical user interface (GUI). Using simple engineering mine model calculations, the RAEF tool evaluates the fraction of simulated deposits that would be profitable and provides an estimate of economic recoverable resources in the study area (Shapiro and Robinson, 2019).

Input parameters for the RAEF analysis are: (1) the Monte Carlo simulation results generated using the MapMark4GUI (Shapiro, 2018) which include simulated ore tonnage, commodity grades, and in-ground contained resources; (2) deposit characteristics including deposit geometry, tract area, depth profile, and mine type; (3) mill method, which defines the beneficiation methods for commodities to be recovered and the costs and metallurgical recovery rates (MRR); and (4) waste management, either a tailings pond and dam or an optional tailings pond liner. Specific input parameters for evaluation of the GFTZ-Cretaceous tract are presented in appendix 7. The assigned deposit type for tungsten skarn was "flat-bedded/stratiform," the maximum deposit depth considered was 1,000 feet, and the MRR was 0.75.

The RAEF reports the cumulative ore tonnage of the deposits, the tonnage of contained in-ground mineral resources, the tonnage of recovered mineral resources, and the net present value (NPV) of the tract. Results for estimated tungsten skarn resources in undiscovered deposits of the GFTZ-Cretaceous tract are displayed as histograms, quantile box plots, and outlier box plots in figure 33, with selected quantile levels and summary statistics reported below. The RAEF estimates the ore deposit cutoff grade and recovered ore value as a function of ore tonnage, mine and mill methods, and deposit depth. Cutoff grade is the ore grade at which the revenue generated by the mining and beneficiation is equal to the capital expenditures and operating costs. Below this grade, ore is not economical to extract and will typically not be mined until economic factors change. In order to compare economic ore grades across commodities and byproducts, the mining industry calculates a copper equivalence for all metals of interest. Copper equivalence (*CuEQ%*) is calculated in equation 1 as

$$CuEQ\% = G_{Cu} \times [\sum_i R_i V_i G_i] / (R_{Cu} V_{Cu} G_{Cu}) \quad (1)$$

where

$R$ is the metallurgical recovery rate,
$V$ is time-averaged metal price per ton, and
$G$ is metal commodity grade in percent of ore for the suite of potentially recoverable commodities, $i$, relative to copper (Cu).

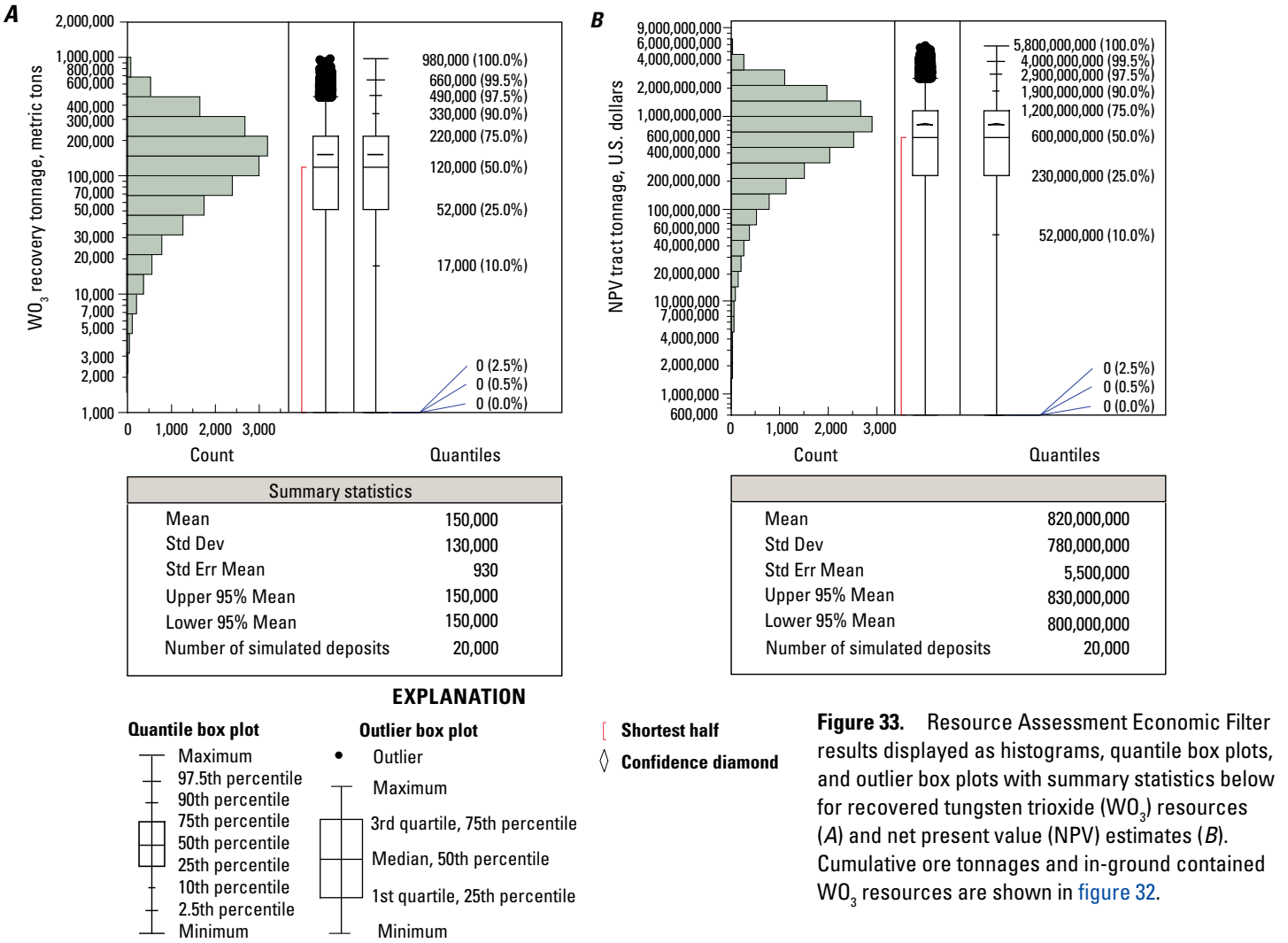


**Figure 33.** Resource Assessment Economic Filter results displayed as histograms, quantile box plots, and outlier box plots with summary statistics below for recovered tungsten trioxide ($WO_3$) resources (*A*) and net present value (NPV) estimates (*B*). Cumulative ore tonnages and in-ground contained $WO_3$ resources are shown in figure 32.

The RAEF generates two graphs that show calculated mine cutoff grades as a function of ore tonnage, mine type, and deposit depth (Shapiro and Robinson, 2019). Figure 34 shows cutoff grade as *CuEQ%* (left axis) and cutoff ore value in dollars per ton (right axis; adjusted to 2008 U.S. dollars) versus total ore tonnage as a function of depth to the top of the deposit in meters. The depth contours show how variations of ore tonnage and deposit depth influence the cutoff grade and ore value.

## Assessment Summary

The median estimate for undiscovered tungsten skarn resources in the GFTZ-Cretaceous tract projected by the Monte Carlo simulation is 43,000,000 metric tons of mineralized rock with a total contained $WO_3$ resource of 200,000 metric tons (figs. 32 and 35). This requires an average grade of approximately 0.46 percent $WO_3$, which is consistent with the Browns Lake deposit and other prospects throughout

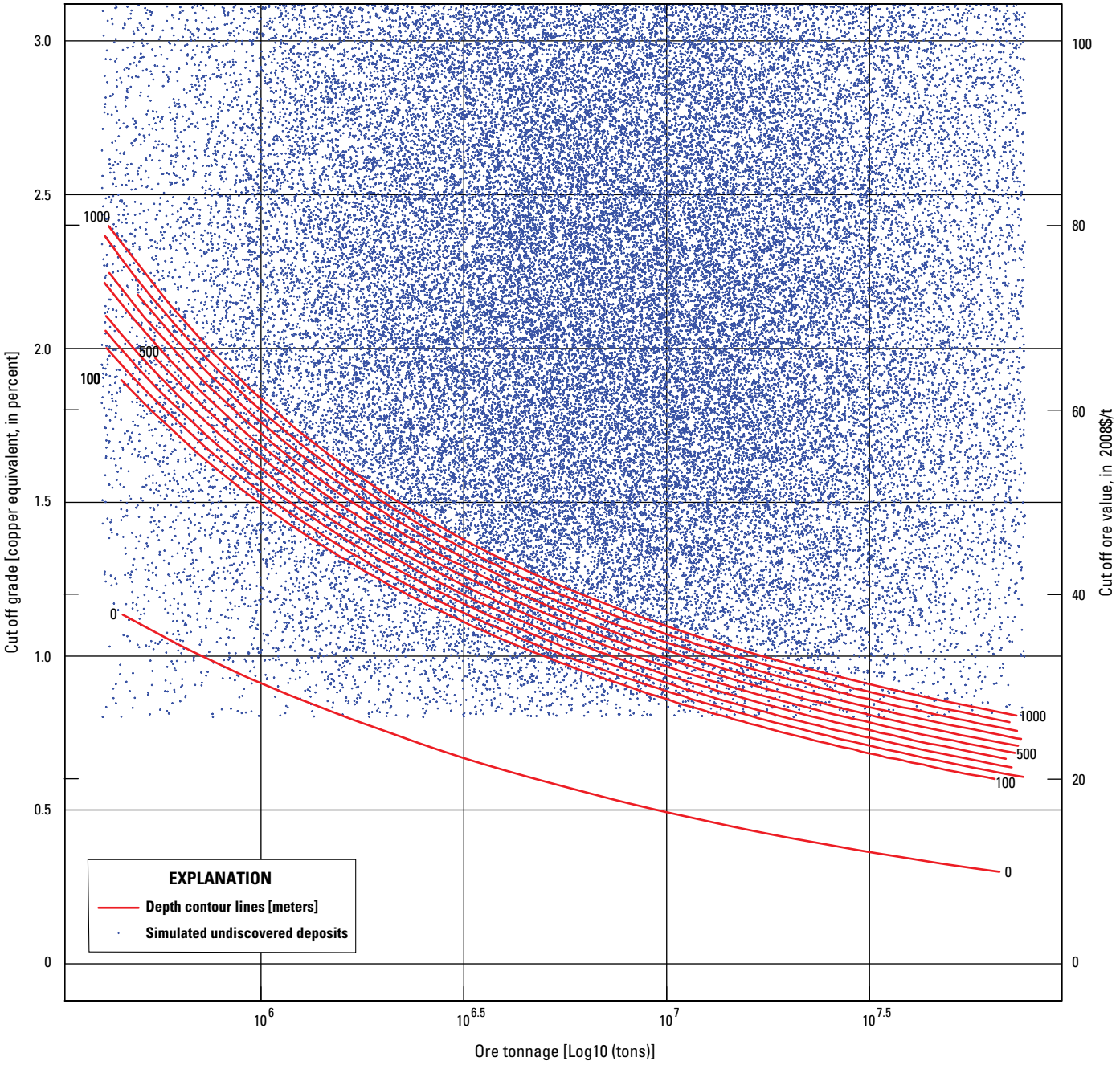


**Figure 34.** Density plot of simulated ore tonnages and values (grades) modified from Resource Assessment Economic Filter output; number of simulated ore deposits = 20,000. The economic cutoffs at a given depth and ore tonnage are indicated by the red contours. 2008$/t, dollar amount in year 2008 per ton.

the study area (table 1). The median estimate represents approximately seven deposits with grades and tonnages similar to that of Browns Lake, whereas the estimate at the 10 percent quantile represents undiscovered resources approximately 61 percent larger than the Browns Lake deposit. Past production and historical resource estimates at the two known deposits (Browns Lake and Calvert) represent approximately 12–13 percent of the total $WO_3$ ore from known deposits and median undiscovered estimates combined. The mean number of expected undiscovered deposits predicted by the Monte Carlo simulation ($n = 4$), with an ore tonnage similar to that of Browns Lake (~6,000,000 metric tons) is approximately equal to the estimated ore tonnage at the 25 percent quantile (22,000,000 metric tons). Simulation results are inclusive of tungsten skarn resources that might exist at significantly greater depths (up to 1,000 m) compared to what has likely been explored (~300 m). Therefore, the 50–100 percent quantile values represent estimates of total $WO_3$ endowment, while values at the 10 and 25 percent quantiles estimate resources that could reasonably be discovered with additional exploration in the near future (figs. 32, 35).

Although eastern Idaho and western Montana have seen significant metal exploration in the years since the DMEA, there have been very few tungsten-focused exploration ventures using modern methods. A portion of the remaining reserves likely exist in proximity to known deposits including Calvert, Browns Lake (Lentung resource), Tungsten Jim (Thompson Creek tungsten deposit), and Finley Basin. Historical reserve estimates and associated exploration data may permit a shorter path toward modern resource estimates at these sites. The Pioneer, Philipsburg, Northern Boulder, Thompson Creek, and Yellow Pine focus areas are all permissive for additional skarn-hosted tungsten resources.

## Metallogenic Controls on Tungsten Mineralization

The northern Rocky Mountains region of Montana and Idaho has seen periods of prolonged crust building, continental amalgamation, and accretionary events that reactivated structures, thickened crust, and recycled crustal

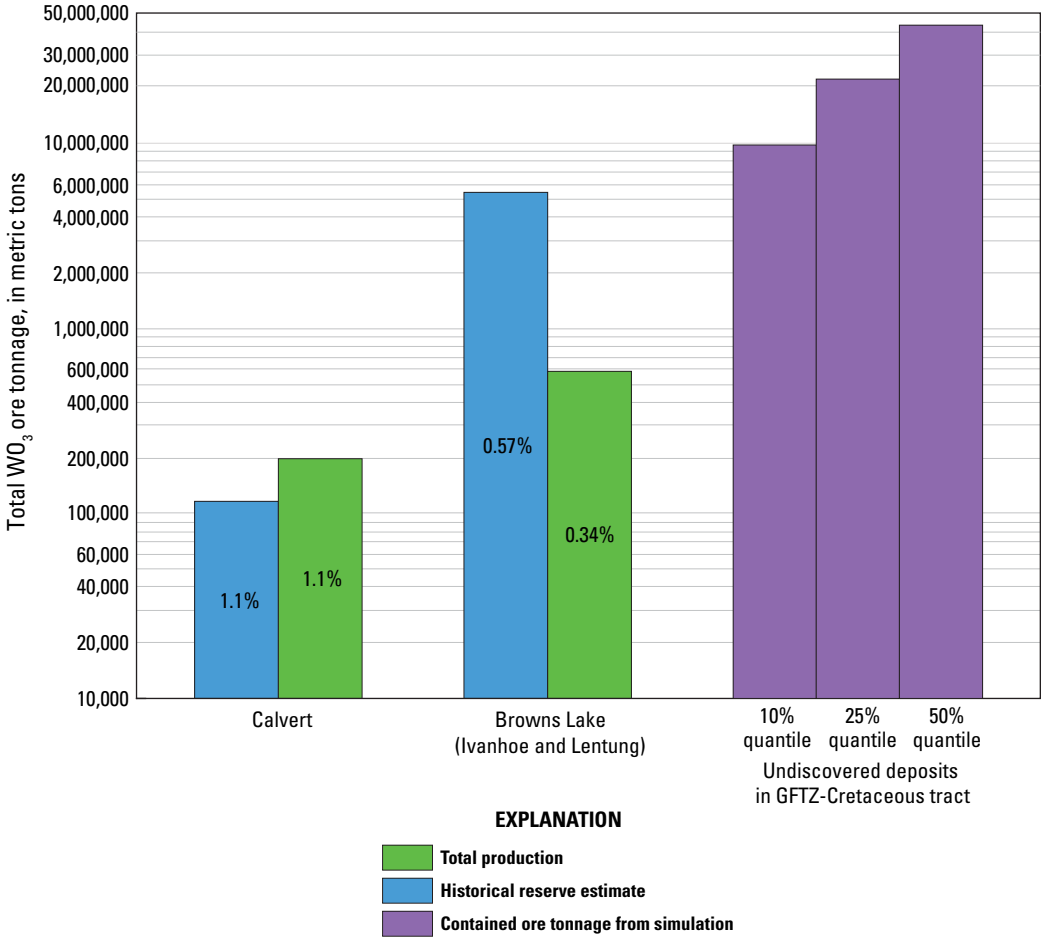


**Figure 35.** Chart showing total tungsten trioxide ($WO_3$) ore tonnage from production and resource data from the two known deposits compared with the $WO_3$ ore tonnage at the 10, 25, and 50 percent (%) quantiles from the undiscovered resource estimate for the GFTZ-Cretaceous tract. Ore grades in percent shown on the bars for the Calvert and Browns Lake deposits.

materials, all of which may influence metal endowment and mineral deposit formation (Lund and others, 2015). The composition and initial metal endowments of Archean and Paleoproterozoic basement domains and the underlying mantle may be instrumental in the occurrence of specific types of younger mineral deposits (Titley, 2001; Groves and Bierlein, 2007). Subsequent orogenic, postorogenic, and hydrothermal processes may remobilize and recycle metals leading to selective metal enrichment. For example, the mostly concealed arc-related(?) Paleoproterozoic crust of the Great Falls and Wallace domains (fig. 6) may have contributed metals to the Cretaceous and Tertiary upper crustal Idaho-Montana porphyry Cu-Mo belt (Lund and others, 2015).

The Great Falls tectonic zone is marked by a series of high-angle faults, lineaments, and northeast-trending magnetic and gravity anomalies (O'Neill and Lopez, 1985; O'Neill, 1998; Vervoort and others, 2016). This zone has been described as a collapsed Paleoproterozoic (1.9–1.7 Ga) arc and collisional suture between the Archean Wyoming province and Medicine Hat block during which time juvenile oceanic lithosphere was subducted northward beneath the Medicine Hat block (fig. 6; Foster and others, 2006; 2012; Mueller and others, 2002). An alternative model suggests that the Great Falls tectonic zone is an intracontinental shear zone (Boerner and others, 1998; Lemieux and others, 2000).

Exposures of magmatic rocks in the Little Belt Mountains, within the Great Falls tectonic zone, have been dated at 1.9–1.8 Ga (Mueller and others, 2002; Foster and others, 2006). However, the known extent of Paleoproterozoic crust west of the Great Falls tectonic zone was expanded with studies of orthogneisses in northern Idaho. Vervoort and others (2016) report Neoarchean (2.67–2.65 Ga) and Paleoproterzoic (1.88–1.84 Ga) ages for these orthogneisses of the Clearwater and Priest River complexes. These results suggest that at least parts of the area west of the Great Falls tectonic zone—known as the Selway terrane (Foster and others, 2006; 2012) or Wallace domain (fig. 6; Sims and others, 2004; 2005; Lund and others, 2015)—is underlain by Paleoproterozoic (~1.86 Ga) basement that is contemporaneous with the exposures in the Great Falls tectonic zone to the east-southeast.

Relative to adjacent Archean sialic protocontinental domains (Archean Wyoming province), the Paleoproterozoic intracratonic domains (Great Falls and Wallace domains) subsequently produced more voluminous Phanerozoic magma, with the northeast-trending Great Falls tectonic zone imparting a structural control on the location of metal-bearing intrusions (Foster and others, 2006; Klein and Sims, 2007; Lund and others, 2015). Plutons of the Idaho batholith, Bitterroot lobe, the northern Atlanta lobe, and a majority of those Cretaceous and Tertiary plutons east of the Idaho batholith are likely underlain by Paleoproterozoic mafic lower crust. Isotopic evidence (strontium, neodymium, lead, and hafnium) further supports derivation of Cretaceous I-type granitoids in the study area by melting of one or more predominantly mafic, ancient, lower crustal sources (Probst, 2007).

Foster and others (2006) suggest that the region experienced a Paleoproterozoic to Mesoproterozoic history of enrichment in incompatible and heat-producing elements (K, Th, U) by primitive, asthenospheric-derived material. The radiometric signatures produced from such heat-producing elements are illustrated in maps of eTh, eU, and K concentrations based on the airborne radiometric survey of the NURE program that are presented in appendix 4. Integration of Cretaceous and Tertiary intrusive igneous polygons (IgneousUnits, I_POLYID from accompanying data release; Goldman and others, 2022) and median airborne radiometric measurements within each individual polygon reveals a clear spatial correlation between the Great Falls domain and the most highly radiometric Phanerozoic plutons of the region (fig. 36). This study has also established a spatial relationship between tungsten skarn mineral sites, the Great Falls tectonic zone, and some of these plutons.

In addition to the numerous tungsten skarn and wolframite-quartz stockwork sites, the Idaho-Montana porphyry copper-molybdenum belt contains granitoid or porphyry deposits in which molybdenum or tungsten are the principal metal (Thompson Creek, Ima, Big Ben, Browns Lake, Calvert). Based on the spatial relationship between (1) epigenetic mineral deposits, (2) juvenile Paleoproterozoic magmatic rocks in the underlying basement, and (3) reactivated structures of the Great Falls tectonic zone, the tectonic history and composition of individual basement domains (Great Falls and Wallace) appear to have influenced the location, size, and ore-element variations of successive mineralizing systems (Klein and Sims, 2007). The ancient collisional suture or intracontinental shear zone controlled the locus of emplacement, while the melting of the fertile Paleoproterozoic basement probably controlled the bulk granodioritic composition of magmas and possible remobilization of metals like copper, molybdenum, and tungsten.

Redox conditions are also known to influence ore-element (molybdenum, tin, and tungsten) variations in large metallogenic provinces. For example, tin enrichment is favored under more reducing conditions where it occurs as $Sn^{2+}$ rather than as $Sn^{4+}$. Tetravalent tin is favored in more oxidized magmas, but its substitution for $Fe^{3+}$ and $Ti^{4+}$ in early-forming mafic silicates inhibits subsequent tin enrichment (Ishihara, 1978; Hart and others, 2004b). Tungsten enrichment is also favored under more reducing conditions, although causative plutons span a greater range of $fO_2$ (Ishihara, 1981; Hart and others, 2004b;). Whole-rock $Fe_2O_3$:FeO ratios can be used as an approximation of redox potential, provided samples are unaltered. Samples from the dataset compiled to investigate pluton chemistry show that Cretaceous to Tertiary plutons of the Idaho batholith and Challis magmatic belt are relatively oxidizing with median $Fe_2O_3$:FeO ratios between 0.71 and 0.87. Plutons of western Montana are more oxidized with a median $Fe_2O_3$:FeO value of 1.0 (fig. 22). These ratios are considerably higher than those reported for middle Cretaceous plutons of the northern cordillera in the

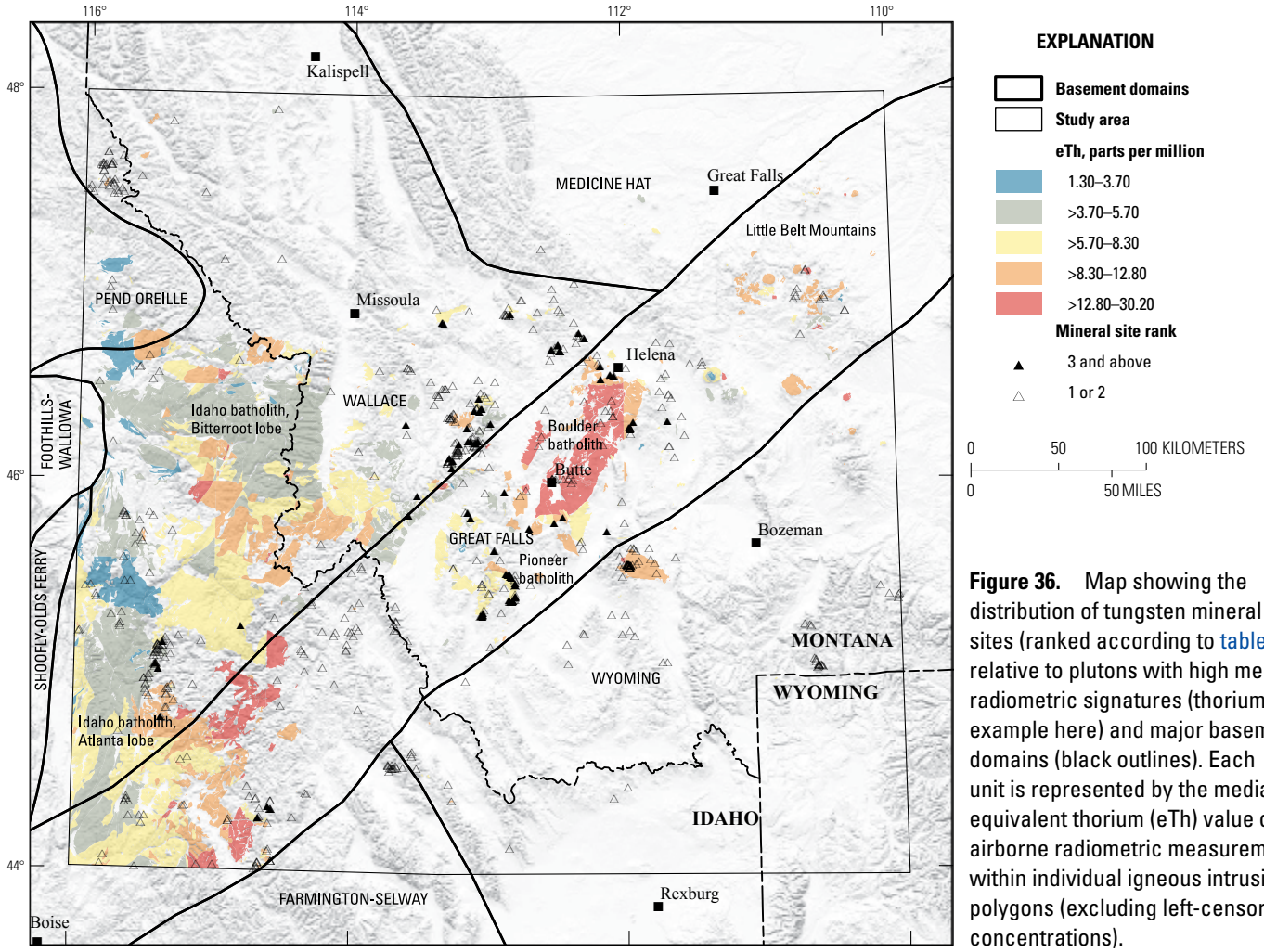


Political boundaries from U.S. Department of State (2009); Shaded relief from U.S. Geological Survey, National Geospatial Program; USA contiguous Albers Equal Area Conic Projection, central meridian 113° W. latitude of origin, 0°; North American Datum of 1983

**Figure 36.** Map showing the distribution of tungsten mineral sites (ranked according to table 2) relative to plutons with high median radiometric signatures (thorium [Th] example here) and major basement domains (black outlines). Each unit is represented by the median equivalent thorium (eTh) value of the airborne radiometric measurements within individual igneous intrusive polygons (excluding left-censored concentrations).

Northwest Territories and Yukon. Hart and others (2004a) report $Fe_2O_3$:FeO ratios of 0.1–0.3 for granitoids of the Tungsten plutonic suite. This suite is a northwest-trending belt of plutons along the eastern margin of the Selwyn basin that hosts the world-class Mactung and Cantung scheelite skarn deposits. Methane-bearing skarn-forming fluids and reduced mineral assemblages (accessory ilmenite) at these deposits are characteristic of very low $fO_2$ environments (Dick and Hodgson, 1982; Bowman and others, 1985; Gerstner and others, 1989).

Across the northern Rocky Mountains study area, some of the more significant tungsten skarn deposits and prospects show a range of redox states. The Browns Lake tungsten deposit (Montana) formed along the contact of a relatively oxidized, metaluminous pluton (Pioneer batholith) with hematitic silty, argillaceous dolomitic limestone. As expected, the associated skarn assemblage is oxidized and consists of magnetite, chalcopyrite, pyrite, bornite, high-andradite garnet, low-hedenbergite pyroxene, hornblende, epidote, and tremolite. Southwest of the fold-and-thrust belt, the Tungsten Jim deposit (Idaho) is hosted by a package of carbonaceous argillite with thin bedded limestones that belong to the Idaho black shale mineral belt, with nearby granite and granodiorite. Pyrrhotite, pyrite, molybdenite, bismuth minerals, hedenbergitic pyroxene, and low-andradite garnet form the reduced skarn assemblage at the Tungsten Jim deposit. Sedimentary host rocks represent a clear change in redox conditions across the study area: oxidized to the east and reduced to the west. The host rocks belong to a Laurentian Proterozoic to Paleozoic passive margin sequence and segmented miogeocline that stretches nearly 5,000 km from southern Nevada through Idaho, Montana, British Columbia, Yukon Territory, and Alaska, including the well-known Selwyn basin in Yukon (Cook, 2015; Johnson and others, 2020; fig. 37). Magma interaction with platform carbonates to the east and carbonaceous slope and basin facies to the west

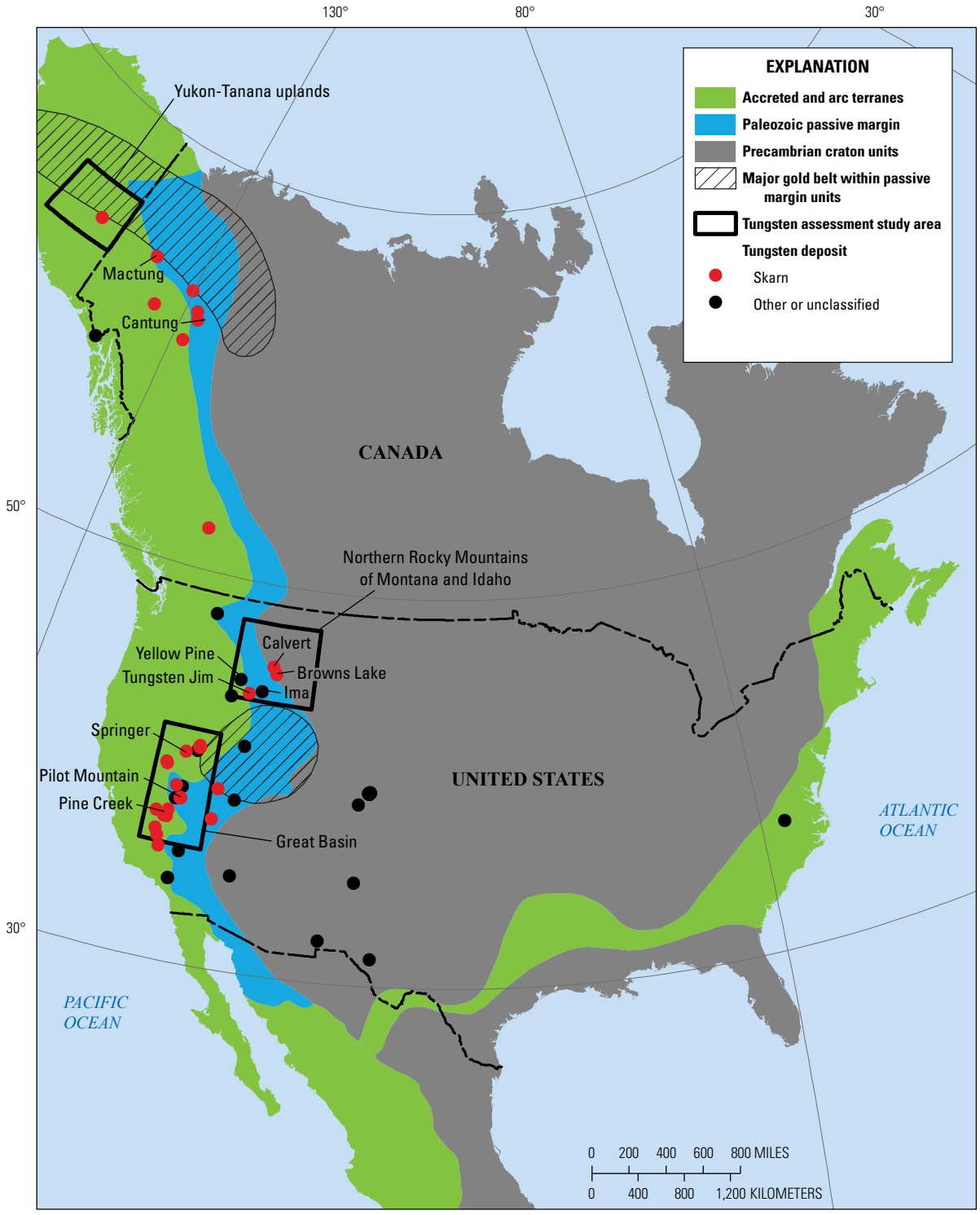


**Figure 37.** Simplified geologic terrane map of North America, highlighting the location of major tungsten provinces and gold belts relative to the Paleozoic passive margin carbonate platform (modified from Johnson and others, 2020). Tungsten assessment study areas include the Yukon-Tanana uplands (Case and others, 2022), Great Basin (Lederer and others, 2021), and Northern Rocky Mountains of Montana and Idaho (this study). Tungsten deposits are compiled from Green and others (2020) and Carroll and others (2018).

may have resulted in the more reduced intrusions and reduced skarn assemblages in eastern Idaho. The same mechanism proposed by Johnson and others (2020), is thought to control intrusion-related metallogeny of the Great Basin with more reduced, gold-rich Carlin-type systems developing to the west and more oxidized, copper-rich porphyry systems developing to the east. Evidence indicates that the eastern edge of the passive margin sequence containing more carbonaceous slope and basin facies is permissive for reduced-intrusion related tungsten skarn, sheeted or stockwork polymetallic (Au+Bi+Te+As±W±Mo±Sb) vein systems, distal mesothermal to epithermal gold-antimony-arsenic±bismuth vein systems, and perhaps Carlin-type gold deposits.

As shown by present-day erosion levels (Barton, 1996; John and others, 2010), plutons of the study area formed at greater depths (7–12 km at the Butte copper-molybdenum deposit, for example) than those of classic porphyry copper deposits (1–6 km). However, study-area plutons formed under conditions more oxidizing than those that produce world-class tungsten skarn deposits and districts with consistently higher tungsten:(molybdenum+copper) ratios. Although the Idaho black shale mineral belt may have provided a local reducing environment, the intruding magmas forming the early border-zone suite of the Idaho batholith would not have been the most highly differentiated, peraluminous, S-type granitoids which are typically more favorable for tungsten mineralization. The relative amounts of copper, molybdenum, and tungsten across the study area—and particularly in those deposits of the Idaho-Montana porphyry belt—are probably controlled by depth, $fO_2$, water saturation, and fluid-melt element partitioning at different stages of crystallization. Intrusion of Cretaceous granitoids into the large thrust sheets dominated by carbonate-shale and argillite sequences was a key factor controlling formation of tungsten skarn deposits of the region. The numerous skarn sites throughout the Montana-Idaho study area, both oxidized and reduced, show that the region is permissive for additional skarn-hosted tungsten resources.

## Acknowledgments

This work was funded by the USGS Mineral Resources Program. We thank leaders of the Mineral Resource Assessment Training (MRAT) project: Jane Hammarstrom, Mark Mihalasky, Patricia Loferski, Gilpin Robinson, and Michael Zientek. We also acknowledge the contribution of the MRAT participants: Damon Bickerstaff, George Case, Joshua Coyan, Kevin Denton, Garth Graham, Carlin Green, Graham Lederer, Erin Marsh, Celestine Mercer, Federico Solano, Ryan Taylor, and Kathryn Watts. We gratefully acknowledge John Wallis for assistance with figures and Alexander Navarra for help with formatting. This report and accompanying data release benefited from reviews by Garth Graham, Stephen Box, Federico Solano, Jeffrey Mauk, and Phil Frederick.

## References Cited

Anderson, J.L., 1983, Proterozoic anorogenic granite plutonism of North America: Geological Society of America Memoir, v. 161, p. 133–154.

Armstrong, R.L., Hollister, V.F., and Harakel, J.E., 1978, K-Ar dates for mineralization in the White-Cloud-Cannivan porphyry molybdenum belt of Idaho and Montana: Economic Geology, v. 73, p. 94–96.

Aro, D.E., 1966, Evaluation of the Calvert Mine, Beaverhead County, Montana: Beaverhead Development Ventures and Minerals Engineering Company. [Private report]

Audétat, A., and Li, W., 2017, The genesis of Climax-type porphyry Mo deposits—Insights from fluid inclusions and melt inclusions: Ore Geology Reviews, v. 88, p. 436–460.

Ballard, W., Bluemie, J., and Gerhard, L., 1983, Northern Rockies/Williston Basin region, correlation of stratigraphic units of North America (COSUNA) project: Tulsa, Okla., American Association of Petroleum Geologists, 1 sheet.

Bankey, V., Cuevas, A., Daniels, D., Finn, C.A., Hernandez, I., Hill, P., Kucks, R., Miles, W., Pilkington, M., Roberts, C., Roest, W., Rystrom, V., Shearer, S., Snyder, S., Sweeney, R.E., Velez, J., Phillips, J.D., and Ravat, D.K.A., 2002, Digital data grids for the magnetic anomaly map of North America: U.S. Geological Survey Open-File Report 2002-414, https://doi.org/10.3133/ofr02414. [Data available at https://mrdata.usgs.gov/magnetic/.]

Barton, M.D., 1996, Granitic magmatism and metallogeny of southwestern North America: Earth and Environmental Science Transactions of the Royal Society of Edinburgh, v. 87, no. 1–2, p. 261–280.

Benjamin, D.A., 1981, Thompson Creek Tungsten mine, Custer County, Idaho: U.S. Bureau of Mines Minerals Availability System Property Evaluation Report—Tungsten, 30 p.

Blevin, P.L., 1998, Paleozoic tin ± tungsten deposits in eastern Australia: AGSO Journal of Australian Geology Geophysics, v. 17, no. 4, p. 75–79.

Blevin, P.L., 2004, Metallogeny of granitic rocks, *in* The Ishihara Symposium—Granites and Associated Metallogenesis, Sydney, Australia, Macquarie University, July 22–24, 2003, Proceedings: Geoscience Australia, p. 1–4.

Blevin, P.L., and Chappell, B.W., 1992, The role of magma sources, oxidation states and fractionation in determining the granite metallogeny of eastern Australia: Earth and Environmental Science Transactions of the Royal Society of Edinburgh, v. 83, no. 1–2, p. 305–316.

Blevin, P.L., and Chappell, B.W., 1995, Chemistry, origin and evolution of mineralized granites in the Lachlan Fold Belt, Australia—The metallogeny of I- and S-type granites: Economic Geology, v. 90, p. 1604–1619.

Boerner, D.E., Craven, J.A., Kurtz, R.D., Ross, G.M., and Jones, F.W., 1998, The Great Falls tectonic zone—Suture or intra-continental shear zone?: Canadian Journal of Earth Sciences, v. 35, p. 175–183.

Bonvalot, S., Balmino, G., Briais, A., Kuhn, M., Peyrefitte, A., Vales, N., Biancale, R., Gabalda, G., Moreaux, G., Reinquin, F., and Sarrailh, M., 2012, World gravity map: Bureau Granimetrique International, 3 plates, scale 1:50,000,000.

Bowman, J.R., Covert, J.J., Clark, A.H., and Mathieson, G.A., 1985, The CanTung E zone scheelite skarn orebody, Tungsten, Northwest Territories—Oxygen, hydrogen, and carbon isotope studies: Economic Geology, v. 80, p. 1872–1895.

Boyle, H.C., and Leitch, C.M.B., 1983, Geology of the Trout Lake molybdenum deposit: Canadian Mining and Metallurgical Bulletin, v. 76, no. 849, p. 115–124.

Bradshaw, H.E., 1981, Exploration at the Ima Mine: Inspiration Development Company, p. 1–16. [Internal report]

Brown, T., and Pitfield, P., 2014, Tungsten, *in* Gunn, G., ed., Critical metals handbook: West Sussex, U.K., John Wiley & Sons, Ltd., p. 385–413.

Burt, D.M., 1982, Skarn deposits—Historical bibliography through 1970: Economic Geology, v. 77, no. 4, p. 755–763.

Camp, V.E., Pierce, K.L., and Morgan, L.A., 2015, Yellowstone plume trigger for Basin and Range extension, and coeval emplacement of the Nevada–Columbia Basin magmatic belt: Geosphere, v. 11, no. 2, p. 203–225.

Carroll, T.R., Schmeda, G., Karl, N.A., Burger, M.H., Long, K.R., and Reyes, T.A., 2018, Tungsten deposits in the United States: U.S. Geological Survey data release, https://doi.org/10.5066/P9XA8MJ4.

Case, G.N.D, Graham, G.E., Marsh, E.E., Taylor, R.D., Green, C.J., Brown P.J., Labay, K.A., 2022, Tungsten skarn potential of the Yukon-Tanana Upland, eastern Alaska, USA—A mineral resource assessment: Journal of Geochemical Exploration, v. 232, no. 106700, 21 p.

Chappell, B.W., and White, A.J.R., 1974, Two contrasting granite types: Pacific Geology, v. 8, p. 173–174.

Chen, Y., Li, H., Sun, W., Ireland, T., Tian, X., Hu, Y., Yang, W., Chen, C., and Xu, D., 2016, Generation of Late Mesozoic Qianlishan A2-type granite in Nanling Range, South China—Implications for Shizhuyuan W–Sn mineralization and tectonic evolution: Lithos, v. 266–267, no. C, p. 435–452.

Chen, Y.-J., Wang, P., Li, N., Yang, Y.-F., and Pirajno, F., 2017a, The collision-type porphyry Mo deposits in Dabie Shan, China: Ore Geology Reviews, v. 81, p. 405–430.

Chen, Y.-J., Zhang, C., Wang, P., Prajno, F., and Li, N., 2017b, The Mo deposits of Northeast China—A powerful indicator of tectonic settings and associated evolutionary trends: Ore Geology Reviews, v. 81, p. 602–640.

Cline, J.S., and Bodnar, R.J., 1991, Can economic porphyry copper mineralization be generated by a typical calc-alkaline melt?: Journal of Geophysical Research, v. 96, no. B5, p. 8113–8126.

Cook, E.F., 1956, Tungsten deposits of south-central Idaho: Idaho Bureau of Mines and Geology Pamphlet No. 108, 40 p., accessed June 8, 2020, at https://www.idahogeology.org/product/p-108.

Cook, H.E., 2015, The evolution and relationship of the western North American Paleozoic carbonate platform and basin depositional environments to Carlin-type gold deposits in the context of carbonate sequence stratigraphy, *in* Pennell, W.M., and Garside, L.J., eds., New concepts and discoveries: Geological Society of Nevada Symposium Proceedings, p. 1–78.

Cookro, T.M., 1985, Depositional controls of breccia-fill and skarn tungsten deposits in the Challis Quadrangle, *in* McIntyre, D.H., ed., Symposium on the geology and mineral deposits of the Challis 1 × 2 Quadrangle, Idaho: U.S. Geological Survey Bulletin 1658 A-S, p. 193–201.

Cookro, T.M., Hall, W.E., and Hobbs, S.W., 1987, Polymetallic skarn deposits, *in* Fisher, F.S., and Johnson, K.M., eds., Preliminary manuscript for "Mineral-resource potential and geology of the Challis 1°×2° quadrangle, Idaho": U.S. Geological Survey Open-File Report 87–480, p. 172–175.

Cookro, T.M., Hall, W.E., and Hobbs, S.W., 1995a, Polymetallic skarn deposits, *in* Fisher, F.S., and Johnson, K.M., eds., Geology and mineral resource assessment of the Challis 1°×2° Quadrangle, Idaho: U.S. Geological Survey Professional Paper 1525, p. 143–145.

Cookro, T.M., Hobbs, S.W., and Hall, W.E., 1995b, Tungsten vein and replacement deposits, *in* Fisher, F.S., and Johnson, K.M., eds., Geology and mineral resource assessment of the Challis 1°×2° Quadrangle, Idaho: U.S. Geological Survey Professional Paper 1525, p. 122–124.

Cox, D.P., 1986, Descriptive model of W skarn deposits, *in* Cox, D.P., and Singer, D.A., eds., Mineral deposit models: U.S. Geological Survey Bulletin 1693, p. 55–57.

Dawson, K.M., 1995, Skarn tungsten, *in* Eckstrand, O.R., Sinclair, W.D., and Thorpe, R.I., eds., Geology of Canadian mineral deposit types: Geological Survey of Canada, Geology of Canada Series, v. 8, p. 495–502.

DeCelles, P.G., 2004, Late Jurassic to Eocene evolution of the Cordilleran thrust belt and foreland basin system, western U.S.A.: American Journal of Science, v. 304, p. 105–168.

Dick, L.A., and Hodgson, C.J., 1982, The MacTung W-Cu-(Zn) contact metasomatic and related deposits of the northeastern Canadian Cordillera: Economic Geology, v. 77, p. 845–867.

du Bray, E.A., Aleinikoff, J.N., and Lund, K., 2012, Synthesis of petrographic, geochemical, and isotopic data for the Boulder batholith, southwest Montana: U.S. Geological Survey Professional Paper 1793, 39 p.

Duval, J.S., Carson, J.M., Holman, P.B., and Darnley, A.G., 2005, Terrestrial radioactivity and gamma-ray exposure in the United States and Canada: U.S. Geological Survey Open-File Report 2005–1413, https://pubs.usgs.gov/of/2005/1413/.

Duval, J.S., Cook, B., and Adams, J.A.S., 1971, Circle of investigation of an air-borne gamma-ray spectrometer: Journal of Geophysical Research, v. 76, no. 35, p. 8466–8470.

Ebbley, N.E., 1966, Review of various methods of developing the Calvert Mine Tungsten Deposit, Montana: Minerals Engineering Company. [Private report]

Einaudi, M.T., and Burt, D.M., 1982, Introduction—Terminology, classification, and composition of skarn deposits: Economic Geology, v. 77, no. 4, p. 745–754.

Einaudi, M.T., Meinert, L.D., and Newberry, R.J., 1981, Skarn deposits, in Skinner, B.J., ed., Seventy-fifth anniversary volume: Society of Economic Geologists, p. 317–391.

Ellefsen, K.J., 2017a, Probability calculations for three-part mineral resource assessments: U.S. Geological Survey Techniques and Methods, book 7, chap. C15, 14 p., https://doi.org/10.3133/tm7C15.

Ellefsen, K.J., 2017b, User's guide for MapMark4—An R package for the probability calculations in three-part mineral resource assessments: U.S. Geological Survey Techniques and Methods, book 7, chap. C14, 23 p., https://doi.org/10.3133/tm7C14.

Ellefsen, K.J., Goldman, M.A., and Van Gosen, B.S., 2020, User guide to the bayesian modeling of non-stationary, univariate, spatial data using R language package BMNUS: U.S. Geological Survey Techniques and Methods, book 7, chap. 20, 27 p., https://doi.org/10.3133/tm7C20.

Elliott, J.E., 1981, Model for contact metasomatic tungsten/copper/gold deposits, *in* Erickson, R.L., ed., Characteristics of mineral deposit occurrences: U.S. Geological Survey Open-File Report 82–795, p. 49–54, https://doi.org/10.3133/ofr82795.

Elliott, J.E., Trautwein, C.M., Wallace, C.A., Lee, G.K., Rowan, L.C., Hanna, W.F., 1993, The Conterminous United States Mineral Assessment Program; background information to accompany folio of geologic, geochemical, remote sensing, and mineral resources maps of the Butte 1°x2° quadrangle, Montana: U.S. Geological Survey Circular 1088, 17p., https://doi.org/10.3133/cir1088.

Elliott, J.E., Wallace, C.A., Lee, G.K., Antweiler, J.C., Lidke, D.J., Rowan, L.C., Hanna, W.F., Trautwein, C.M., Dwyer, J.L., and Moll, S.H.,1992a, Maps showing mineral resource assessment for vein and replacement deposits of gold, silver, copper, lead, zinc, manganese, and tungsten in the Butte 1°x2° quadrangle, Montana: U.S. Geological Survey Map 1-2050-D, scales 1:250,000 and 1:500,000, 31-p. pamphlet, https://doi.org/10.3133/i2050D.

Elliott, J.E., Wallace, C.A., Lee, G.K., Antweiler, J.C., Lidke, D.J., Rowan, L.C., Hanna, W.F., Trautwein, C.M., Dwyer, J.L., and Moll, S.H., 1992b, Maps showing mineral resource assessment for skarn deposits of gold, silver, copper, tungsten, and iron in the Butte 1°×2° quadrangle, Montana: U.S. Geological Survey Miscellaneous Investigation Series Map I–2050–E, scales 1:250,000 and 1:500,000, 30-p.pamphlet, https://doi.org/10.3133/i2050E.

Erickson, G.E., Leinz, R.W., and Marks, L.Y., 1981, Mineral resources of the Flint Creek Range Wilderness Study Area, Granite and Powell Counties, Montana: U.S. Geological Survey Open-File Report 81–1095, 8 p.

Evans, K.V., Aleinikoff, J.N., Obradovich, J.D., and Fanning, C.M., 2000, SHRIMP U-Pb geochronology of volcanic rocks, Belt Supergroup, western Montana—Evidence for rapid deposition of sedimentary strata: Canadian Journal of Earth Sciences, v. 37, no. 9, p. 1287–1300.

Eyde, T.H., 1958, The Potosi tungsten district Madison County, Montana: Montana Bureau of Mines and Geology, Information Circular 21, 51 p.

Fisher, F.S., and Johnson, K.M., 1995, Geology and mineral resource assessment of the Challis 1°×2° Quadrangle, Idaho: U.S. Geological Survey Professional Paper 1525, 205 p., 23 plates.

Fortier, S.M., Nassar, N.T., Lederer, G.W., Brainard, J., Gambogi, J., and McCullough, E.A., 2018, Draft critical mineral list—Summary of methodology and background information—U.S. Geological Survey technical input document in response to Secretarial Order No. 3359: U.S. Geological Survey Open-File Report 2018–1021, 15 p., https://doi.org/10.3133/ofr20181021.

Foster, D.A., Grice, W.C., Jr., and Kalakay, T.J., 2010, Extension of the Anaconda metamorphic core complex—$^{40}Ar/^{39}Ar$ thermochronology and implications for Eocene tectonics of the northern Rocky Mountains and the Boulder batholith: Lithosphere, v. 2, no. 4, p. 232–246.

Foster, D.A., Mueller, P.A., Heatherington, A., Gifford, J.N., and Kalakay, T.J., 2012, Lu-Hf systematics of magmatic zircons reveal a Proterozoic crustal boundary under the Cretaceous Pioneer batholith, Montana: Lithos, v. 142–143, p. 216–225.

Foster, D.A., Mueller, P.A., Mogk, D.W., Wooden, J.L., and Vogl, J.J., 2006, Proterozoic evolution of the western margin of the Wyoming Craton—Implications for the tectonic and magmatic evolution of the northern Rocky Mountains: Canadian Journal of Earth Sciences, v. 43, no. 10, p. 1601–1619.

Frank, D.G., 2016, Historical files from Federal Government mineral exploration-assistance programs, 1950 to 1974: U.S. Geological Survey Data Series 1004, https://pubs.usgs.gov/ds/1004/index.htm.

Frost, B.R., Barnes, C.G., Collins, W.J., Arculus, R.J., Ellis, D.J., and Frost, C.D., 2001, A geochemical classification for granitic rocks: Journal of Petrology, v. 42, p. 2033–2048.

Frost, B.R., and Frost, C.D., 2008, A geochemical classification for feldspathic igneous rocks: Journal of Petrology, v. 49, p. 1955–1969.

Galli, P.E., 1964, Golden Gate tungsten property—Yellow Pine, Idaho: Union Carbide Corporation mine examination, 8 p. [Internal report]

Gaschnig, R.M., Vervoort, J.D., Lewis, R.S., and McClelland, W.C., 2010, Migrating magmatism in the northern US Cordillera—In situ U–Pb geochronology of the Idaho batholith: Contributions to Mineralogy and Petrology, v. 159, no. 6, p. 863–883.

Gaschnig, R.M., Vervoort, J.D., Lewis, R.S., and Tikoff, B., 2011, Isotopic evolution of the Idaho batholith and Challis intrusive province, Northern US Cordillera: Journal of Petrology, v. 52, no. 12, p. 2397–2429.

Gaschnig, R.M., Vervoort, J.D., Lewis, R.S., and Tikoff, B., 2013, Probing for Proterozoic and Archean crust in the northern U.S. cordillera with inherited zircon from the Idaho batholith: Geological Society of America Bulletin, v. 125, no. 1–2, p. 73–88.

Gentor Resources Inc., 2008, Technical Report on the Ima Mine Molybdenum Project: Gentor Resources Inc., prepared by Duke, C. of Wardrop Engineering Inc., 52 p.

Gerstner, M.R., Bowman, J.R., and Pasteris, J.D., 1989, Skarn formation at the Macmillan Pass tungsten deposit (MacTung), Yukon and Northwest Territories—I. P-T-X-V characterization of the methane-bearing skarn-forming fluids: The Canadian Mineralogist, v. 27, no. 4, p. 545–563.

Gifford, J.N., Mueller, P.A., Foster, D.A., and Mogk, D.W., 2014, Precambrian crustal evolution in the Great Falls tectonic zone—Insights from xenoliths from the Montana alkali province: The Journal of Geology, v. 122, no. 5, p. 531–548.

Goldman, M.A., Dicken, C.L., Brown, P.J., Andersen, A.K., Bennett, M.M., and Parks, H.L., 2022, Spatial data associated with tungsten skarn resource assessment of the Northern Rocky Mountains, Montana and Idaho: U.S. Geological Survey data release, https://doi.org/10.5066/P9094RVV.

Green, C., Lederer, G.W., Parks, H.L., and Zientek, M.L., 2020, Grade and tonnage model for tungsten skarn deposits—2020 update: U.S. Geological Survey Scientific Investigations Report, 2020-5085, 23 p., https://doi.org/10.3133/sir20205085.

Groves, D.I., and Bierlein, F.P., 2007, Geodynamic settings of mineral deposit systems: London, Geological Society Journal, v. 164, p. 19–30.

Gustafson, L.B., and Hunt, J.P., 1975, The porphyry copper deposit at El Salvador, Chile: Economic Geology, v. 70, no. 5, p. 857–912.

Hall, W.E., 1985, Stratigraphy of and mineral deposits in the middle and upper Paleozoic rocks of the black-shale mineral belt, central Idaho, chap. J *in* McIntyre, D.H., ed., Symposium on the geology and mineral deposits of the Challis 1°×2° Quadrangle, Idaho: U.S. Geological Survey Bulletin 1658 A-S, p. 117–131., at https://doi.org/10.3133/b1658AS.

Hammarstrom, J.M., Elliott, J.E., Kotlyar, B.B., Theodore, T.G., Nash, J.T., John, D.A., Hoover, D.B., and Knepper, D.H.J., 1995, Sn and (or) W skarn and replacement deposits, chap. 8 *of* du Bray, E.A., ed., Preliminary compilation of descriptive geoenvironmental mineral deposit models: U.S. Geological Survey Open-File Report 95–831, p. 54–61., at https://doi.org/10.3133/ofr95831.

Hart, C.J.R., Goldfarb, R.J., Lewis, L.L., and Mair, J.L., 2004a, The Northern Cordilleran Mid-Cretaceous Plutonic Province—Ilmenite/magnetite-series granitoids and intrusion-related mineralization: Resource Geology, v. 54, no. 3, p. 253–280.

Hart, C.J.R., Mair, J.L., Goldfarb, R.J., and Groves, D.I., 2004b, Source and redox controls on metallogenic variations in intrusion-related ore systems, Tombstone-Tungsten Belt, Yukon Territory, Canada: Earth and Environmental Science Transactions of the Royal Society of Edinburgh, v. 95, no. 1–2, p. 339–356.

Hill, P.L., Kucks, R.P., and Ravat, D., 2009, Aeromagnetic and aeroradiometric data for the conterminous United States and Alaska from the National Uranium Resources Evaluation (NURE) Program of the U.S. Department of Energy: U.S. Geological Survey Open-File Report 2009–1129, https://doi.org/10.3133/ofr20091129.

Hobbs, S.W., and Elliot, J.E., 1973, Tungsten, in Brobst, D.A., and Pratt, W.P., eds., United States Mineral Resources: U.S. Geological Survey Professional Paper 820, p. 667–678.

Hobbs, S.W., and Hays, W.H., 1990, Ordovician and older rocks of the Bayhorse area, Custer County, Idaho: U.S. Geological Survey Bulletin 1891, 50 p., at https://doi.org/10.3133/b1891.

Hobbs, S.W., and Tooker, E.W., 1979, Preliminary map of tungsten provinces in the conterminous United States: U.S. Geological Survey Open-File Report 79–576-C, 1 plate., at https://doi.org/10.3133/ofr79576C.

Horton, J.D., 2017, The state geologic map compilation (SGMC) geodatabase of the conterminous United States (ver. 1.1, August 2017): U.S. Geological Survey data release, https://doi.org/10.5066/F7WH2N65.

Hyndman, D.W., 1983, The Idaho batholith and associated plutons, Idaho and Western Montana: Memoir of the Geological Society of America, v. 159, no. 1, p. 213–240.

Ishihara, S., 1978, Metallogenesis in the Japanese island-arc system: Journal of the Geological Society, v. 135, p. 389–406.

Ishihara, S., 1981, The granitoid series and mineralization: Economic Geology, 75th Anniversary Volume, p. 456–484.

Jayne, D.I., 1984, Gold and antimony resources of the Yellow Pine and Homestake deposits Valley County, Idaho: U.S. Bureau of Mines Minerals Availability System Property Evaluation Report, Gold/Antimony, 74 p.

Jerome, S.E., and Cook, D.R., 1967, Relation of some metal mining districts in the western United States to regional tectonic environments and igneous activity: Nevada Bureau of Mines Bulletin 69, 35 p.

John, D.A., Ayuso, R.A., Barton, M.D., Blakely, R.J., Bodnar, R.J., Dilles, J.H., Gray, F., Graybeal, F.T., Mars, J.C., McPhee, D.K., Seal, R.R., Taylor, R.D., and Vikre, P.G., 2010, Porphyry copper deposit model, chap. B *of* John, D.A., ed., Mineral deposit models for resource assessment: U.S. Geological Survey Scientific Investigations Report 2010–5070-B, 169 p.

Johnson, C.L., Ressel, M.W., and Ruprecht, P., 2020, Toward a global Carlin-Type exploration model—The relationship between Eocene magmatism and diverse gold-rich deposits in the Great Basin, USA, *in* Koutz, F.R., and Pennell, W.M., eds., Vision for discovery: Geological Society of Nevada Symposium Proceedings, p. 28.

Johnson, M.R., Anderson, E.D., Ball, L.B., Drenth, B.J., Grauch, V.J.S., McCafferty, A.E., Scheirer, D.S., Schweitzer, P.N., Shah, A.K., and Smith, B.D., 2019, Airborne geophysical survey inventory of the conterminous United States, Alaska, Hawaii, and Puerto Rico (ver. 2.0, June 2020): U.S. Geological Survey data release, https://doi.org/10.5066/P9K8YTW1.

Jones, V.E., 1934, Spring Hill gold deposit near Helena, Montana: Economic Geology, v. 29, p. 544–559.

Kelbert, A., Egbert, G.D., and DeGroot-Hedlin, C., 2012, Regional 3-D electrical conductivity model of Snake River Plain/Yellowstone, USA based on magnetotelluric data: Geology, v. 40, p. 447–450.

Kiilsgaard, T.H., 1996, Mining properties in Montana that were involved in the DMA, DMEA, OME mineral exploration programs, 1950–1974: U.S. Geological Survey Open-File Report 96–501, 33 p., 1 sheet, scale 1:100,000, at https://doi.org/10.3133/ofr96501.

Kiilsgaard, T.H., 1997, Mining properties in Idaho that were involved in the DMA, DMEA, or OME mineral exploration programs, 1950–1974: U.S. Geological Survey Open-File Report 97–439, 34 p., 1 map., at https://doi.org/10.3133/ofr97439.

Kiilsgaard, T.H., and Lewis, R.S., 1985, Plutonic rocks of Cretaceous age and faults in the Atlanta lobe of the Idaho batholith, Challis quadrangle, chap. B *of* McIntyre, D.H., ed., Symposium on the geology and mineral deposits of the Challis 1°×2° Quadrangle, Idaho: U.S. Geological Survey Bulletin 1658-A-S, p. 29–42.

King, E.M., and Valley, J.W., 2001, The source, magmatic contamination, and alteration of the Idaho batholith: Contributions to Mineralogy and Petrology, v. 142, no. 72–88.

Klein, T.L., 2004, Mineral deposit data for epigenetic base- and precious-metal and uranium-thorium deposits in south-central and southwestern Montana and southern and central Idaho: U.S. Geological Survey Open-File Report 2004–1005, 16 p., https://doi.org/10.3133/ofr20041005.

Klein, T.L., and Sims, P.K., 2007, Control of epigenetic metal deposits by Paleoproterozoic basement architecture, *in* Lund, K., ed., Earth science studies in support of public policy development and land stewardship—Headwaters province, Idaho and Montana: U.S. Geological Survey Circular 1305, 92 p.

Kotlyar, B.B., Ludington, S.D., and Mosier, D.L., 1995, Descriptive, grade, and tonnage models for molybdenum-tungsten greisen deposits: U.S. Geological Survey Open-File Report 95–584, 30 p.

Kuntz, M.A., Covington, H.R., and Schoor, L.J., 1992, An overview of basaltic volcanism of the eastern Snake River Plain, Idaho, *in* Link, P.K., Kuntz, M.A., and Platt, L.B., eds., Regional geology of eastern Idaho and western Wyoming: Geological Society of America Memoir 179, p. 227–267.

Kwak, T.A.P., 1987, W-Sn skarn deposits—And related metamorphic skarns and granitoids: Developments in Economic Geology, v. 24, p. 1–451.

Larson, L.P., Lowrie, R.L., and Leland, G.R., 1971, Availability of tungsten at various prices from resources in the United States: U.S. Bureau of Mines Information Circular 8500, 65 p.

Lawley, C.J.M., Richards, J.P., Anderson, R.G., Creaser, R.A., and Heaman, L.M., 2010, Geochronology and geochemistry of the MAX porphyry Mo deposit and its relationship to Pb-Zn-Ag mineralization, Kootenay Arc, southeastern British Columbia, Canada: Economic Geology, v. 105, p. 1113–1142.

Lederer, G.W., Solano, F., Coyan, J.A., Denton, K.M., Watts, K.E., Mercer, C.N., Bickerstaff, D.P., and Granitto, M., 2021, Tungsten skarn mineral resource assessment of the Great Basin region of western Nevada and eastern California: Journal of Geochemical Exploration, v. 223, no. 106712, 24 p.

Lehnert, K.A., Su, Y., Langmuir, C.H., Sarbas, B., and Nohl, U., 2000, A global geochemical database structure for rocks: Geochemistry, Geophysics, Geosystems, v. 1, no. 5, p. 1–14.

Lemieux, S., Ross, G.M., and Cook, F.A., 2000, Crustal geometry and tectonic evolution of the Archean crustal basement beneath the southern Alberta Plains, from new seismic reflection and potential field studies: Canadian Journal of Earth Sciences, v. 37, p. 1473–1491.

Lewis, R.S., Link, P.K., Stanford, L.R., and Long, S.P., 2012, Geologic map of Idaho: Idaho Geological Survey Geologic Map 9, scale 1:750,000.

Link, P.K., and DeGrey, L., 2020, Digital geology of Idaho, Module 5—Mesozoic thrust belt: Pocatello, Idaho, Idaho State University Department of Geosciences, accessed June 13, 2020, at https://digitalgeology.aws.cose.isu.edu/Digital_Geology_Idaho/Module5/mod5.htm.

Link, P.K., and Janecke, S.U., 1999, Geology of east-central Idaho—Geologic roadlogs for the Big and Little Lost River, Lemhi, and Salmon River Valleys, *in* Hughes, S.S., and Thackray, G.D., eds., Guidebook to the geology of eastern Idaho: Pocatello, Idaho, Idaho Museum of Natural History in cooperation with the ISU Press, p. 295–334.

Ludington, S.D., Moring, B.C., Miller, R.J., Stone, P.A., Bookstrom, A.A., Bedford, D.R., Evans, J.G., Haxel, G.A., Nutt, C.J., Flyn, K.S., and Hopkins, M.J., 2007, Preliminary integrated geologic map databases for the United States, Western States—California, Nevada, Arizona, Washington, Oregon, Idaho, and Utah (ver. 1.3, December 2007): U.S. Geological Survey Open-File Report 2005–1305, digital data.

Lund, K., Box, S.E., Holm-Denoma, C.S., San Juan, C.A., Blakely, R.J., Saltus, R.W., Anderson, E.D., and Dewitt, E.H., 2015, Basement domain map of the conterminous United States and Alaska: U.S. Geological Survey Data Series 898, 41 p., https://doi.org/10.3133/ds898.

Lund, K., Zürcher, L., Hofstra, A.H., Van Gosen, B.S., Benson, M.E., Box, S.E., Anderson, E.D., Bleiwas, D.I., DeAngelo, J., Drake, R.M., II, Fernette, G.L., Giles, S.A., Glen, J.M.G., Haacke, J.E., Horton, J.D., John, D.A., Robinson, G.R., Jr., Rockwell, B.W., San Juan, C.A., Shaffer, B.N., Smith, S.M., and Williams, C.F., 2016, Geology and mineral resources of the north-central Idaho Sagebrush focal area (ver. 1.1, October 27, 2016): U.S. Geological Survey Scientific Investigations Report 2016–5089–C, 147 p.

Lydon, J.W., 2000, A synopsis of the current understanding of the geological environment of the Sullivan deposit: Geological Association of Canada, Mineral Deposits Division, v. 1, p. 12–31.

Mair, J.L., Goldfarb, R.J., Craig, A.J., Hart, C.J.R., and Marsh, E.E., 2006, Geochemical constraints on the genesis of the Scheelite Dome intrusion-related god deposit, Tombstone gold belt, Yukon, Canada: Economic Geology, v. 101, p. 523–553.

McCullough, E.A., and Nassar, N.T., 2017, Assessment of critical minerals—Updated application of an early-warning screening methodology: Mineral Economics, v. 30, p. 257–272.

McDonald, C., Mosolf, J.G., Vuke, S.M., and Lonn, J.D., 2020, Geologic Map of the Elliston 30' × 60' Quadrangle, west-central Montana: Montana Bureau of Mines and Geology, Geologic Map 77, 1 plate, scale 1:100,000.

McFaul, E.J., Mason, G.T., Ferguson, W.B., and Lipin, B.R., 2005, U.S. Geological Survey mineral databases—MRDS and MAS/MILS: U.S. Geological Survey Data Series 52.

McIntyre, D.H., 1985, Symposium on the geology and mineral deposits of the Challis 1°×2° Quadrangle, Idaho: U.S. Geological Survey Bulletin 1658-A-S, 227 p.

Meinert, L.D., 1992, Skarns and skarn deposits: Geoscience Canada, v. 19, no. 4, p. 145–162.

Meinert, L.D., Dipple, G.M., and Nicolescu, S., 2005, World skarn deposits, *in* Hedenquist, J.W., Thompson, J.F.H., Goldfarb, R.J., and Richards, J.P., eds., One hundredth anniversary volume: Society of Economic Geologists, p. 299–336.

Menzie, W.D., and Jones, G.M., 1983, Tungsten skarn, *in* Singer, D.A., and Mosier, D.L., eds., Mineral deposit grade-tonnage models: U.S. Geological Survey Open-File Report 83–623, p. 49–51.

Menzie, W.D., and Jones, G.M., 1986, Grade and tonnage model of W skarn deposits, *in* Cox, D.P., and Singer, D.A., eds., Mineral deposit models: U.S. Geological Survey Bulletin 1693, p. 55–57.

Menzie, W.D., Jones, G.M., and Elliott, J.E., 1992, Tungsten—Grades and tonnages of some deposits, chap. J *of* DeYoung, J.H., and Hammarstrom, J.M., eds., Contributions to commodity geology research: U.S. Geological Survey Bulletin 1877, p. J1–J7.

Meyer, B., Saltus, R., Chulliat, A., 2017, EMAG2v3—Earth magnetic anomaly grid (2-arc-minute resolution): National Centers for Environmental Information, NOAA, accessed June 30, 2020, at https://doi.org/10.7289/V5H70CVX.

Mi, M., Chen, Y.-J., Yang, Y.-F., Wang, P., Li, F.-L., Wan, S.-Q., and Xu, Y.-L., 2015, Geochronology and geochemistry of the giant Qian'echong Mo deposit, Dabie Shan, eastern China—Implications for ore genesis and tectonic setting: Gondwana Research, v. 27, no. 3, p. 1217–1235.

Minty, B., Franklin, R., Milligan, P., Richardson, M., and Wilford, J., 2009, The radiometric map of Australia: Exploration Geophysics, v. 40, no. 4, p. 325–333.

Mitchell, V.E., 1999, History of the Ima Mine, Lemhi County, Idaho: Idaho Geological Survey Staff Report 99-2, 39 p., accessed August 17, 2020, at https://www.idahogeology.org/pub/Staff_Reports/1999/S-99-2.pdf.

Monecke, T., Monecke, J., Reynolds, T. J., Tsuruoka, S., Bennett, M. M., Skewes, W. B., and Palin, R. M., 2018, Quartz Solubility in the H2O-NaCl System—A Framework for Understanding Vein Formation in Porphyry Copper Deposits: Economic Geology, v. 113, p. 1007–1046.

Montana Bureau of Mines and Geology, 2006, Montana Bureau of Mines and Geology abandoned and inactive mines database, 2006: Montana State Library, accessed June 30, 2020, at https://mslservices.mt.gov/Geographic_Information/Data/DataList/datalist_Details?did=%7B2F348EE2-7AB1-4708-8CD1-E56683EB2084%7D.

Mueller, P.A., Burger, H.R., Wooden, J.L., Brady, J.B., Cheney, J.T., Harms, T.A., Heatherington, A.L., and Mogk, D.W., 2005, Paleoproterozoic metamorphism in the northern Wyoming province—Implications for the assembly of Laurentia: The Journal of Geology, v. 113, no. 2, p. 169–179.

Mueller, P.A., Heatherington, A.L., Kelly, D.M., Wooden, J.L., and Mogk, D.W., 2002, Paleoproterozoic crust within the Great Falls tectonic zone—Implications for the assembly of southern Laurentia: Geology, v. 30, no. 2, p. 127–130.

Mutschler, F.E., Wright, E.G., Ludington, S.D., and Abbott, J.T., 1981, Granite molybdenite systems: Economic Geology, v. 76, no. 4, p. 874–897.

Nabighian, M.N., 1972, The analytic signal of two-dimensional magnetic bodies with polygonal cross-section—Its properties and use for automated anomaly interpretation: Geophysics, v. 37, no. 3, p. 507–517.

Newberry, R.J., 1982, Tungsten-bearing skarns of the Sierra Nevada—I—The Pine Creek mine, California: Economic Geology, v. 77, no. 4, p. 823–844.

Newberry, R.J., and Einaudi, M.T., 1981, Tectonic and geochemical setting of tungsten skarn mineralization in the Cordillera: Arizona Geological Society Digest, v. 14, p. 99–112.

Newberry, R.J., and Swanson, S.E., 1986, Scheelite skarn granitoids—An evaluation of the roles of magmatic source and process: Ore Geology Reviews, v. 1, no. 1, p. 57–81.

Noble, S.R., Spooner, E.T.C., and Harris, F.R., 1984, The Logtung large tonnage, low-grade W (scheelite)-Mo porphyry deposit, south-central Yukon Territory: Economic Geology, v. 79, p. 848–868.

O'Neill, J.M., 1998, The Great Falls tectonic zone, Montana-Idaho—An early Proterozoic collisional orogen beneath and south of the Belt basin, *in* Berg, R.B., ed., Belt Symposium III: Montana Bureau of Mines and Geology Special Publication 112, p. 222–228.

O'Neill, J.M., and Lopez, D.A., 1985, Character and regional significance of Great Falls tectonic zone, east-central Idaho and west-central Montana: American Association of Petroleum Geologists Bulletin, v. 69, no. 3, p. 437–447.

Olmore, S.D., 1991, Geologic summary of the Big Ben Molybdenum Deposit near Neihart, Montana, *in* Baker, D.W., and Berg, R.B., eds., Guidebook of the Central Montana Alkalic Province—Geology, ore deposits and origin: Montana Bureau of Mines and Geology Special Publication 100, p. 124–127.

Pardee, J.T., and Schrader, F.C., 1933, Metalliferous deposits of the greater Helena mining region, Montana: U.S. Geological Survey Bulletin 842, 318 p.

Pattee, E.C., 1960, Tungsten resources of Montana—Deposits of the Mount Torrey Batholith, Beaverhead County: U.S. Bureau of Mines Report of Investigations 5552, 41 p.

Pearson, R.C., Trautwein, C.M., Berger, B.R., Hanna, W.F., Jenson, S.K., Loen, J.S., Moll, S.H., Purdy, T.L., Rowan, L.C., Ruppel, E.T., and Segal, D.B., 1992a, Maps showing mineral resource assessment for copper and molybdenum in porphyry and stockwork deposits and for tungsten, iron, gold, copper, and silver in skarn deposits, Dillon 1°×2° quadrangle, Idaho and Montana: U.S. Geological Survey Miscellaneous Investigations Series Map I-1803-G, 3 sheets, scales 1:250,000 and 1:500,000, 28-p. pamphlet, https://doi.org/10.3133/i1803G.

Pearson, R.C., Trautwein, C.M., Ruppel, E.T., Hanna, W.F., Rowan, L.C., Loen, J.S., Berger, B.R., 1992b, Mineral resource assessment of the Dillon 1°×2° quadrangle, Idaho and Montana: U.S. Geological Survey Circular 1077, 15p., https://doi.org/10.3133/cir1077.

Phillips, J.D., 2002, Processing and interpretation of aeromagnetic data for the Santa Cruz Basin—Patagonia Mountains area, south-central Arizona: U.S. Geological Survey Open-File Report 02–98, https://doi.org/10.3133/ofr0298.

Phillips, J.D., Duval, J.S., and Ambroziak, R.D., 1993, National geophysical data grids—Gamma-ray, gravity, magnetic, and topographic data for the conterminous United States: U.S. Geological Survey Digital Data Series DDS-9, https://doi.org/10.3133/ds9.

Pilkington, M., and Keating, P., 2006, The relationship between local wavenumber and analytic signal in magnetic interpretation: Geophysics, v. 71, no. 1, p. L1–L3.

Polya, D.A., Foxford, K.A., Stuart, F., Boyce, A., and Fallick, A.E., 2000, Evolution and paragenetic context of low δD hydrothermal fluids from the Panasqueira W-Sn deposit, Portugal—New evidence from microthermometric, stable isotope, noble gas and halogen analyses of primary fluid inclusions: Geochimica et Cosmochimica Acta, v. 64, p. 3357–3371.

Probst, K.R., 2007, Geochemistry of Cretaceous and Tertiary plutons of the Great Falls Tectonic Zone—Implications for crustal evolution: Gainesville, Florida, University of Florida, M.S. thesis, 50 p.

R Core Team, 2019, R—A language and environment for statistical computing: R Foundation for Statistical Computing, Vienna, accessed on August 1, 2019, at https://www.R-project.org.

Ray, G.E., 1995, W skarns, *in* Lefebure, D.V., and Ray, G.E., eds., Selected British Columbia mineral deposit profiles, volume I—Metallics and coal: British Columbia Ministry of Energy, Mines and Petroleum Resources Open-File Report 1995–20, p. 71–74.

Ray, G.E., 2013, A review of skarns in the Canadian Cordillera: British Columbia Geological Survey Open-File Report 2013–08, 50 p.

Reynolds, M.W., 1979, Character and extent of Basin-Range faulting, western Montana and east-central Idaho, *in* Newman, G.W., and Goode, H.D., eds., 1979 Basin and Range Symposium: Denver, Colo., Rocky Mountain Association of Geologists and the Utah Geological Association, p. 185–193.

Roby, R.N., Ackerman, F.B., Fulkerson, F.B., and Crowley, F.A., 1960, Mines and mineral deposits (except fuels) Jefferson County, Montana: Montana Bureau of Mines and Geology Bulletin 16, 122 p.

Roedder, E., 1984, Fluid inclusions: Mineralogical Society of America, Reviews in Mineralogy & Geochemistry, v. 12, 652 p.

Rostad, O.H., 1978, K-Ar dates for mineralization in the White Cloud-Cannivan porphyry molybdenum belt of Idaho and Montana—A discussion: Economic Geology, v. 73, p. 1366–1368.

Ruppel, E.T., and Lopez, D.A., 1984, The thrust belt in southwest Montana and east-central Idaho: U.S. Geological Survey Professional Paper 1278, 41 p.

Sawkins, F.J., 1984, Metal deposits in relation to plate tectonics: Berlin, Heidelberg, Springer-Verlag, Minerals and rock series, v. 17, 325 p.

Schaltegger, U., Pettke, T., Audétat, A., Reusser, E., and Heinrich, C.A., 2005, Magmatic-to-hydrothermal crystallization in the W–Sn mineralized Mole Granite (NSW, Australia)—Part I—Crystallization of zircon and REE-phosphates over three million years—A geochemical and U–Pb geochronological study: Chemical Geology, v. 220, no. 3–4, p. 215–235.

Schmidt, E.A., Broch, M.J., and White, R.O., 1982, Geology of the Thompson Creek molybdenum deposit, Custer County, Idaho, *in* Ranta, D.E., Kamilli, R.J., and Pansze, A.J., eds., Denver Region Exploration Geologists Society Symposium on the genesis of Rocky Mountain ore deposits—Changes with time and tectonics, Denver, Colorado, November 4–5, 1982, Proceedings: Denver, Colo., Denver Region Exploration Geologists Society, p. 79–84.

Schulz, K.J., DeYoung, J.H., Jr., Seal, R.R., II, and Bradley, D.C., eds., 2017, Critical mineral resources of the United States—Economic and environmental geology and prospects for future supply: U.S. Geological Survey Professional Paper 1802, 797 p.

Sears, J.W., 2007, Belt-Purcell Basin—Keystone of the Rocky Mountain fold-and-thrust belt, United States and Canada: Special Paper of the Geological Society of America, v. 433, no. 7, p. 147–166.

Seedorff, E., Dilles, J.H., Proffett, J.M., Jr., and Einaudi, M.T., Zurcher, L., Stavast, W.J.A., Johnson, D.A., Barton, M.D., 2005, Porphyry deposits—Characteristics and origin of hypogene features: Economic Geology, v. 100, p. 251–298.

Shand, S.J., 1943, The eruptive rocks (2d ed.): John Wiley, New York, 444 p.

Shand, S.J., 1947, The eruptive rocks (3d ed.): John Wiley, New York, 444 p.

Shapiro, J.L., 2018, User's guide for MapMark4GUI—A graphical user interface for the MapMark4 R package: U.S. Geological Survey Techniques and Methods, book 7, chap. C18, 19 p., https://doi.org/10.3133/tm7c18.

Shapiro, J.L., and Robinson, G.R., 2019, Resource assessment economic filter (RAEF)—A graphical user interface supporting implementation of simple engineering mine cost analyses of quantitative mineral resource assessment simulations: U.S. Geological Survey Techniques and Methods, book 7, chap. C23, 18 p., https://doi.org/10.3133/tm7c23.

Sims, P.K., Lund, K., and Anderson, E., 2005, Precambrian crystalline basement map of Idaho—An interpretation of aeromagnetic anomalies: U.S. Geological Survey Scientific Investigations Map 2884, 1 sheet, scale 1:1,000,000.

Sims, P.K., O'Neill, J.M., Bankey, V., and Anderson, E., 2004, Precambrian basement geologic map of Montana—An interpretation of aeromagnetic anomalies: U.S. Geological Survey Scientific Investigations 2829, 1 sheet, scale 1:1,000,000.

Singer, D.A., 1993, Basic concepts in three-part quantitative assessments of undiscovered mineral resources: Nonrenewable Resources, v. 2, no. 2, p. 69–81.

Singer, D.A., 2007, Estimating amounts of undiscovered mineral resources, *in* Briskey, J.A., and Schulz, K.J., eds., Proceedings for a workshop on deposit modeling, mineral resource assessment, and their role in sustainable development: U.S. Geological Survey Circular 1294, p. 79–84.

Singer, D.A., 2010, Progress in integrated quantitative mineral resource assessments: Ore Geology Reviews, v. 38, p. 242–250.

Singer, D.A., Berger, V.I., and Moring, B.C., 2008, Porphyry copper deposits of the world—Database and grade and tonnage models, 2008: U.S. Geological Survey Open-File Report 2008–155, 45 p.

Singer, D.A., and Menzie, W.D., 2010, Quantitative mineral resource assessments—An integrated approach: New York, Oxford University Press, 219 p.

Smith, S.M., Azain, J.S., Bueghly, Z.C., and Olinger, D.A., 2018, Reanalysis of selected archived NURE-HSSR sediment and soil samples from Arizona, California, Idaho, Montana, Nevada, New Mexico, and Utah (ver. 5.0, October 2019): U.S. Geological Survey data release, https://doi.org/10.5066/F7765DHF.

Sonder, L.J., and Jones, C.H., 1999, Western United States extension—How the west was widened: Annual Review of Earth and Planetary Sciences, v. 27, p. 417–462.

Spanski, G.T., 2004, Inventory of significant mineral deposit occurrences in the Headwaters project area in Idaho, Western Montana, and extreme eastern Oregon and Washington: U.S. Geological Survey Open-File Report 2004–1038, 13 p., and digital data, https://doi.org/10.3133/ofr20041038.

Steefel, C.I., and Atkinson, W.W., Jr., 1984, Hydrothermal andalusite and corundum in the low district, Montana: Economic Geology, v. 79, p. 573–579.

Stewart, D.E., Stewart, E.D., Lewis, R.S., Weppner, K.N., and Isakson, V.H., 2016, Geologic map of the Stibnite Quadrangle, Valley County, Idaho: Idaho Geological Survey, Geologic Map 51, 2 plates, scale 1:24,000.

Stoeser, D.B., Green, G.N., Morath, L.C., Heran, W.D., Wilson, A.B., Moore, D.W., and Van Gosen, B.S., 2007, Preliminary integrated geologic map databases for the United States—Central states—Montana, Wyoming, Colorado, New Mexico, North Dakota, South Dakota, Nebraska, Kansas, Oklahoma, Texas, Iowa, Missouri, Arkansas, and Louisiana (ver. 1.2, December 2007): U.S. Geological Survey Open-File Report 2005–1351, digital data, https://doi.org/10.3133/ofr20051351.

Strong, D.F., 1988, A model for granophile mineral deposits, *in* Roberts, R.G., and Sheahan, P.A., eds., Ore deposit models, Volume 1: Geological Association of Canada, p. 155–161.

Tate, C.A., Mitchell, V.E., and Stanford, L.R., 2018, Database of the mines and prospects of Idaho (version 1.2018.1): Idaho Geological Survey Digital Databases (DD-1), digital data, accessed June 8, 2020, at https://www.idahogeology.org/product/dd-1.

Taylor, R.D., Hammarstrom, J.M., Piatak, N.M., and Seal, R.R., 2010, Arc-related porphyry molybdenum deposit model, chap. D of Mineral deposit models for resource assessment: U.S. Geological Survey Scientific Investigations Report 2010–5070-D, 64 p.

Titley, S.R., 2001, Crustal affinities of metallogenesis in the American southwest: Economic Geology, v. 96, p. 1323–1342.

Truckle, D.M., 1988, Geology of the Calvert Hill area, Beaverhead County, Montana: Butte, Montana, Montana Technological University, M.S. thesis, 94 p., scale 1:24,000.

U.S. Bureau of Mines, 1960, Defense minerals exploration administration exploration project contract, Salmon River Scheelite Corporation, Custer County, Idaho: U.S. Bureau of Mines Docket no. 3667, 11 p.

U.S. Bureau of Mines, 1945, Tungsten, antimony, gold—Bradley (Yellowpine) Mine Valley County, Idaho, in War minerals report: U.S. Bureau of Mines, W.M.R. 461, 18 p.

U.S. Department of Defense, 2022, DoD Issues $24.8M Critical Minerals Award to Perpetua Resources: U.S. Department of Defense release, December 19, 2022, accessed February 21, 2023, at https://www.defense.gov/News/Releases/Release/Article/3249350/dod-issues-248m-critical-minerals-award-to-perpetua-resources/.

U.S. Office of the Secretary, 2018, Final list of critical minerals 2018: Federal Register, v. 83, no. 97, p. 23295–23296. [Also available at https://www.federalregister.gov/documents/2018/05/18/2018-10667/final-list-of-critical-minerals-2018.]

U.S. Environmental Protection Agency, 1992, Mine site visit—Cyprus Thompson Creek: U.S. Environmental Protection Agency Archive Document, 31 p.

U.S. Geological Survey, 1999, Digitized aeromagnetic datasets for the conterminous United States, Hawaii, and Puerto Rico: U.S. Geological Survey Open-File Report 99–557, digital data, https://doi.org/10.3133/ofr99557.

U.S. Geological Survey, 2019, Mineral commodity summaries 2019: U.S. Geological Survey, 204 p., https://doi.org/10.3133/70202434.

U.S. Geological Survey and National Geophysical Data Center, 2002, Digital aeromagnetic datasets for the conterminous United States and Hawaii—A companion to the North American magnetic anomaly map: U.S. Geological Survey Open-File Report 2002–361, digital data, https://doi.org/10.3133/ofr02361.

U.S. Tungsten Corporation, 2013, Geological report on the Calvert Tungsten Property, Beaverhead County, Montana and form 8-K: United States Securities and Exchange Commission Form, accessed June 8, 2020, at https://sec.report/Document/0001376474-13-000281.

U.S. Tungsten Corporation, 2014, U.S. Tungsten Corporation amended annual report and form 10-K/A: United States Securities and Exchange Commission, accessed June 8, 2020, at https://www.sec.gov/Archives/edgar/data/0001436309/000127351114000041/us-tungsten_10ka.htm.

Van Gosen, B.S., Eppinger, R.G., Hammarstrom, J.M., Briggs, P.H., Crock, J.G., Gent, C.A., Meier, A.L., Sutley, S.J., and Theodorakos, P.M., 2000, Analytical data for reconnaissance geochemical samples from mine dumps, stream sediments and waters at the Thompson Creek Tungsten Mine, Custer County, Idaho: U.S. Geological Survey Open-File Report 2000–239, 28 p.

Vervoort, J.D., Lewis, R.S., Fisher, C., Gaschnig, R.M., Jansen, A.C., and Brewer, R., 2016, Neoarchean and Paleoproterozoic crystalline basement rocks of north-central Idaho—Constraints on the formation of western Laurentia: Geological Society of America Bulletin, v. 128, no. 1/2, p. 94–109.

Vitz, H.E., 1964, The Bradley antimony-gold-tungsten and gold-antimony deposits, Stibnite, Idaho: Union Carbide Corporation, 6 p. [Internal report]

Volin, M.E., Roby, R.N., and Cole, J.W., 1952, Investigation of the combination silver-tungsten mine, Granite County, Montana: U.S. Bureau of Mines Report of Investigations 4914, 25 p.

Vuke, S.M., Porter, K.W., Lonn, J.D., and Lopez, D.A., 2007, Geologic map of Montana (1st ed.): Montana Bureau of Mines and Geology Geologic Map 62, 67 p., 2 plates.

Walker, D.D., 1960, Tungsten resources of Montana—Deposits of the Philipsburg batholith, Granite and Deer Lodge Counties: U.S. Bureau of Mines Report of Investigations 5612, 55 p.

Walker, D.D., 1963, Tungsten resources of western Montana—Miscellaneous deposits: U.S. Bureau of Mines Report of Investigations 6334, 60 p.

Werner, A.B.T., Sinclair, W.D., and Amey, E.B., 2014, International strategic mineral issues summary report—Tungsten: U.S. Geological Survey Circular 930-O, 86 p.

Westra, G., and Keith, S.B., 1981, Classification and genesis of stockwork molybdenum deposits: Economic Geology, v. 76, p. 844–873.

Wintzer, N.E., 2019, Geology, geochronology, and geochemistry of the Stibnite-Yellow Pine gold-antimony-tungsten mining area, Idaho: Pullman, Wash., Washington State University, Ph.D. thesis, 282 p.

Zientek, M.L., Derkey, P.D., Miller, R.J., Causey, J.D., Bookstrom, A.A., Carlson, M.H., Green, G.N., Frost, T.P., Boleneus, D.E., Evans, K.V., Van Gosen, B.S., Wilson, A.B., Larsen, J.C., Kayser, H.Z., Kelley, W.N., and Assmus, K.C., 2005, Spatial databases for the geology of the Northern Rocky Mountains—Idaho, Montana, and Washington: U.S. Geological Survey Open-File Report 2005–1235, 201 p., https://doi.org/10.3133/ofr200512.

# Glossary

**A-type** Granite which forms in an anorogenic environment and often in stable cratonic interiors, along tectonic rifts, or after an orogenic event. Typically enriched in silica and large-ion lithophile elements.

**I-type** Granite in which geochemical and isotopic characteristics are primarily inherited through the melting of older igneous sources.

**Mineral deposit** An occurrence of a valuable commodity or mineral that is of sufficient size and grade that it might, under the most favorable of circumstances, be considered to have potential for economic development.

**Mineral prospect** A mineral concentration that is being or has been examined to determine whether a mineral deposit exists.

**Mineral occurrence** A locality where a useful mineral or material is found.

**Past producer** A mine formerly operating that has closed and where the equipment or structures may have been removed or abandoned.

**Permissive tract** The surface projection of a volume of rock whose geologic characteristics permit the existence of a specified type of mineral deposit. The probability that deposits of the type being studied occur outside the boundary of the tract is negligible. In this report, the term is commonly abbreviated to "tract."

**Producer** A mine in production at the time the data were entered.

**Resource** A mineral concentration of sufficient size and grade and in such form and amount that economic extraction of a commodity from the concentration is currently or potentially feasible.

**Stockwork** A mineral deposit consisting of a three-dimensional network of planar to irregular veinlets closely enough spaced that the whole mass can be mined.

**S-type** Granite in which geochemical and isotopic characteristics are primarily inherited through partial melting of a crustal sedimentary source.

**Tungstate** A mineral whose essential anionic structure is the orthotungstate tetrahedron ($WO_4^{2-}$), usually combined with $Fe^{2+}$ ($FeWO_4$: ferberite), $Mn^{2+}$ ($MnWO_4$: hübnerite), or $Ca^{2+}$ ($CaWO_4$: scheelite).

**Undiscovered mineral deposit** A mineral deposit that is believed to exist or an incompletely explored mineral occurrence or prospect that could have sufficient size and grade to be classified as a deposit.

**Wolframite** Name for a solid solution that extends from ferberite ($FeWO_4$) to hübnerite ($MnWO_4$). Complete substitution occurs between $Fe^{2+}$ and $Mn^{2+}$ cations. Ferberite is the mineral name used when Fe > Mn and hübnerite is used when Mn > Fe. In this report, the term wolframite is used when the Fe to Mn ratio is unknown.

# Appendix 1-7

# Appendix 1. Pluton Chemistry

By Allen K. Andersen

The three maps in this appendix show plutonic rock classification by sample site. Whole-rock geochemical data for samples within the study area were retrieved from the EarthChem PetDB Website (available at https://search.earthchem.org/; Lehnert and others, 2000), with additional data from du Bray and others (2012) and selected samples for the Pioneer batholith from the National Geochemical Database (available at https://mrdata.usgs.gov/#geochemistry). Samples were classified based on alkalinity index, aluminum saturation index, iron index, modified alkali-lime index, and silicon dioxide content as shown in figures 19, 20, and 21.

# References Cited

du Bray, E.A., Aleinikoff, J.N., and Lund, K., 2012, Synthesis of petrographic, geochemical, and isotopic data for the Boulder batholith, southwest Montana: U.S. Geological Survey Professional Paper 1793, 39 p.

Lehnert, K.A., Su, Y., Langmuir, C.H., Sarbas, B., and Nohl, U., 2000, A global geochemical database structure for rocks: Geochemistry, Geophysics, Geosystems, v. 1, no. 5, p. 1–14.

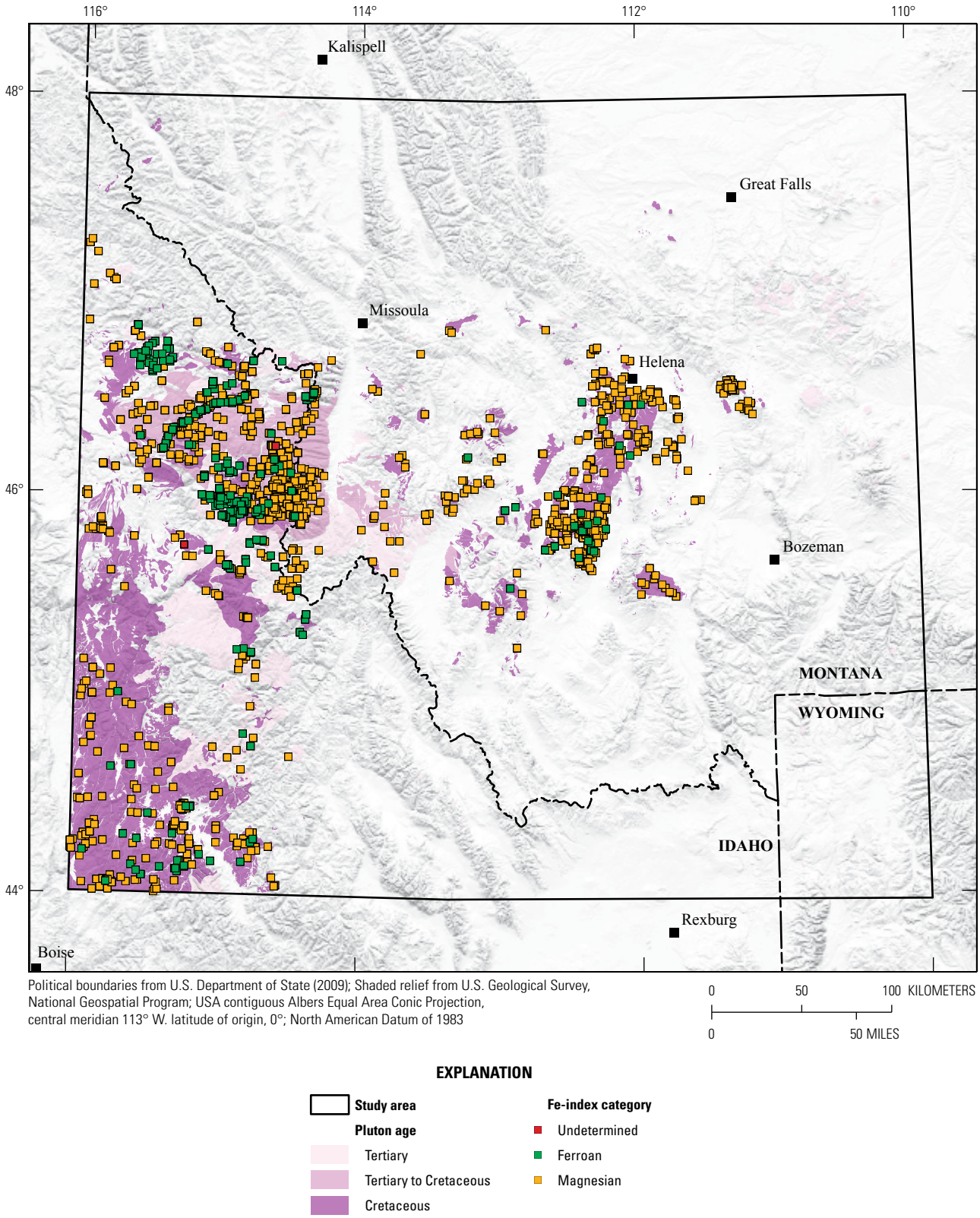


**Figure 1.1.** Map showing the distribution of granitoid samples classified as ferroan or magnesian according to their iron (Fe)-index [$FeO^{total}/(FeO^{total}+MgO)$] and weight percent silicon dioxide content.

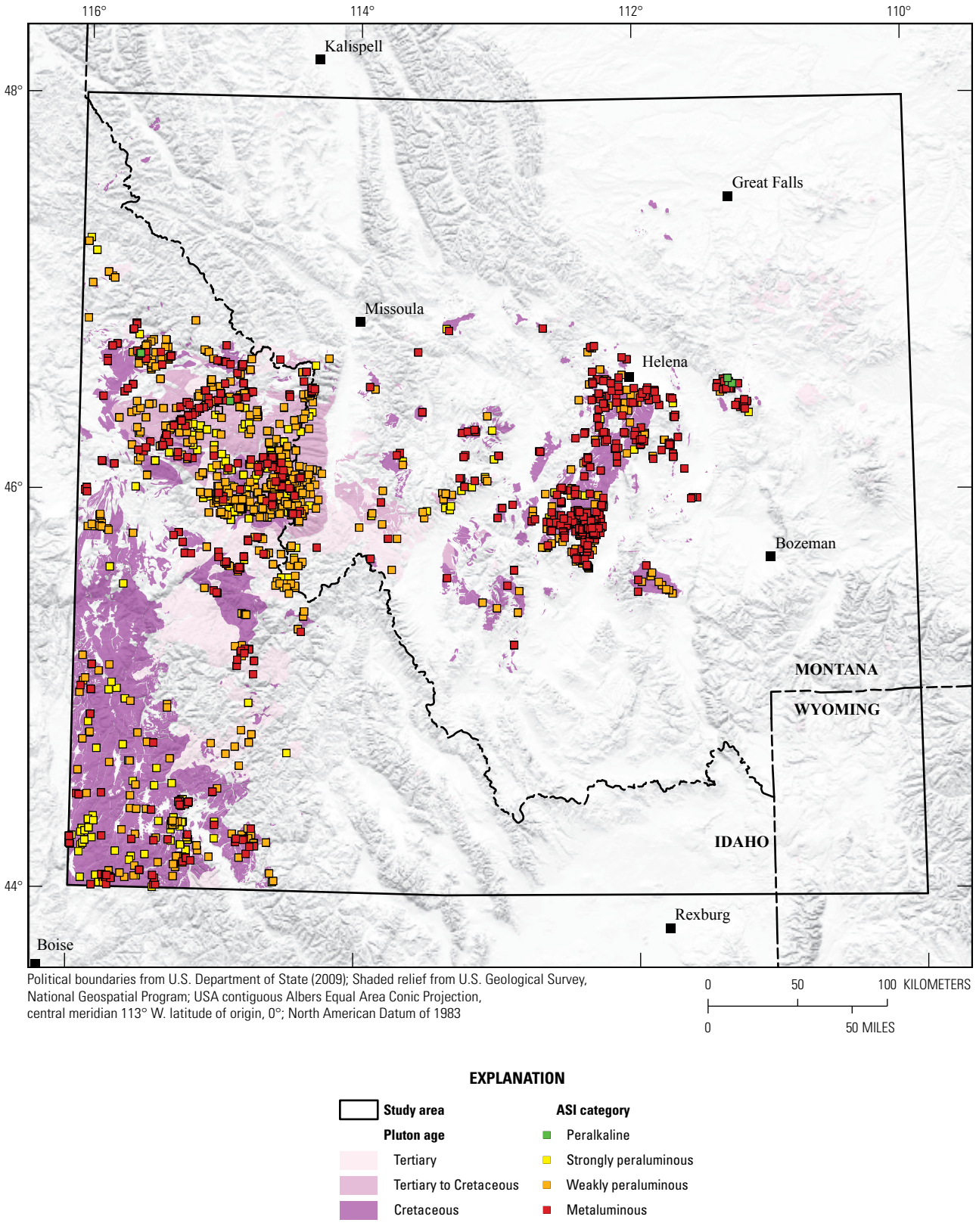


**Figure 1.2.** Map showing the distribution of granitoid samples classified as metaluminous, peraluminous, and peralkaline based on alkalinity index [Al/(Na+K)] and aluminum saturation index [Al/(Na+K+Ca)]. ASI, aluminum saturation index.

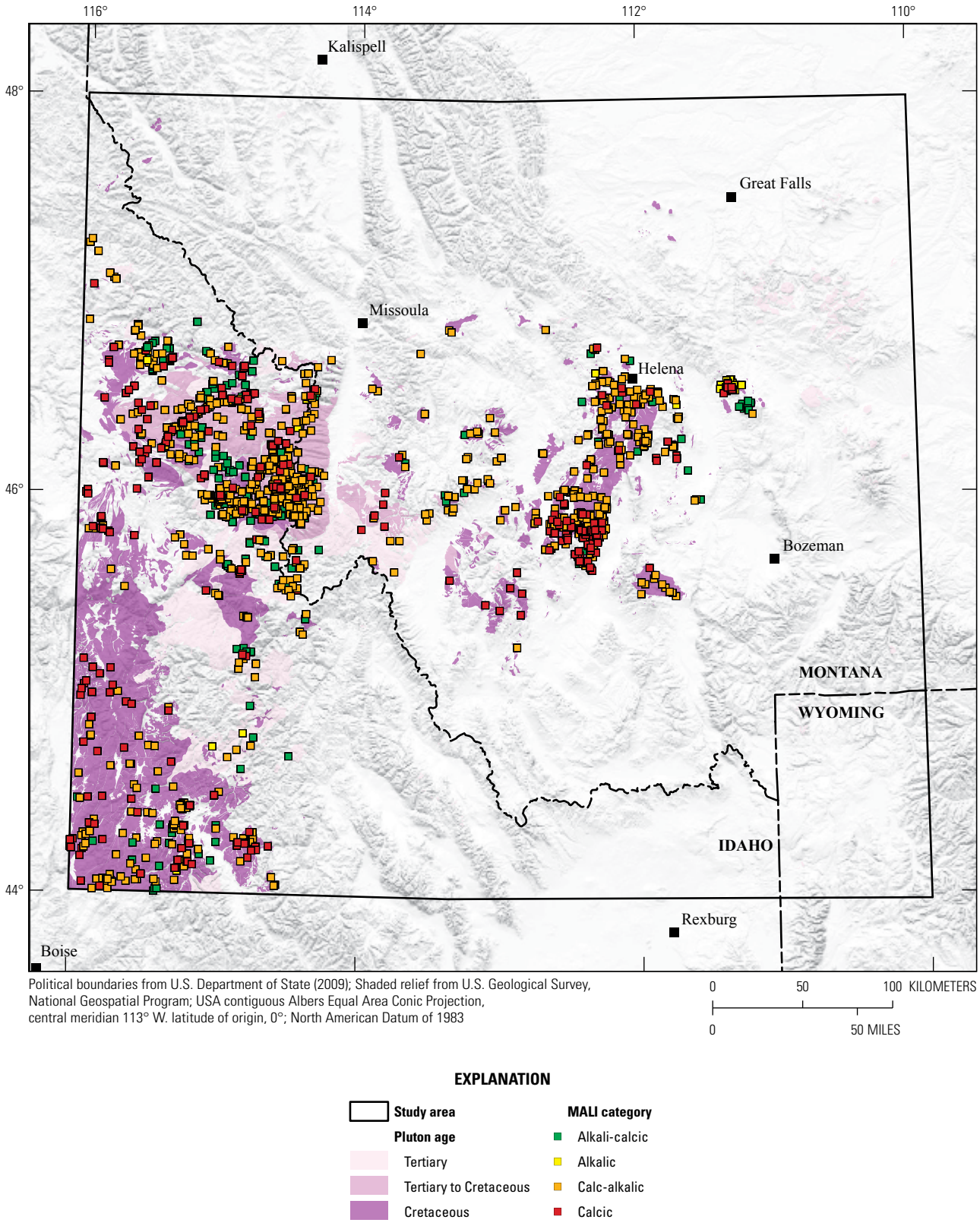


**Figure 1.3.** Map showing the distribution of granitoid samples classified as alkalic, alkali-calcic, calc-alkalic, and calcic based on the modified alkali-lime index ($Na_2O+K_2O-CaO$) and weight percent silicon dioxide content. MALI, modified alkali-lime index.`

# Appendix 2. Components of Histograms and Box Plots Explained

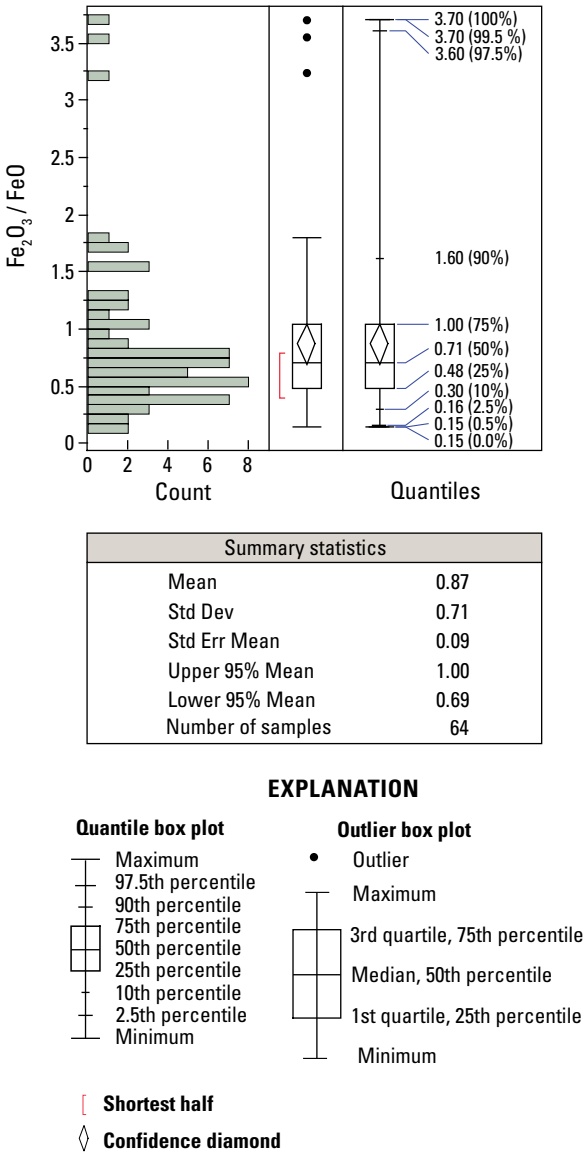


**Figure 2.1.** Histogram and box plot examples with explanation detailing different components of each. On the quantile box plot and outlier box plot, the ends of the box represent the 25th and 75th quantiles, also expressed as the 1st and 3rd quartile, respectively. The difference between the 1st and 3rd quartiles is the interquartile range. Outliers are points that fall outside the distances (length of whiskers, computed as follows: 1st quartile–1.5x(interquartile range) and 3rd quartile+1.5x (interquartile range). The horizontal line within the box represents the median value. The center of the confidence diamond is the mean and the top and bottom points of the diamond represent the upper and lower 95 percent of the mean. The red bracket identifies the shortest half, which is the densest 50 percent of the observations (Rousseeuw and Leroy, 1987).

# Reference Cited

Rousseeuw, P.J., and Leroy, A.M., 1987, Robust regression and outlier detection: New York, John Wiley and Sons, 329 p.

# Appendix 3. Tract Delineation Steps

By Margaret A. Goldman

This appendix provides details on the geoprocessing steps used to delineate tracts in ArcGIS 10.7 (Esri, Redlands, CA). Steps are divided into three parts: initial tract delineation, pre-assessment tract modification, and post-assessment tract modification.

## Input Datasets

- Spatial Databases for the Geology of the Northern Rocky Mountains—Idaho, Montana, and Washington (Northern Rockies; v. 1.0, Zientek and others, 2005)
- The State Geologic Map Compilation (SGMC) Geodatabase of the Conterminous United States (Horton, 2017).

## Initial Tract Delineation

1. Definition queries were used to select polygons from the Northern Rockies and SGMC datasets where carbonate rocks were present.

Northern Rockies feature class: Geology_1235_clip_nr_geo_lith
Definition query:

LNAME_2 LIKE '%carbonat%' OR LNAME_2 LIKE '%calcareous%' OR LNAME_2 = 'mixed siliceous/phosphatic rocks') AND NOT ( nr_geo_mu_AGE = 'Quaternary' OR nr_geo_mu_AGE = 'Quaternary-Tertiary' OR nr_geo_mu_AGE = 'Tertiary' OR nr_geo_mu_AGE = 'Cretaceous')

SGMC feature class: SGMC_Geology (polygon)
Definition query:

MAJOR1 = 'Dolostone' OR MAJOR1 = 'Limestone' OR MAJOR1 = 'Marble' OR MAJOR2 = 'Dolostone' OR MAJOR2 = 'Limestone' OR MAJOR3 = 'Dolostone' OR MAJOR3 = 'Limestone'

2. Definition queries were used to select polygons from the Northern Rockies and SGMC datasets where igneous rocks of appropriate composition and depth of emplacement were present.

Northern Rockies feature class: Geology_1235_clip_nr_geo_igmu
Definition query:

(NOT (IG_STYLE LIKE '%volc%' OR IG_STYLE = 'pyroclastic, sedimentary' OR IG_STYLE LIKE '%hypa%')) AND (IG_AGE LIKE '%Creta%' OR IG_AGE LIKE '%Tert%') AND NOT ( IG_NAME = 'Cretaceous-Jurassic meta-gabbro' OR IG_NAME = 'Cretaceous-Middle Proterozoic meta-intrusive rocks, mafic' OR IG_NAME = 'Cretaceous-Middle Proterozoic meta-ultramafic rocks' OR IG_NAME = 'Cretaceous gabbro' OR IG_NAME = 'Cretaceous syenite-pyroxenite suite' OR IG_NAME = 'Tertiary syenite suite')

SGMC feature class: SGMC_Geology (polygon)
Definition query:

(AGE_MIN LIKE '%Creta%' OR AGE_MIN LIKE '%Tert%' OR AGE_MAX LIKE '%Creta%' OR AGE_MAX LIKE '%Tert%') AND GENERALIZED_LITH = 'Igneous, intrusive'

3. SGMC igneous and carbonate units within the extent of the Northern Rockies dataset were removed, leaving selected only those units outside the Northern Rockies extent and within the study area.
4. The selected igneous units from the Northern Rockies and SGMC datasets were merged.
5. The selected carbonate units from the Northern Rockies and SGMC datasets were merged.
6. Merged carbonate polygons were buffered using a 2,000-meter (m) buffer and dissolved into a single polygon.
7. Merged igneous polygons were buffered using a 2,000-m buffer and dissolved into a single polygon.

8. The buffered igneous and buffered carbonate polygons were intersected, resulting in a preliminary tract of approximately 15,600 square kilometers ($km^2$).
9. Polygon parts and holes less than 1 $km^2$ were removed.

## Pre-Assessment Tract Modification

1. The initial multipart tract was exploded, resulting in the parts becoming independent features.
2. The resulting polygons were classified as Bitterroot, GFTZ–Cretaceous, GFTZ–Tertiary, and Yellowstone/Jardine.
3. Minor adjustments to some polygons were made manually in the geographic information system (GIS; see the "Tract Delineation" section) prior to the assessment.
4. The Bitterroot and GFTZ–Cretaceous tracts were selected for the assessment. The GFTZ–Tertiary and Yellowstone/Jardine tracts were removed. The Bitterroot tract (5,217 $km^2$) was then assessed qualitatively and the GFTZ–Cretaceous tract (7,576 $km^2$) was assessed quantitatively.

## Post-Assessment Tract Modification

1. Additional minor adjustments to some polygons were made manually in the GIS (see "Tract Delineation" section) following the assessment.
2. Used the *Aggregate* tool to aggregate polygons within 200 m (by tract).
3. Removed polygons with less than 1 $km^2$ extent.
4. Used the *Smooth Polygons* tool with a 10-km tolerance to smooth polygon boundaries.
5. Calculated the difference in area of each polygon between polygons from steps 3 and 2 and classified polygons based on the difference in area: 3 classes, using quantile breaks.
6. Added a column with buffer values based on the classes defined in Step 5. A value of 100 m was assigned to the class with the smallest area difference; 300 m was assigned to the class with a moderate area difference, and 600 m was assigned to the class with the largest area difference. The *Buffer* tool was then run using this column to set the buffer distance for the smoothed polygons.
7. Dissolved polygons by tract and calculated the final area. These steps resulted in a total tract area of 5,770 $km^2$ for the Bitterroot tract and 7,946 $km^2$ for the GFTZ–Cretaceous tract.

# References Cited

Horton, J.D., 2017, The state geologic map compilation (SGMC) geodatabase of the conterminous United States (ver. 1.1, August 2017): U.S. Geological Survey data release, https://doi.org/10.5066/F7WH2N65.

Zientek, M.L., Derkey, P.D., Miller, R.J., Causey, J.D., Bookstrom, A.A., Carlson, M.H., Green, G.N., Frost, T.P., Boleneus, D.E., Evans, K.V., Van Gosen, B.S., Wilson, A.B., Larsen, J.C., Kayser, H.Z., Kelley, W.N., and Assmus, K.C., 2005, Spatial databases for the geology of the Northern Rocky Mountains—Idaho, Montana, and Washington, Version 1.0: U.S. Geological Survey Open-File Report 2005–1235, 201 p., https://doi.org/10.3133/ofr20051235.

# Appendix 4. Radiometric Data

By Margaret A. Goldman

The radiometric maps in this appendix show similar geographic trends for all three elements: equivalent thorium (eTh), equivalent uranium (eU), and potassium (K). Higher concentrations of these elements, inferred from airborne radiometric measurements, occur in proximity to the Great Falls tectonic zone and in the southeast corner of the study area around the Yellowstone and Island Park calderas. In maps showing element enrichments summarized by igneous intrusive units (figs. 4.1, 4.2, 4.3), the Boulder batholith shows the highest concentrations in eTh, eU, and K. Elevated concentrations of all three elements are also found in the Atlanta lobe of the Idaho batholith including areas near the Thompson Creek and Yellow Pine Mines. Tertiary plutons in the Bitterrot Lobe of the Idaho batholith also show slightly elevated concentrations in eTh, eU, and K. Similar results were obtained on maps showing prediction surfaces of eTh, eU, and K for the study area derived from Bayesian kriging of the national airborne radiometric dataset (figs. 4.4, 4.5, 4.6). Although not used quantitatively in this assessment, the maps demonstrate how radiometric data could be useful, in combination with other data, in data-driven delineation of tract boundaries for other mineral resource assessments.

## References Cited

Duval, J.S., Carson, J.M., Holman, P.B., and Darnley, A.G., 2005, Terrestrial radioactivity and gamma-ray exposure in the United States and Canada: U.S. Geological Survey Open-File Report 2005–1413, https://doi.org/10.3133/ofr20051413.

Ellefsen, K.J., Goldman, M.A., and Van Gosen, B.S., 2020, User guide to the Bayesian modeling of non-stationary, univariate, spatial data using R language package BMNUS: U.S. Geological Survey Techniques and Methods, book 7, chap. 20, 27 p., https://doi.org/10.3133/tm7C20.

Ellefsen, K.J., and Van Gosen, B.S., 2020, Bayesian modeling of non-stationary, univariate, spatial data for the Earth sciences: U.S. Geological Survey Techniques and Methods, book 7, chap. C24, 20 p., https://doi.org/10.3133/tm7C24.

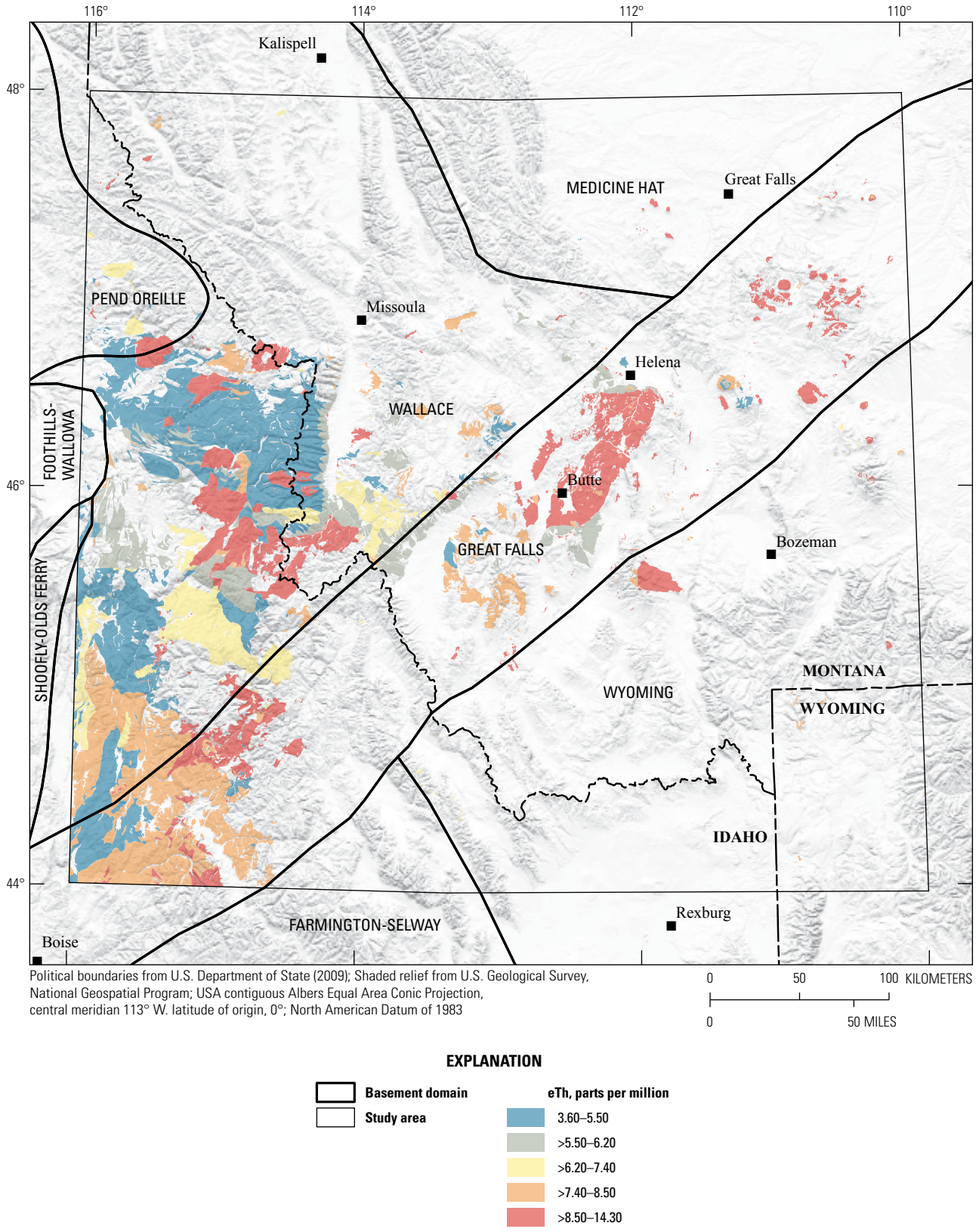


**Figure 4.1.** Map showing equivalent thorium (eTh) concentrations summarized by igneous intrusive unit in the northern Rocky Mountains tungsten skarn study area. Each unit is represented by the median eTh value of the airborne radiometric measurements within the unit (excluding left-censored concentrations).

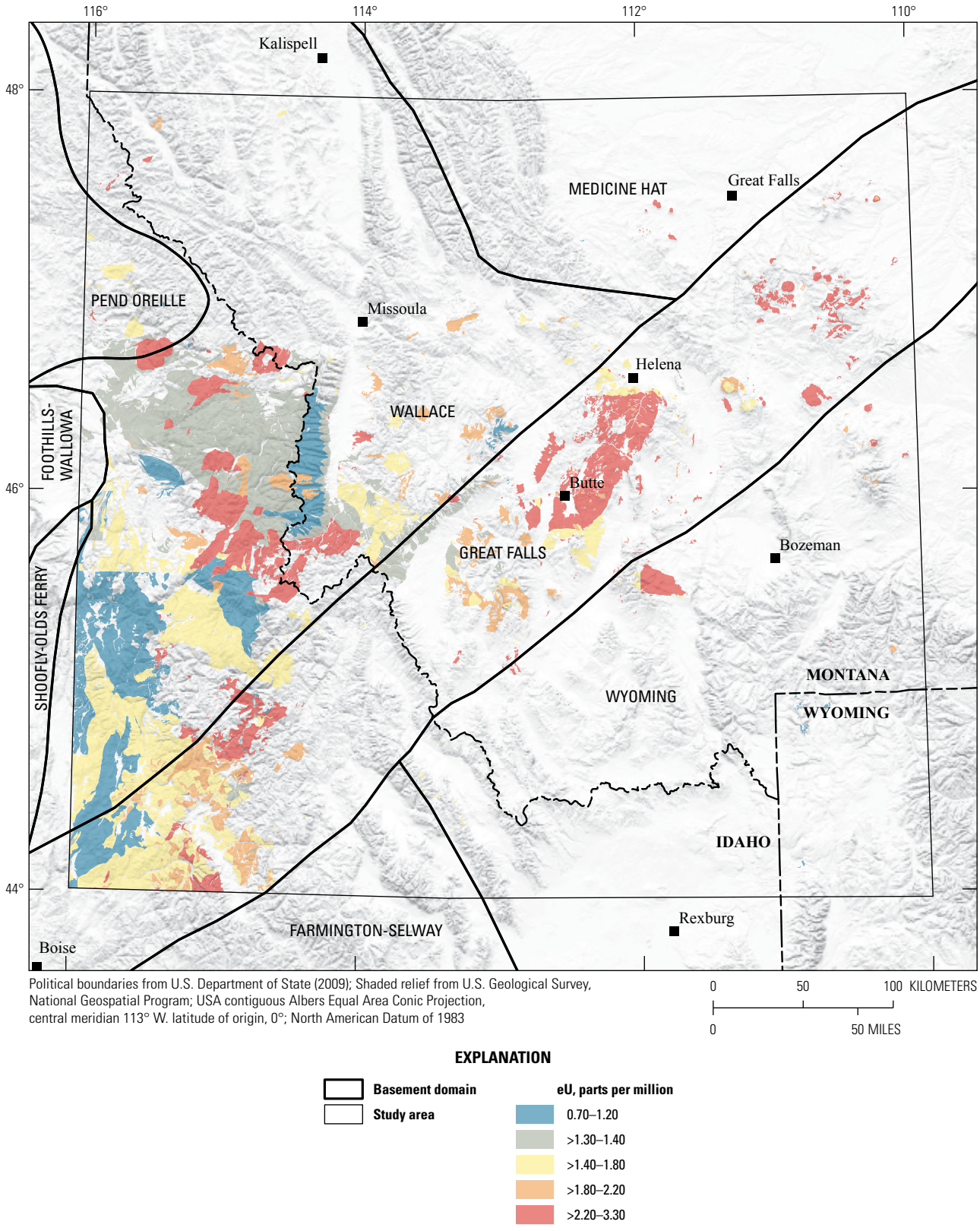


**Figure 4.2.** Map showing equivalent uranium (eU) concentrations summarized by igneous intrusive unit in the northern Rocky Mountains tungsten skarn study area. Each unit is represented by the median eU value of the airborne radiometric measurements within the unit (excluding left-censored concentrations).

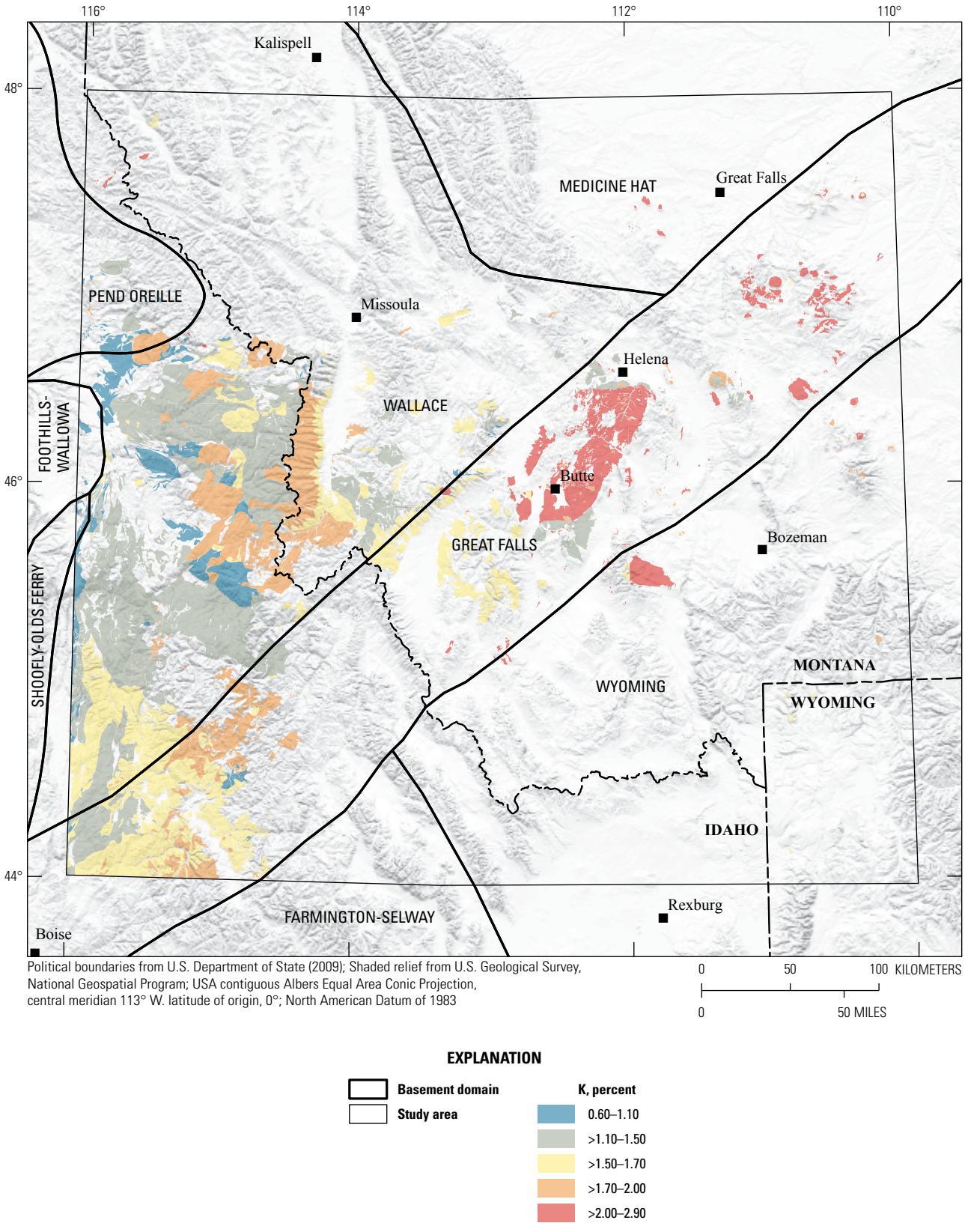


**Figure 4.3.** Map showing potassium (K) concentrations summarized by igneous intrusive unit in the northern Rocky Mountains tungsten skarn study area. Each unit is represented by the median K value of the airborne radiometric measurements within the unit (excluding left-censored concentrations).

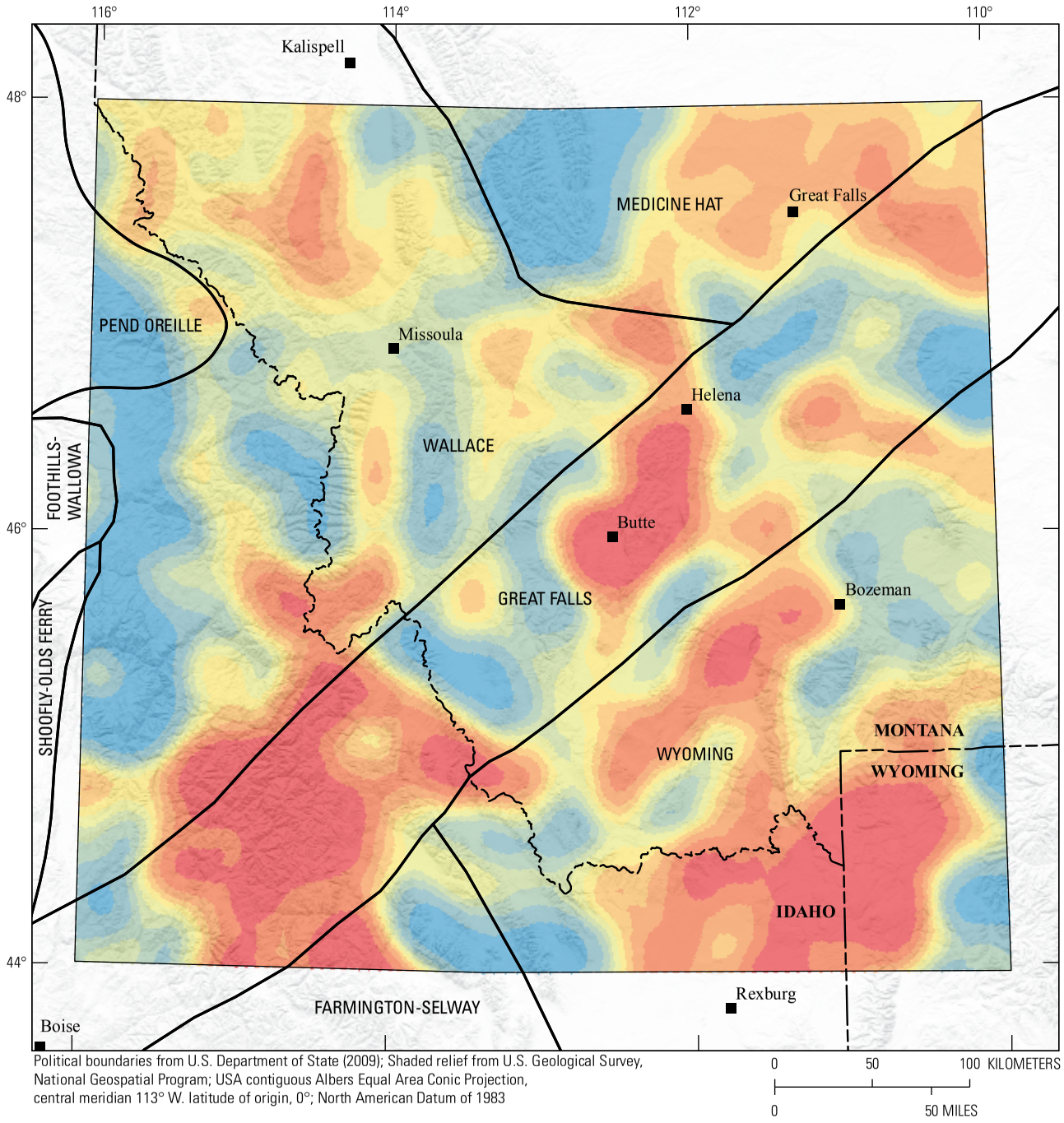


Political boundaries from U.S. Department of State (2009); Shaded relief from U.S. Geological Survey, National Geospatial Program; USA contiguous Albers Equal Area Conic Projection, central meridian 113° W. latitude of origin, 0°; North American Datum of 1983

**Figure 4.4.** Map showing predicted equivalent thorium (eTh) concentrations in the northern Rocky Mountains tungsten skarn study area derived from Bayesian kriging of the national airborne radiometric dataset (Duval and others, 2005; Ellefsen and others, 2020; Ellefsen and Van Gosen, 2020).

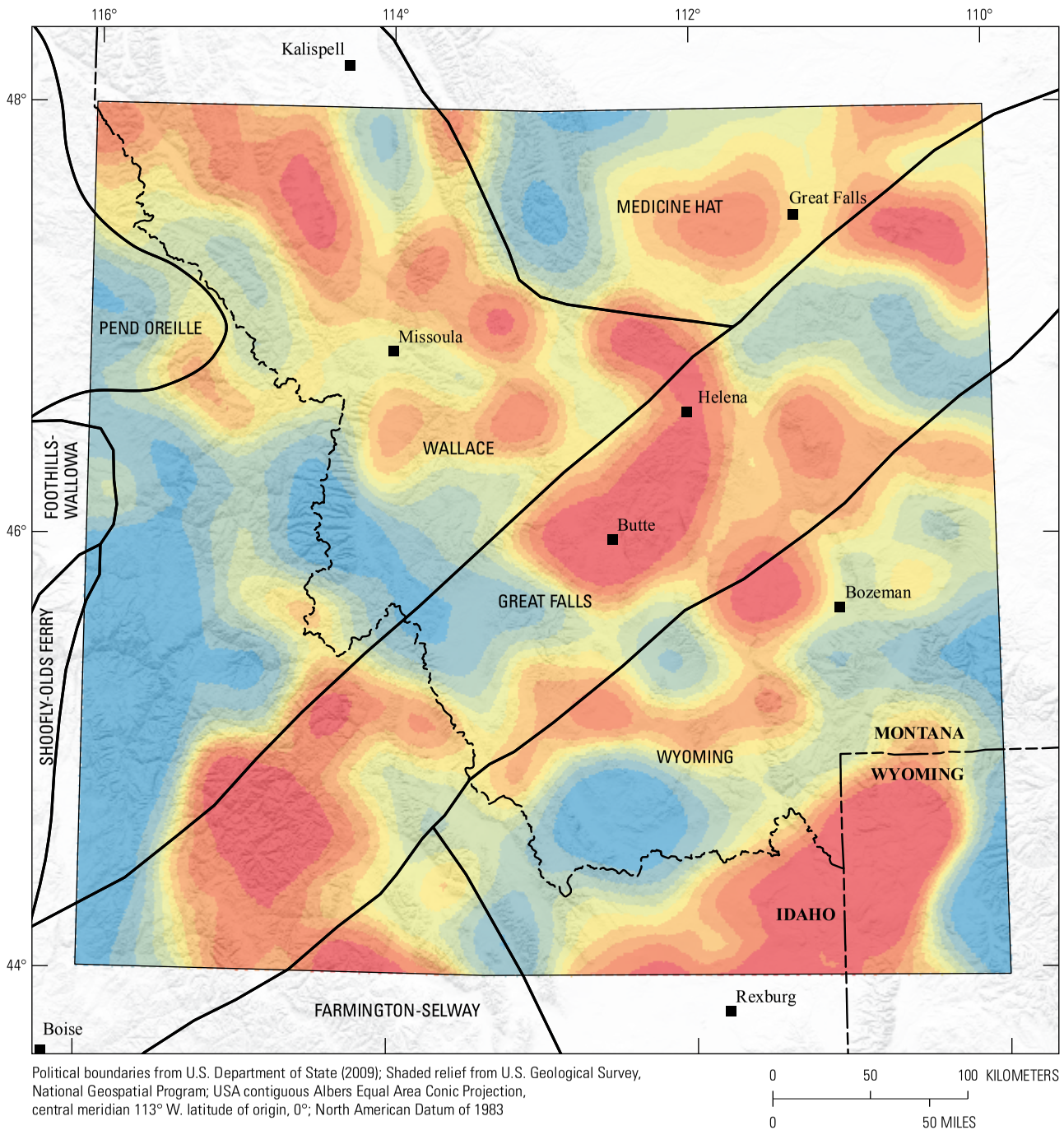


**Figure 4.5.** Map showing predicted equivalent uranium (eU) concentrations in the northern Rocky Mountains tungsten skarn study area derived from Bayesian kriging of the national airborne radiometric dataset (Duval and others, 2005; Ellefsen and others, 2020; Ellefsen and Van Gosen, 2020).

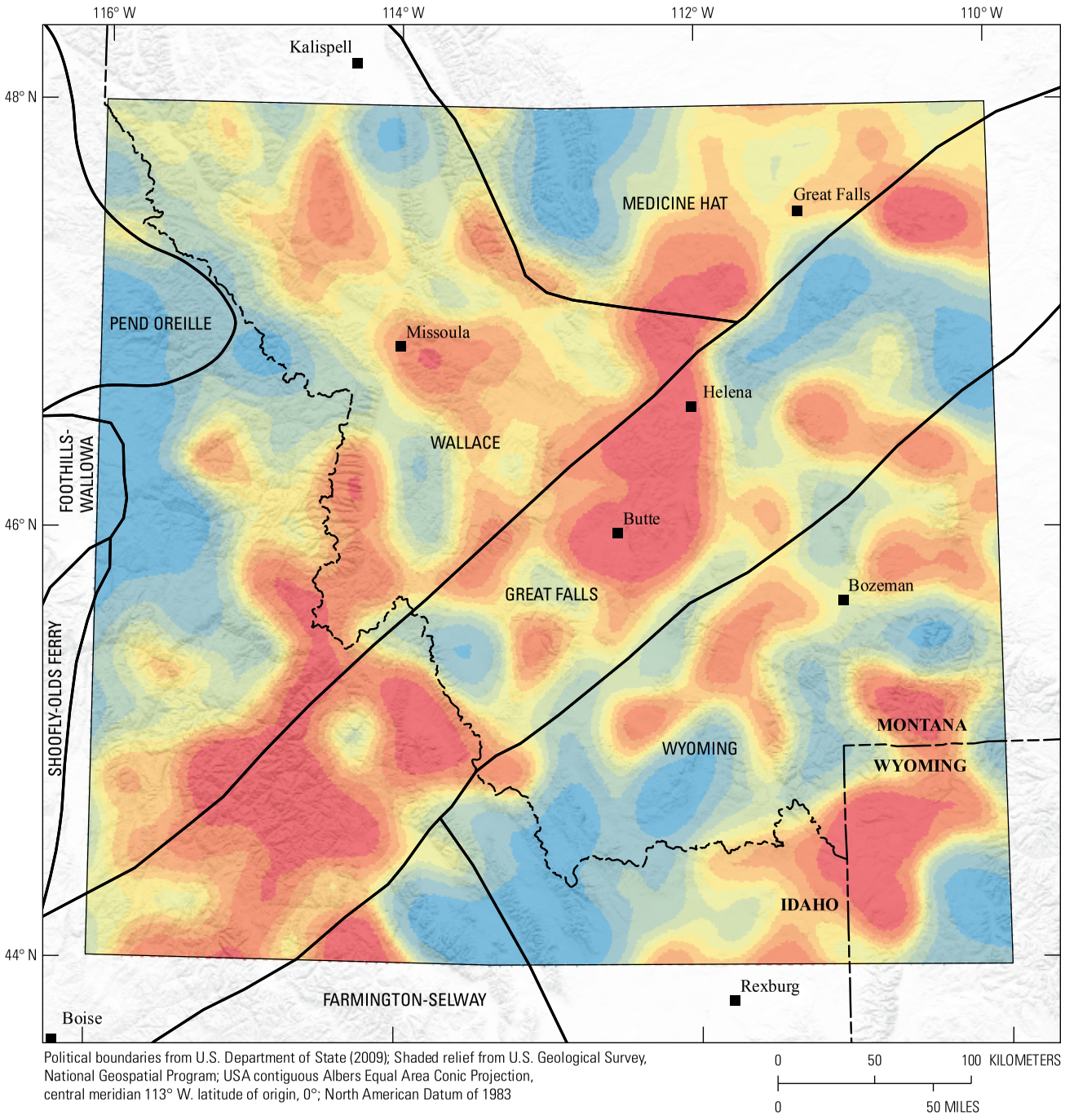


**Figure 4.6.** Map showing predicted K concentrations in the northern Rocky Mountains tungsten skarn study area derived from Bayesian kriging of the national airborne radiometric dataset (Duval and others, 2005; Ellefsen and others, 2020; Ellefsen and Van Gosen, 2020).

# Appendix 5. Airborne Magnetic Data

By Philip J. Brown

The merged airborne magnetic datasets from the U.S. Geological Survey (Bankey and others, 2002) and the National Oceanic and Atmospheric Administration (Meyer and others, 2017) were processed to enhance qualities of interest in the data. For skarn systems of the northern Rocky Mountains study area, zones of greatest tungsten potential are considered to be within 2 kilometers (km) of igneous intrusions and at a depth of less than 1 km. Given the depth and spatial extent of the targets being considered, the airborne data do not have high enough resolution to quantitatively model tungsten deposits. To enhance the signal from the shallower source bodies, a residual map was created from the Magnetic Map of North America (Bankey and others, 2002) and the lower-frequency content earth magnetic anomaly grid (EMAG2) data (Meyer and others, 2017). This creates a residual total magnetic field intensity map which is similar to running a high-pass filter on the Magnetic Map of North America data in the Frequency Domain but is simpler to create.

Analytic Signal and Local Wave Number algorithms (Nabighian, 1972; Phillips, 2002; Pilkington and Keating, 2006) were then applied to the total field EMAG North American Magnetic residual data. After these processing steps, it was observed that anomalous areas of the Local Wavenumber Grid consistently overlap areas of known tungsten mineral occurrences. Plotting the local wavenumber values ranging in amplitude from 50 to 65 produces a map of filtered magnetic responses that envelop igneous body edges known to be associated with tungsten skarn mineralization. The resulting map in effect is a plan-view "target-map" that may be used with other geologic and geochemical information to identify areas permissive for undiscovered or covered tungsten skarn deposits.

Although aeromagnetic data were not used quantitatively in this assessment, these data positively correlate with zones permissive for tungsten mineralization based upon known prospects, geochemical information, and geologic mapping (figure 5.1). For future assessments, these data could be utilized in select areas to extend permissive areas under-cover and downslope of known mineral-producing contacts. Combined with geological and geochemical information, these data could be used as part of a data-driven interpretation algorithm used to automatically determine tract boundaries.

## References Cited

Bankey, V., Cuevas, A., Daniels, D., Finn, C.A., Hernandez, I., Hill, P., Kucks, R., Miles, W., Pilkington, M., Roberts, C., Roest, W., Rystrom, V., Shearer, S., Snyder, S., Sweeney, R.E., Velez, J., Phillips, J.D., and Ravat, D.K.A., 2002, Digital data grids for the magnetic anomaly map of North America: U.S. Geological Survey Open-File Report 2002-414, https://doi.org/10.3133/ofr02414. [Data available at https://mrdata.usgs.gov/magnetic/.]

Meyer, B., Saltus, R., Chulliat, A., 2017, EMAG2v3—Earth magnetic anomaly grid (2-arc-minute resolution): National Centers for Environmental Information, NOAA, accessed June 30, 2020, at https://doi.org/10.7289/V5H70CVX.

Nabighian, M.N., 1972, The analytic signal of two-dimensional magnetic bodies with polygonal cross-section—Its properties and use for automated anomaly interpretation: Geophysics, v. 37, no. 3, p. 507–517.

Phillips, J.D., 2002, Processing and interpretation of aeromagnetic data for the Santa Cruz Basin—Patagonia Mountains area, south-central Arizona: U.S. Geological Survey Open-File Report 02–98, https://doi.org/10.3133/ofr0298.

Pilkington, M., and Keating, P., 2006, The relationship between local wavenumber and analytic signal in magnetic interpretation: Geophysics, v. 71, no. 1, p. L1–L3.

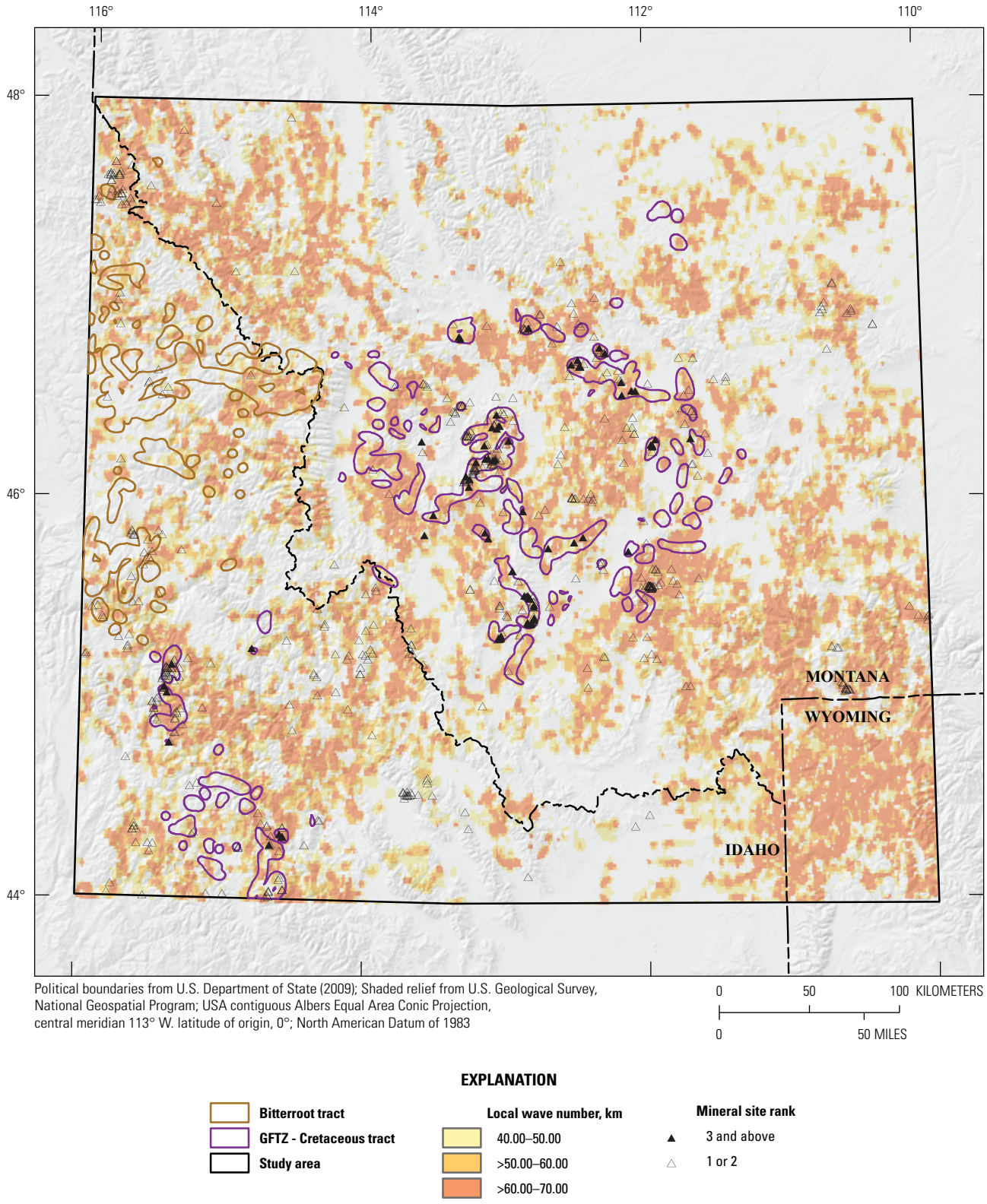


**Figure 5.1.** Map showing local wave number for the northern Rocky Mountains tungsten skarn study area. km, kilometers.

# Appendix 6. Impact of Experience on Undiscovered Deposit Estimates

By Allen K. Andersen and Heather L. Parks

Each member of the 21-person assessment panel convened in August 2019 made an independent estimate of the number of undiscovered deposits for the GFTZ-Cretaceous tract. After an initial round of estimates, results were shared and discussed, resulting in panelists adjusting some estimates during a second round. Results of the two rounds of assessments are presented in figure 6.1 and table 6.1, categorized by estimator experience level (high, medium, low, and none). In each round, 19 of the 21 panelists provided estimates. Details on estimator experience level are shown in table 6.2. Estimators with a greater level of experience in making undiscovered-deposit estimates generally gave higher estimates for each percentile. The discussion between rounds one and two had minimal impact on the estimates with novice estimators still generally giving lower estimates than more experienced estimators. The second-round consensus was chosen for the assessment.

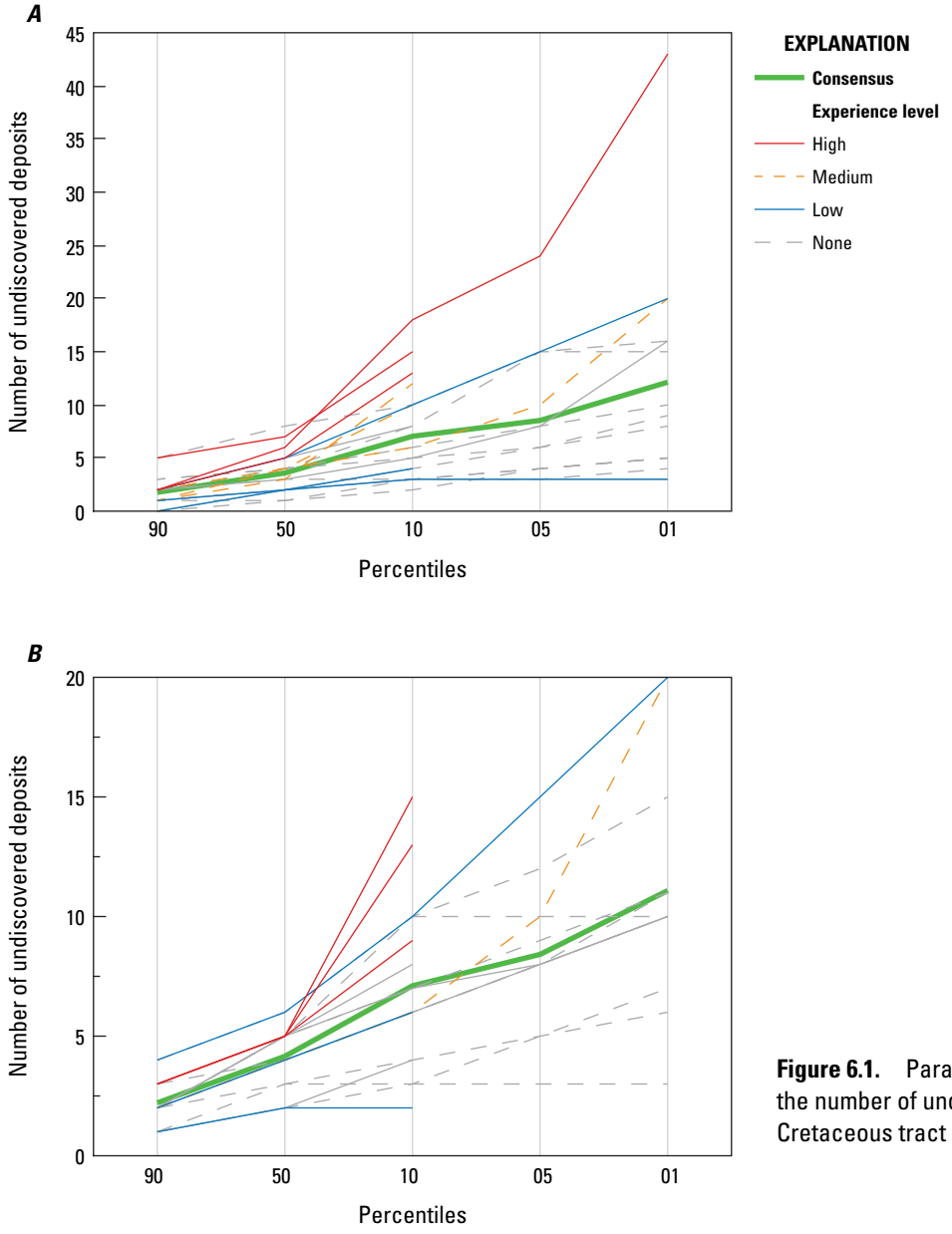


**Figure 6.1.** Parallel plots showing estimates of the number of undiscovered deposits for the GFTZ-Cretaceous tract during *A*, round one and *B*, round two.

**Table 6.1.** Individual and consensus estimates of undiscovered number of deposits.

[The values under NXX refer to the estimated number of deposits associated with the xxth percentile]

| Experience level | N90 | N50 | N10 | N05 | N01 |
|---|---|---|---|---|---|
| Estimation round 1 | | | | | |
| Consensus | 2 | 4 | 7 | 9 | 12 |
| High | 5 | 7 | 15 | | |
| High | 2 | 6 | 18 | 24 | 43 |
| High | 2 | 5 | 13 | | |
| Medium | 2 | 4 | 6 | 10 | 20 |
| Medium | 1 | 4 | 10 | | |
| Medium | 1 | 3 | 12 | | |
| Low | 2 | 5 | 10 | 15 | 20 |
| Low | 1 | 2 | 4 | | |
| Low | 0 | 2 | 3 | 3 | 3 |
| None | 5 | 8 | 10 | 15 | 16 |
| None | 3 | 4 | 6 | 8 | 10 |
| None | 3 | 4 | 5 | 6 | 9 |
| None | 2 | 5 | 8 | | |
| None | 2 | 4 | 8 | 15 | 15 |
| None | 2 | 3 | 5 | 8 | 16 |
| None | 2 | 3 | 3 | 4 | 5 |
| None | 1 | 2 | 4 | 6 | 8 |
| None | 1 | 2 | 4 | | |
| None | 1 | 2 | 3 | 4 | 5 |
| Estimation round 2 | | | | | |
| Consensus | 2 | 4 | 7 | 8 | 11 |
| High | 3 | 5 | 15 | | |
| High | 3 | 5 | 13 | | |
| High | 3 | 5 | 9 | | |
| Medium | 2 | 4 | 6 | 10 | 20 |
| Low | 4 | 6 | 10 | 15 | 20 |
| Low | 2 | 4 | 6 | | |
| Low | 1 | 2 | 2 | | |
| None | 4 | 6 | 10 | 12 | 15 |
| None | 3 | 4 | 6 | 8 | 11 |
| None | 2 | 5 | 10 | 10 | 10 |
| None | 2 | 5 | 8 | | |
| None | 2 | 5 | 7 | 9 | 11 |
| None | 2 | 5 | 7 | 8 | 10 |
| None | 2 | 4 | 6 | 8 | 10 |
| None | 2 | 4 | 6 | 8 | 10 |
| None | 2 | 3 | 4 | 5 | 6 |
| None | 1 | 3 | 3 | 5 | 7 |
| None | 1 | 2 | 4 | | |
| None | 1 | 2 | 3 | 3 | 3 |

**Table 6.2.** Explanation of experience level for estimators of undiscovered number of deposits.

| Experience level | Experience level details |
|---|---|
| High | This task has been a central or major part of the estimator's work. The estimator has performed it routinely, has trained others in performance of this task, and others have consulted the estimator as an expert for assistance in performing this task. |
| Medium | The estimator has performed this task as a regular part of a job, independently and usually without review by a supervisor, manager, or senior employee. |
| Low | The estimator has performed this task on the job under close supervision by a supervisor, manager, or senior employee to ensure compliance with correct procedures. |
| None | The estimator has completed formal education or training in performing this task but has not performed this task on the job. |

# Appendix 7. Resource Assessment Economic Filter Input Parameters

The Resource Assessment Economic Filter (RAEF), introduced by Shapiro and Robinson (2019), is applied to Monte Carlo simulation results derived from three-part quantitative mineral resource assessments. In addition to the undiscovered deposit simulation results, the RAEF utilizes a set of economic filter parameters including, cost-inflation factors, a depth profile of undiscovered deposits, mine and mill type selections appropriate for the deposit type, and engineering cost models for different mine and mill types. Input parameters for evaluation of the GFTZ-Cretaceous tract in the northern Rocky Mountain tungsten skarn study area are presented in Table 7.1.

**Table 7.1.** Input parameters for the Resource Assessment Economic Filter of Shapiro and Robinson (2019) applied to simulation results of the GFTZ-Cretaceous tract.

[MSC, Marshall-Swift cost updating index; $WO_3$, tungsten trioxide; CV_$WO_3$, commodity value for $WO_3$; MRR_$WO_3$, metallurgical recovery rate for $WO_3$]

| Parameter | Value |
|---|---|
| Number of depth intervals | 1 |
| Minimum depth (meters) | 0 |
| Maximum depth (meters) | 1,000 |
| Deposit type | Flat-bedded/stratiform |
| Mine method | Room and pillar |
| Mill Type | 1: Product flotation |
| Days of operation | 350 |
| Environment choice | Tailings pond and dam |
| Liner | Yes |
| MSC | 1.26 |
| Investment rate of return (decimal fraction) | 0.15 |
| Cap cost inflation factor | 1 |
| Operating cost inflation factor | 1 |
| Area (square kilometers) | 7,576 |
| CV_WO3 (U.S. dollars per metric ton) | 26,500 |
| MRR_WO3 (decimal fraction) | 0.75 |

# Reference Cited

Shapiro, J.L., and Robinson, G.R., 2019, Resource assessment economic filter (RAEF)—A graphical user interface supporting implementation of simple engineering mine cost analyses of quantitative mineral resource assessment simulations: U.S. Geological Survey Techniques and Methods, book 7, chap. C23, 18 p., https://doi.org/10.3133/tm7c23.

Moffett Field Publishing Service Center, California
Manuscript approved for publication February 02, 2023
Edited by Phil A. Frederick and John Mark Brigham
Layout by Kimber Petersen

ISSN 2328-0328 (online)
https://doi.org/10.3133/sir20235012